Fabian Zierler
Mat. No. 01310461

Lattice studies of Sp(4) as a candidate Dark Matter theory

PhD Thesis

Doctoral thesis to achieve the university degree of
Doctor of Natural Sciences (Dr.rer.nat.)

University of Graz
Institute of Physics

Supervisor: Prof. Axel Maas
2nd Examiner: Prof. Biagio Lucini

Graz, May 2023

Abstract

The microscopic nature of Dark Matter is one of the most pressing and challenging problems in current particle physics. There is strong observational evidence for its existence based on astrophysical and cosmological observations on large scales. Searches for direct detection of particle Dark Matter at dedicated experiments and at colliders have not found any concrete signals that would illuminate our understanding of Dark Matter at the microscopic level. This has lead to an increased interest in novel ways of constructing microscopic Dark Matter models. Among them are non-Abelian, confining gauge theories in which the Dark Matter candidates are bound states within a rich sector of further dark states. Their bound state nature poses challenges in providing theoretical description and necessitates the use of non-perturbative methods. In this thesis Sp(4) gauge theory with two fermions is investigated as a model of composite Dark Matter. There are several open questions relevant for this model in a Dark Matter context. What are the symmetries of the theory with non-degenerate fermions and what are the symmetries of the dark hadron sector? What is the mesonic spectrum of the non-Abelian theory as a function of the fermion masses? Which degrees of freedom describe the low-energy physics? In order to answer this, the methods of lattice gauge theory are used. The spectrum of low-lying pseudoscalar, vector and scalar states is determined and a description of their multiplet structures based on global symmetries is given. The numerical investigation of the mesonic spectrum includes flavour non-singlet and singlet states for degenerate and non-degenerate fermions. The mass hierarchies of the non-singlet states and the pseudoscalar singlets are established as a function of the fermion masses. The results on the scalar singlet are inconclusive, but they are consistent with potentially light masses. A first exploratory investigation of pseudoscalar scattering lengths is performed.

Kurzfassung

Die mikroskopische Struktur Dunkler Materie ist eines der größten und wichtigsten ungelösten Probleme der modernen Teilchenphysik. Astrophysikalische und kosmologische Beobachtungen liefern starke Indizien für dessen Existenz. Suchen, an Teilchenbeschleunigern und in eigens dafür geschaffenen Experimenten, nach neuen Elementarteilchen, die Dunkle Materie bilden können, konnten bisher nicht Klarheit in unser Verständnis der mikroskopischen Struktur Dunkler Materie bringen. Das Ausbleiben eines direkten Nachweises motiviert die Konstruktion von neuartigen mikroskopischen Modellen der Dunklen Materie. Dazu zählen nicht-abelsche Eichtheorien, in denen Dunkle Materie ein Bindungszustand innerhalb eines Dunklen Sektors ist, der Confinement unterliegt. Die theoretische Beschreibung von Bindungszuständen ist herausfordernd und benötigt nicht-perturbative Methoden. In dieser Arbeit wird eine Sp(4) Eichtheorie mit zwei fundamentalen Fermionen als Modell von Dunkler Materie untersucht. Im Kontext eines Modells von Dunkler Materie bestehen einige offene Fragen zu dieser Theorie. Was sind die globalen Symmetrien mit nichtentarteten Fermionen und was sind die Symmetrien des dazugehörigen Hadronenspektrums? Wie sieht das Mesonenspektrum als Funktion der Fermionmassen aus? Welche Freiheitsgrade beschreiben die Niederenergiephysik dieses Modells. Um diese Fragen zu beantworten, wird die Methodik der Gittereichfeldtheorien verwendet. Die Massen der niederenergetischen pseudoskalaren, vektoriellen und skalaren Mesonen werden bestimmt und eine Beschreibung der Symmetriestrukturen des Spektrums wird beschrieben. Die numerische Untersuchung des Mesonenspektrums beinhaltet die Singulett- und nicht-Singulettzustände der globalen Flavoursymmetrie. Die Massenhierarchie der nicht-Singulettzustände und pseudoskalaren Singulettzustände als Funktion Fermionmassen werden ermittelt. Die Massen der skalaren Singulettzuständen konnten nicht ausreichend signifikant bestimmt werden, sie sind allerdings konsistent mit relativ leichten Massen. Eine explorative Untersuchung der Streulängen der pseudoskalaren Mesonen wurde durchgeführt.

Acknowledgements

First of all, I want to thank my advisor Axel Maas for his guidance and encouragement throughout the last years. I want to thank the members of the research group FG1 and all my collaborators, in particular, Suchita Kulkarni, Marko Nikolic, Seán Mee, Yannick Dengler, Joachim Pomper, and Joshua Lockyer for countless discussion on Dark Matter, symmetries, parities and everything related to it.

I greatly appreciated the discussions on physics as well as all the coffee breaks with the particle physics students here in Graz. I am particularly thankful for Bernd Riederer for always having time to discuss technical problems and his insights into creating beautiful plots and Elizabeth Dobson for a careful reading of the manuscript.

I am thankful for the opportunity to have been a visiting graduate student at Swansea University and want to thank everyone for their hospitality and kindness.

This work was supported by the Austrian Science Fund research teams grant STRONG-DM (FG1). I acknowledge travel support from the City of Graz and the Doctoral School of Physics at the University of Graz. The computations used throughout this thesis have been partially performed on the Sauron and GSC clusters at the University of Graz and on the Vienna Scientific Cluster (VSC4).

Zuallerletzt, möchte ich mich bei meiner Familie und insbesondere bei meinen Eltern für die jahrelange Unterstützung, Zuspruch und ihr Vertrauen in mich bedanken. Alles, was ich bis hierher erreichen konnte, wurde durch sie möglich.

Contents

Publications

Some parts of this thesis are adapted and have been expanded upon from previously published works.

- Bennett, H. Hsiao, J.-W. Lee, B. Lucini, A. Maas, M. Piai et al., *Singlets in gauge theories with fundamental matter*, 2304.07191, [1]
- S. Kulkarni, A. Maas, S. Mee, M. Nikolic, J. Pradler and F. Zierler, *Low-energy effective description of dark $Sp(4)$ theories*, *SciPost Phys.* **14** (2023) 044 [2202.05191], [2]
- F. Zierler, J.-W. Lee, A. Maas and F. Pressler, *Singlet Mesons in Dark $Sp(4)$ Theories*, *PoS* **LATTICE2022** (2023) 225 [2210.11187], [3]
- F. Zierler, S. Kulkarni, A. Maas, S. Mee, M. Nikolic and J. Pradler, *Strongly Interacting Dark Matter from Sp(4) Gauge Theory*, *EPJ Web Conf.* **274** (2022) 08014 [2211.11272], [4]
- A. Maas and F. Zierler, *Strong isospin breaking in $\boldsymbol{Sp}(4)$ gauge theory*, *PoS* **LATTICE2021** (2022) 130 [2109.14377], [5]
- F. Zierler and A. Maas, *$Sp(4)$ SIMP Dark Matter on the Lattice*, *PoS* **LHCP2021** (2021) 162, [6]

Specifically, earlier versions of Sec. 2.5.6, Sec. 2.5.7, Sec. 3.1.1, Sec. 3.1.2, Sec. 3.1.3, Sec. 3.2 and Sec. 3.3, as well as the appendices A.2, A.3, B and C have first been published [2]. Preliminary results were published in [5] and [6] and a summary of the results was published in [4]. Similarly, an earlier version of Sec. 3.4 was first published in [1] and preliminary results were published in [3]. Section 3.5 is based on earlier results that first appeared in [3].

Chapter 1

Introduction

The Standard Model (SM) of particle physics is currently the best available description of three out of the four fundamental forces in nature. It describes electromagnetism and the weak interaction combined in a unified description as well as the strong interaction. Mathematically it is formulated as quantum field theory (QFT). So far, it successfully describes all experimental observations made in dedicated particle physics experiments.

While the SM is extremely successful at explaining almost all observed physical phenomena, it is still incomplete. It does not contain a quantum description of gravity, where the most accurate description is currently given by the general theory of relativity (general relativity, GR). The SM is unable to explain astrophysical observations of Dark Matter (DM), whose gravitational effects in astronomy and cosmology are a well-established empirical fact. It is, however, completely unknown what causes these effects on a microscopic level.

The main motivation for models of particle DM are briefly reviewed in Sec. 1.1. This includes an overview of astrophysical and cosmological evidence for DM in Sec. 1.1.1, a discussion of the small structure problems in Sec. 1.1.2 and a review of constraints on self-interacting DM in Sec. 1.1.3. In Sec. 1.1.4 DM as a thermal relic is discussed and the *Strongly Interacting Massive Particles* (SIMP) paradigm is introduced. In Sec. 1.2 the core concepts of non-Abelian gauge theories such as asymptotic freedom and chiral symmetry breaking will be discussed. This will be complemented by discussions of specifics of Quantum Chromodynamics (QCD) which motivate DM model building with other non-Abelian theories as a model of SIMP DM. In Sec. 1.2.8 the symmetry patterns of QCD will be generalized to real and pseudo-real representations and the construction of an effective field theory (EFT) will be discussed in Sec. 1.3. In Sec. 1.4 a model of SIMP DM based on $\mathrm{Sp}(2N)$ gauge theories is introduced which will be studied throughout the remainder of the thesis. In Sec. 1.5 the relevance of $\mathrm{Sp}(2N)$ theories for other models of Physics Beyond the Standard Model (BSM

physics) is briefly discussed.

1.1 Dark Matter

1.1.1 Observational evidence

Empirical evidence of Dark Matter comes from observations on a variety of different scales – see e.g. [7–9] for overviews. On a galactic scale, the rotation curves of spiral galaxies [10, 11] are one piece of evidence. The rotational velocity is expected to fall off as a function of the distance to the centre of the galaxy. However, a roughly constant velocity distribution is observed, indicating the existence of additional non-visible matter surrounding the galaxy.

On larger scales, observations of gravitational lensing caused by a cluster of galaxies allows a determination off the mass distribution within the cluster [12]. A particularly important case of (weak) gravitational lensing is seen in the bullet cluster merger where the reconstructed gravitational potential is offset from the centre of the visible mass implying the existence of another form of non-visible matter. The astrophysics of the merging galaxy clusters provide constraints on the self-interaction of DM [13]. The strong lensing of galaxy clusters [14] and measurements of their internal density profiles [15] provide further constraints on these scales.

Further evidence for DM can be extracted from the anisotropies of the cosmic microwave background (CMB). In a world without DM, the density perturbations in the early universe would not have been sufficiently strong in order for the currently observed structures of visible matter to form. This implies, that non-visible matter, i.e. DM, is required to facilitate the structure formation from the observed small CMB anisotropies [7, 8].

This is not an exhaustive list of empirical evidence for the existence of DM. A discussion of further observations as well as a guide to further literature can be found in Ref. [9].

These observations suggest the existence of an additional form of non-standard matter. Given that all aforementioned observations are of gravitational origin, it cannot be excluded that they are caused by an incomplete description of gravity at galactic scales and beyond. This has lead to the development of modified theories of gravity [16]. These approaches often have difficulties describing the observed effects of DM on all length scales – see the Particle Data Group's (PDG) review [17] and references therein. As of now, particle DM is the most widely pursued hypothesis.

Assuming particle DM, some constraints on its properties can be deduced. It is required that all astrophysical observations can be explained by the additional particle content beyond the SM. Furthermore, any candidate theory must be compatible with the non-observation

of any physics beyond the SM at current collider and direct detection experiments. This entails that DM can have only minuscule charges under any other SM charge. Astrophysical observations further constrain DM self-interaction. This will be discussed in more detail in Sec. 1.1.3. While model specific limits on DM candidates can impose strong constraints, model independent bounds on the DM itself are extremely loose with a lower bound on fermionic DM of $m \geq 70$ eV and $m \geq 10^{-22}$ eV for bosonic DM. Assuming that particle DM is point-like, an upper limit of 5 solar masses can be established [17]. Note, that some of these constraints are modified if DM is made of more than one species of particles.

1.1.2 Small-scale structure problems

While the hypothesis of cold, non-interacting DM is extremely successful at explaining the observed astrophysical structures at large scales, i.e. at the scales above 1 Mpc. Below these scales, tensions appear when comparing gravitational simulations of DM to observation. The most pressing small-scale issues are known as the *core-vs-cusp* problem, the *too-big-to-fail* and, initially, the *missing satellites* problem – see [18] for a review.

The core-vs-cusp problem refers to the mismatch between the expected DM density profiles close to the galactic centre within DM dominated galaxies. Simulations of cold, collisionless DM predict a *cusp-like* rising density profile towards the galactic centre whereas a flat density profile is observed. An open question here is the influence of baryonic matter on the density profiles obtained from numerical simulation. Present-day simulations have mostly been performed with DM only due to the increased complexity of adding the baryonic feedback [18, 19].

The too-big-to-fail problem concerns galaxies whose DM halos have a large central mass of roughly 10^{10} solar masses. Galaxies with halos of this mass are believed to always facilitate star creation of its enclosed baryonic matter. However, fewer galaxies of this kind have been observed than predicted. Since the associated baryonic mass is expected to be a small fraction of the total mass in these systems, the effects of neglected baryonic feedback are likely smaller than in the core-vs-cusp problem [17, 18].

The missing satellites problem refers to the non-observation of comparatively small satellite galaxies with masses as low as 300 solar masses. This is in tension with simulations of cold non-interacting DM which predict a larger number based on the expected number of DM halos that can accommodate such satellite galaxies [17, 18]. Recent investigations suggest that based on recently improved detections of satellite galaxies and a better understanding of dwarf galaxies in general might explain the apparent mismatch and might even provide an excess of satellite galaxies [20]. The missing satellite problem is now thought to

be resolved [21].

1.1.3 Self-Interacting Dark Matter

One way to explain the persisting small scale structure problems is to no longer assume collisionless DM but self-interacting DM (SIDM) with comparatively large self-scattering cross-sections σ [22]. The relevant quantity here is the ratio σ/m between the DM self-scattering cross-section σ and the DM mass m. It is important to note the potential velocity dependence of this quantity. Astrophysical observations and constraints on DM self-interaction are obtained at different scales (galaxy cluster, groups, individual galaxies). The collision velocity of DM particles depends on the scales of the observed systems. Here, a brief overview of the constraints at different collision velocities is given.

Recent analyses of clusters with a mean velocity of about 1500 km/s obtained constraints as low as $\sigma/m \leq 0.13\text{cm}^2/\text{g}$, but noted possible systematic uncertainties at the level of $0.1\text{cm}^2/\text{g}$ [14]. Other studies obtained similar but slightly looser constraints at comparable collision velocities between $1000-2000$ km/s at $\sigma/m \leq 0.19\text{cm}^2/\text{g}$ [15] and $\sigma/m \leq 0.35\text{cm}^2/\text{g}$ [23]. The quoted values are understood at a 95% confidence level. These investigations often prefer a non-vanishing self-scattering cross-section.

At lower velocities the self-interaction cross-section is less constrained. Simulations of SIDM suggest that the too-big-to-fail and the core-cusp problem can be addressed by a (velocity-independent) SIDM cross-sections of around $\sigma/m \approx 0.5 - 10\text{cm}^2/\text{g}$ [17, 24]. In light of the constraints at high collision velocity, a velocity dependent cross-section appears favourable. Much stronger cross-section at velocities below 20 km/s would also be able to fit stellar dispersions [21].

These findings based on SIDM simulations generally assume only a single DM particle coupled through a light scalar or vector mediator to the SM. In particular, the physics of richer dark sectors containing more than a single DM candidate and a mediator is less studied. This is particularly relevant for models of hadron-like DM where dark sector particles are confined under a new gauge force. These sectors additionally permit different, stable DM candidates with distinct masses and interactions. The individual components could then provide different contributions to self-interactions [21].

Overall, the proposition of DM self-interactions is promising. At comparatively large velocities stringent bounds from strong-lensing in galactic clusters and groups exist. In order to explain the small-scale structure problems a velocity dependent self-scattering cross-section appears favourable with scattering cross-sections ranging between $\sigma/m = 0.1-10\ \text{cm}^2/\text{g}$ from large to low velocities.

1.1.4 Thermal Particle Dark Matter: WIMPs and SIMPs

If a dark sector is coupled by any mediator to the SM, then it is reasonable to expect that the dark sector was in thermal and chemical equilibrium with the SM in the early, hot and dense universe. Depending on the mediator, equilibrium between DM and the SM might even be unavoidable. Furthermore, thermal DM can provide production processes of DM. Among these processes the *freeze-out* mechanism has been considered in many DM models – see e.g. [8] for a textbook review. In this scenario DM is thermally coupled to the visible sector in the early universe. As the universe cools and expands a DM number changing process falls out of equilibrium and reduces the overall number of DM particles in the universe. This process is then stopped once the interaction rate drops below the Hubble rate H, which parameterizes the expansion of the universe. At this point the DM number freezes. This scenario places further constraints on the underlying DM model.

The coupling to the SM needs to be sufficiently strong to allow a thermal equilibrium, while simultaneously evading constraints from collider and direct detection searches. The DM number changing process must lead to the observed DM relic density in the current universe after freeze-out. The former constraint restricts the possible coupling strengths between the dark sector and the SM, while the latter requirement can usually be used to constrain the DM particle mass.

A particularly popular case is obtained when the number depletion process is provided by the scattering of two DM particles into two SM particles. Under some assumptions (among them are homogeneity and isotropy [17]) the relic density is obtained by solving the Boltzmann equation

$$\frac{dn}{dt} + 3Hn = -\langle \sigma_{2\mathrm{DM}\to 2\mathrm{SM}} v \rangle \left(n^2 - n_{\mathrm{eq}}^2 \right), \tag{1}$$

where n denotes the DM number density and n_{eq} its value at the equilibrium, H the Hubble rate and $\langle \sigma_{2DM\to 2SM} v \rangle$ the thermal average of the depleting cross-section times the DM collision velocity. This leads to a typical DM mass scale in the range of $m_{\mathrm{DM}} \sim$ TeV, i.e. at the electroweak scale. These DM models are commonly called *Weakly Interacting Massive Particles* (WIMPs) and have attracted substantial theoretical and experimental interest over the past decades. This has lead to stringent exclusion limits of WIMP DM models since many experiments specifically targeted the WIMP scale in their searches.

Recently, in light of the non-detection of DM and the previously discussed small-scale structure problems, other freeze-out mechanisms have gained increasing interest. Specifically, models in which the number depletion process occurs purely in the dark sector through

processes such as nDM $\to$ 2DM. In particular, the 3DM $\to$ 2DM process has gained significant attention. This process already implies the existence of DM self-interaction. By considering cosmological constraints it was shown that such a process points towards strongly interacting DM and this scenario was named *Strongly Interacting Massive Particles* (SIMPs) [25–27]. The relevant Boltzmann equation, using the same assumptions as in the case of the WIMP scenario, reads

$$\frac{dn}{dt} + 3Hn = -\langle \sigma_{3\mathrm{DM}\to 2\mathrm{DM}} v^2 \rangle \left(n^3 - n^2 n_{\mathrm{eq}} \right), \tag{2}$$

Based on the solution to this equation, the typical SIMP DM particle is expected to be below 1 GeV where experimental constraints are relatively loose. These models naturally provide larger self-interactions as WIMP like models and are thus better suited to resolve small-structure problems. Since thermal equilibrium with the SM is required for freeze-out, SIMP models require a mediator into the SM.

Among the many possible models, that can accommodate a SIMP freeze-out, dark sectors based on QCD-like theories, i.e. asymptotically free, non-Abelian, confining gauge theories with fermionic matter which exhibits spontaneous chiral symmetry breaking, are particularly exciting – see Sec. 1.2. They can provide a rich sector of dark hadrons and can naturally have 3DM $\to$ 2DM interactions. The additional global symmetries of the dark sector can guarantee the stability of the DM candidate and portal mediators into the SM allow for the dark hadrons to always be SM singlets. The existence of 3DM $\to$ 2DM interactions can be understood by considering effective descriptions of such theories. This will be discussed in Sec. 1.3.

1.2 Non-Abelian Gauge Theories and Quantum Chromodynamics

Here, the most relevant details of non-Abelian theories in general and QCD in particular will be reviewed. This includes their microscopic description, the global symmetries of the theory itself and the hadron spectrum in particular, and its generalizations to non-SU(N) theories and fermions under different representations.

1.2.1 Lagrangian and Action

The Lagrangian of a set of matter fields $\{\psi_f\}$ with masses of m_f charged under a colour group is given by [1]

$$\mathcal{L}(x) = \frac{1}{2}\mathrm{Tr}\left[\mathrm{F}_{\mu\nu}(\mathrm{x})\mathrm{F}^{\mu\nu}(\mathrm{x})\right] + \sum_{\mathrm{f}} \bar{\psi}^{\mathrm{f}}(\mathrm{x})\left(\gamma_\mu \mathrm{D}_\mu(\mathrm{x}) + \mathrm{m_f}\right)\psi^{\mathrm{f}}(\mathrm{x}) \tag{3}$$

where we consider Euclidean spacetime and the Dirac gamma matrices γ_μ obey $\{\gamma_\mu, \gamma_\nu\} = 2\delta_{\mu\nu}\mathbb{1}$ unless stated otherwise[2]. Additionally, the matrix $\gamma_5 = \gamma_1\gamma_2\gamma_3\gamma_0$ is introduced, which anti-commutes with all other γ-matrices. The adjoint spinor is denoted as $\bar{\psi}_f(x)$ and is defined as

$$\bar{\psi}_f = \psi_f^\dagger \gamma_0. \tag{4}$$

In (3), $F_{\mu\nu}(x)$ is the field-strength tensor and $D_\mu(x)$ is the covariant derivative for a given gauge group. Different fermion species are labelled by the index f. These two quantities can be expressed in terms of the spin-1 gauge fields $A_\mu(x)$ as

$$F_{\mu\nu}(x) = \partial_\mu A_\nu(x) - \partial_\nu A_\mu(x) + ig\left[A_\mu, A_\nu\right] \tag{5}$$

$$D_\mu(x) = \partial_\mu + igA_\mu(x). \tag{6}$$

If the commutator $[A_\mu, A_\nu]$ is non-vanishing then self-interactions of the gauge fields occur in these theories and the gauge theory is called non-Abelian. The Lagrangian is invariant under a local symmetry group generated by the generators τ^a of a symmetry group G which obey the commutation relations $\left[\tau^a, \tau^b\right] = if^{abc}\tau^c$ where the Latin indices a, b, c label the generators. The gauge fields can be expressed as components of the generators $A_\mu(x) = A_\mu^a(x)\tau^a$ and the colour indices can be made explicit as

$$F_{\mu\nu}^a(x) = \partial_\mu A_\nu(x)^a - \partial_\nu A_\mu(x)^a - gf^{abc}A_\mu^b A_\nu^c \tag{7}$$

$$\left(D_\mu(x)\right)_{ij} = \delta_{ij}\partial_\mu + ig\tau_{ij}^a A_\mu^a. \tag{8}$$

Note, that the structure constants f^{abc} are in the adjoint representation of the gauge group while the matter fields can transform under a different representation of the gauge group in

[1] The notation of [28] after rescaling the gauge fields by a factor of $\frac{1}{g}$ is used.

[2] In principle, a term $\theta\epsilon_{\mu\nu\rho\sigma}F^{\mu\nu}(x)F^{\rho\sigma}(x)$ may be added. For the purposes of this thesis the coefficient is set to $\theta = 0$ and only theories where this term is not present are considered.

which the generators are represented by matrices τ_{ij}^{a}[3]. The Lagrangian is invariant under gauge transformations of the local symmetry group G. Specifically, under a hermitian group element U the matter fields in the fundamental representations and the adjoint gauge fields transform as

$$\psi \to U(x)\psi(x) \tag{9}$$

$$\bar{\psi} \to \bar{\psi}(x)U(x)^{\dagger} \tag{10}$$

$$A_{\mu}(x) \to U(x)A_{\mu}(x)U(x)^{\dagger} + i(\partial_{\mu}U(x))U(x)^{\dagger} \tag{11}$$

leaving the Lagrangian invariant. Note, that the transformation acts differently on matter fields if they are charged under a non-fundamental representation – e.g. in the two-index antisymmetric representation the fermion field ψ transforms into $\psi \to U(x)\psi(x)U(x)^{T}$ [29]. In the absence of fermions in a non-Abelian gauge theory, pure Yang-Mills theory is recovered. The Lagrangian is related to the action and the partition function in Euclidean metric as

$$Z = \int \mathcal{D}[A_{\mu}, \psi, \bar{\psi}]e^{-S[A_{\mu},\psi,\bar{\psi}]} \tag{12}$$

$$S[A_{\mu}, \psi, \bar{\psi}] = \int \mathcal{L}(x)dx \tag{13}$$

In this thesis, only Dirac fermions are considered. Note, that other matter fields such as Weyl or Majorana fermions can also be charged under non-Abelian gauge theories.

1.2.2 Asymptotic Freedom and Confinement

One of the key features of non-Abelian gauge theories with a sufficiently small number of matter fields is the existence of asymptotic freedom. This can be read off from the β function which gives the dependence of the running coupling on the renormalization scale μ as $\beta(g) = \frac{dg}{g \ln \mu}$. Given the Lagrangian from above the β-function at one loop in perturbation theory for massless fermions is given by [30, 31]

$$\beta(g) = -\left(\frac{11}{3}C_2(G) - \frac{4}{3}N_f T(R)\right)\frac{g^3}{16\pi^2} + \mathcal{O}(g^5) \tag{14}$$

[3] In QCD the matter fields transform under the three-dimensional fundamental representation of the gauge group $\mathrm{SU}(3)_c$ while the gauge fields are in the eight-dimensional adjoint representation. In this context the fermion fields are the quark fields and the gauge bosons are the gluons.

where the coefficients depend on the gauge group and the fermion representation through $f^{acd}f^{bcd} = C_2(G)\delta_{a,b}$ and $\mathrm{Tr}(\tau^a(R)\tau^b(R)) = T(R)\delta_{ab}$ with $\tau^a(R)$ being the generators of the group G in the representation R. As long as the number of fermion flavours is smaller than

$$N^{\mathrm{AF}} = \frac{11C_2(G)}{4T(R)}, \tag{15}$$

the first coefficient of the β-function is negative, and the running coupling gets arbitrarily small at large energies. Thus, the coupling is small at larger energies and the theories can be treated within perturbation theory (PT) up to genuinely non-perturbative effects. This entails that the theory is consistent up to arbitrarily large energies – the theory is *ultraviolet (UV) complete*.

A key empirical, non-perturbative fact of Quantum Chromodynamics is the absence of free quarks or gluons in the spectrum of observed particles. All observable states need to be singlets under the colour group. Given that neither the gauge fields nor the fermion fields are colour charge singlets (they transform non-trivially under gauge transformations), the observable states need to be bound states of the fundamental fields, called hadrons. See [32,33] for detailed discussion of confinement. The observable spectrum of hadrons of any non-Abelian gauge theory as defined above needs to reflect all possible ways of constructing colour singlets. In QCD, these bound states are either mesons (quark-antiquark-states), baryons (three-quark-state) or other exotic states such as tetraquarks (four quarks), pentaquark (five quarks), glueballs (only gauge fields) and hybrid states. The lightest hadronic states are of particular interest for models of physics beyond the SM. In the following section the light hadronic spectrum of QCD will be reviewed.

1.2.3 The Light Hadron Spectrum of Quantum Chromodynamics

The hadron spectrum of QCD has inspired different models of BSM physics. In particular, the lightest states of the spectrum are of relevance. The most recent experimental results on the hadron spectrum can be found in the PDG review [17]. The lightest states of QCD are the pseudoscalar $J^P = 0^-$ pions π which occur as charged pions $\pi^\pm$ and a neutral pion π^0. The neutral pion π^0 is the lightest state in the QCD spectrum with a mass of roughly 135 MeV while the charged pions are slightly heavier at 139 MeV. Other light pseudoscalar hadrons include the four kaons, where two of them are the charged $K^\pm$ states at 493 MeV while the other two are the neutral K^0 and $\bar{K}^0$ which are slightly heavier at 497 MeV. An eight and ninth light pseudoscalar is given by the η hadron which is slightly heavier than the kaons at around 547 MeV and the η' hadron at 958 MeV. The number of light pseudoscalar states

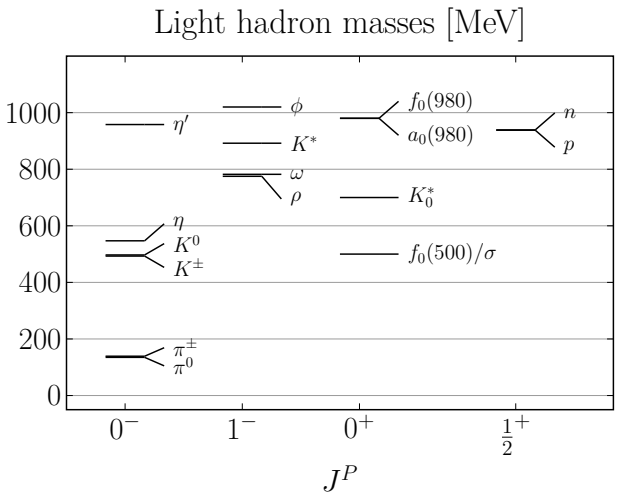

Figure 1: Light hadronic states of the QCD spectrum. These states include the pseudoscalar, scalar and vector mesons as well as the spin-$\frac{1}{2}$ proton and neutron. Note that the experimental uncertainties and the widths of these states can be sizeable. They are omitted for visual clarity and only the currently best estimate [17] is depicted. All other states are heavier than 1 GeV.

can be understood in the context of approximate global symmetries of the QCD Lagrangian. This also applies to the other hadron states and will be discussed in section 1.2.4.

The sector of light, scalar hadrons contains the very broad $f_0(500)$ particle as its lightest state. The experimental status of the light scalar mesons has been a long-standing puzzle. A detailed discussion can be found in the PDG review article "Scalar Mesons below 1 GeV" [17]. Further scalar states are given by the three $a_0(980)$, the single $f_0(980)$ and the four $K_0^*(700)$ which are sometimes denoted as the κ. The numbers in parentheses give their approximate mass in MeV, i.e. the $f_0(500)$ has a mass of roughly 500 MeV.

In the vector sector three vector mesons $\rho^\pm$ and ρ^0 exist at an energy of 775 MeV. Further vector states are given by the $\omega(782)$, the $\phi(1020)$ and the four $K^*(892)$ states. The light hadronic states of QCD are completed by the proton (938 MeV) and the neutron (939 MeV) as the lightest fermionic bound states. All other states are heavier than 1 GeV and heavier than all aforementioned hadrons. A plot of all light states is given in figure 1.

Overall, a pattern of several hadrons that have approximately the same mass appears. Note, that the pion states are substantially lighter than all other states. This pattern can be explained by considering the global symmetries of the theory.

1.2.4 Global Flavour Symmetries, Chiral Symmetry and Hadron Multiplets

The Lagrangian of isolated QCD (i.e. the Lagrangian of quarks and gluons without taking the effects of the electroweak sector into account) is of the form (3) with an SU(3) colour group. The fermionic content is given by six massive quarks called up u, down d, strange s, charm c, bottom b and top t. The latter three are all heavier than all the light hadrons mentioned above and have distinct masses. They will be disregarded for the purposes of this discussion. The other three light quarks are, however, lighter than all the hadrons mentioned above.

Let us focus for now on the pseudoscalar sector of the light meson spectrum. The mesons can be identified as bound states of the three light quarks. Specifically, interpolating fields of the mesons are given in terms of the quark spinors and the adjoint spinors. An appropriate choice of gamma matrices ensures the correct quantum numbers $J^P = 0^-$

$$\begin{aligned}
\pi^+ &= u\gamma_5\bar{d} & K^+ &= u\gamma_5\bar{s} \\
\pi^- &= d\gamma_5\bar{u} & K^- &= s\gamma_5\bar{u} \\
\pi^0 &= \frac{1}{\sqrt{2}}\left(d\gamma_5\bar{d} - u\gamma\bar{u}\right) & K^0 &= d\gamma_5\bar{s} \\
\eta &= \frac{1}{\sqrt{6}}\left(d\gamma_5\bar{d} + u\gamma\bar{u} - 2s\gamma_5\bar{s}\right) & \bar{K}^0 &= s\gamma_5\bar{d} \\
\eta' &= \frac{1}{\sqrt{3}}\left(d\gamma_5\bar{d} + u\gamma\bar{u} + s\gamma_5\bar{s}\right). & &
\end{aligned} \tag{16}$$

Some mesons are almost mass-degenerate as a consequence of the global symmetries. We will mostly follow the treatment in [28]. It is convenient to split the fermion fields into left- and right-handed components by introducing the projection operators $P_{R/L}$ and defining their action on four-component Dirac spinors as

$$\begin{aligned}
P_R &= \frac{\mathbb{1} + \gamma_5}{2} & P_L &= \frac{\mathbb{1} - \gamma_5}{2} \\
P_R\psi &= \psi_R & P_L\psi &= \psi_L
\end{aligned} \tag{17}$$

where $\mathbb{1}$ is the identity matrix in Dirac space. The fermionic part of the Lagrangian density

for a single fermion can be rewritten as

$$\begin{aligned} \bar{\psi}\gamma_\mu D_\mu \psi &= \bar{\psi}_L \gamma_\mu D_\mu \psi_L + \bar{\psi}_R \gamma_\mu D_\mu \psi_R \\ m\bar{\psi}\psi &= m\left(\bar{\psi}_R \psi_L + \bar{\psi}_L \psi_R\right). \end{aligned} \tag{18}$$

Observe that the kinetic part of the Lagrangian does not mix left- and right-handed components. A combination of left- and right-handed spinors only occurs in the Lagrangian in the presence of a fermion mass. For N_f fermions the kinetic part of the Lagrangian is invariant under $\mathrm{SU}(N_f) \times U(1)$ transformations of the left- and right-handed component respectively. The Lagrangian of massless fermions is thus invariant under the group $\mathrm{SU}(N_f)_L \times \mathrm{SU}(N_f)_R \times U(1) \times U(1)$. Since this symmetry does not mix the chiral components of the spinor field, it is usually called *chiral symmetry* and the limit of all masses approaching vanishing masses is referred to as the *chiral limit*. Obviously, the mass term of the Lagrangian breaks this symmetry as the left- and right-handed components are no longer independent. This can be seen by rewriting the spinor fields in a vector notation, i.e. $\bar{\Psi} = \left(\bar{\psi}_1, \ldots, \bar{\psi}_{N_f}\right)$ for the adjoint spinors and accordingly for Ψ and introducing the mass matrix $M = \mathrm{diag}(m_1, \ldots, m_{N_f})$. The fermionic Lagrangian is then given by $\mathcal{L}_f = \bar{\Psi}\left(\gamma_\mu D_\mu \mathbb{1}_{N_f} + M\right)\Psi$ where $\mathbb{1}_{N_f}$ denotes the $N_f \times N_f$ unit matrix. For degenerate masses both kinetic and mass terms are invariant under the transformations

$$\begin{aligned} \Psi' &= e^{i\alpha T_i}\Psi, \\ \Psi' &= e^{i\alpha \mathbb{1}_{N_f}}\Psi, \\ \bar{\Psi}' &= \bar{\Psi} e^{-i\alpha T_i}, \\ \bar{\Psi}' &= \bar{\Psi} e^{-i\alpha \mathbb{1}_{N_f}}. \end{aligned} \tag{19}$$

Here, T_i are the generators of an $\mathrm{SU}(N_f)$ symmetry. The symmetry group is $\mathrm{SU}(N_f)_V \times U(1)_V$. Both terms in the fermionic Lagrangian are invariant because these transformations only mix different fermion flavours but never change the structure of the chiral components. The extra chiral rotations are given by inserting γ_5 into (19)

$$\begin{aligned} \Psi' &= e^{i\alpha\gamma_5 T_i}\Psi, \\ \Psi' &= e^{i\alpha\gamma_5 \mathbb{1}_{N_f}}\Psi, \\ \bar{\Psi}' &= \bar{\Psi} e^{-i\alpha\gamma_5 T_i}, \\ \bar{\Psi}' &= \bar{\Psi} e^{-i\alpha\gamma_5 \mathbb{1}_{N_f}}, \end{aligned} \tag{20}$$

which enlarges the symmetry in the absence of fermion masses to $\mathrm{SU}(N_f)_L \times \mathrm{SU}(N_f)_R \times U(1)_A \times U(1)_V$. Thus, the hadron spectrum of QCD could be explained by an approximate $\mathrm{SU}(N_f)_L \times \mathrm{SU}(N_f)_R \times U(1)_A \times U(1)_V$ symmetry if all fermion masses are relatively light. Additional small corrections due to the small fermion masses, which break the symmetry further down to $\mathrm{SU}(N_f)_V \times U(1)_A \times U(1)_V$, would appear. However, it turns out that this symmetry is *not* realized in nature. The reasons for this are two-fold.

1.2.5 Chiral Symmetry Breaking and the Axial Anomaly

In the previous section, the global symmetries of the fermionic part of the Lagrangian was discussed. The group $\mathrm{SU}(N_f)_L \times \mathrm{SU}(N_f)_R \times U(1)_A \times U(1)_V$ was identified as the global symmetry of the Lagrangian. However, the symmetries of the physical theory are not those of the Lagrangian but those of the partition function. It can be shown that this causes an issue in the case of the chiral rotation generated by the unit matrix $\mathbb{1}_{N_f}$ in (20) which is usually known as the axial $U(1)_A$. This symmetry is broken through quantum effects, i.e. through non-invariance of the fermion measure in the path integral under the global $U(1)_A$. The corresponding current is no longer conserved and thus the symmetry is not manifest in the physical spectrum [34]. In the language of lattice field theory this corresponds to the fermion determinant being non-invariant under this symmetry. See [28] for a demonstration of this property on a lattice. This symmetry is not realized in QCD which is reflected in the meson spectrum. The relatively large mass of the pseudoscalar meson η' and its dependence on the number of colours N_c and fermion flavours N_f are directly linked to the *axial anomaly* [35,36].

In addition to the axial anomaly no effects of the full $\mathrm{SU}(N_f)_L \times \mathrm{SU}(N_f)_R$ symmetry in the meson spectrum are observed. If this were the case, the states with the same J quantum number but opposing parity would be approximately degenerate in the presence of small fermion masses. This is clearly not the case, as can be seen by comparing the pseudoscalar states 0^- to the scalar states 0^+ in fig. 1. The symmetry must be broken by a different mechanism. This can be explained by considering the *chiral condensate* defined as

$$\langle 0|\bar{\Psi}(0)\Psi(0)|0\rangle. \tag{21}$$

It has the same structure as the mass term in the Lagrangian and is therefore not invariant under chiral rotations. If the chiral condensate (21) is non-vanishing, this signals that the ground state of theory is not invariant under the full symmetry of the Lagrangian and this symmetry is said to be *spontaneously broken* and only the $\mathrm{SU}(N_f)_V$ symmetry which leaves the condensate invariant remains. This explains the mass differences between parity partners

in QCD. In this way the chiral condensate acts as an order parameter for chiral symmetry breaking. Note, that this symmetry is not always broken. At high temperatures the theory undergoes a crossover phase transition in which chiral symmetry is again restored and the chiral condensate vanishes. Thus, it is more appropriate to say that chiral symmetry is hidden at low temperatures but re-emerges in the high-temperature case. This effect has also been observed using lattice studies of the finite-temperature particle spectrum [37–39]. The spontaneous breaking of a continuous global symmetry has far-reaching consequences for the mesonic spectrum since Goldstone's theorem now applies (see [40] for a textbook treatment) which implies the existence of massless bosonic states. In particular, when the global symmetry is spontaneously broken from a global group G down to a smaller subgroup H, the number of massless Goldstone states (sometimes also called Nambu-Goldstone bosons) is given by the number of broken generators of G [41]. Here, symmetry breaking from $\mathrm{SU}(N_f) \times \mathrm{SU}(N_f) \to \mathrm{SU}(N_f)$ occurs. This leads to $N_f^2 - 1$ massless Goldstone modes. In the presence of small but non-vanishing fermion masses chiral symmetry is only approximate. Due to the explicit breaking from the mass terms the would-be Goldstone modes acquire a small mass and are commonly referred to as (pseudo-)Nambu-Goldstone bosons ((P)NGB).

Through the axial anomaly the $U(1)_A$ is broken in QCD. At low temperatures the chiral symmetry $\mathrm{SU}(N_f)_L \times \mathrm{SU}(N_f)_R$ is spontaneously broken by the non-vanishing chiral condensate down to $\mathrm{SU}(N_f)_V$. Overall, the global symmetries of this gauge theory with mass-degenerate fermion is given by

$$\mathrm{SU}(N_f)_V \times U(1)_V. \tag{22}$$

This line of reasoning can be straightforwardly generalized to situation where not all fermions are mass-degenerate. For every $N_f^{(i)}$ degenerate fermions a global symmetry (after accounting for the axial anomaly and spontaneous chiral symmetry breaking) of $\mathrm{SU}(N_f^{(i)})$ remains. In the case of fully-degenerate fermion masses, the global symmetry is given by a product of N_f individual $U(1)$ symmetries.

1.2.6 Global $\mathrm{SU}(2)_F$ and $\mathrm{SU}(3)_F$ flavour symmetries in QCD

The similar masses of many hadrons can be understood through the approximate global symmetries of the QCD Lagrangian. Assuming that up and down quark masses are light, an approximate $\mathrm{SU}(2)_F$ symmetry between those fermions manifests. In the context of QCD this symmetry is usually called *strong isospin*. Additionally, the strange quark gives an additional $U(1)$ that preserves its fermion number and the additional $U(1)_V$ symmetry can be shown

to cause baryon number conservation. Specifically, under an element $U \in \mathrm{SU}(2)_F$ the light quark fields transform as

$$\begin{pmatrix} u \\ d \end{pmatrix} \to U \begin{pmatrix} u \\ d \end{pmatrix} = \begin{pmatrix} a & b \\ -b^* & a^* \end{pmatrix} \begin{pmatrix} u \\ d \end{pmatrix} = \begin{pmatrix} a \cdot u + b \cdot d \\ -b^* \cdot u + a^* \cdot d \end{pmatrix} \tag{23}$$

where a and b are complex numbers for which $|a|^2 + |b|^2 = 1$. On any fermion bilinear with two light quarks, such a flavour transformation decomposes into $2 \otimes 2 = 3 \oplus 1$. This means that the bilinear operators are either a triplet or a singlet under $\mathrm{SU}(2)_F$. The pion states in (16) form a triplet under this global symmetry, whereas the η and η' states are singlets. This already can explain the approximate symmetry between all three pions and the distinct masses for the η and η'. Furthermore, the $\mathrm{SU}(2)_F$ transforms a kaon K^+ into a superposition of itself and the K^0. This further explains the near degeneracy between K^+, K^0 and their antiparticles K^- and $\bar{K}^0$.

Since chiral symmetry was spontaneously broken, three almost-massless PNGBs appear. Indeed, three pions are substantially lighter than any other state in the theory. They can be identified as the PNGBs of the $\mathrm{SU}(2)_L \times \mathrm{SU}(2)_R \to \mathrm{SU}(2)_V$.

Similar considerations apply for the vector and scalar mesons. The ρ and $a_0(980)$ mesons form a triplet under $\mathrm{SU}(2)_F$ while the ω, the ϕ and both f_0 scalars appear to be singlets. The approximate degeneracy between the vector K^* mesons and the scalar K_0^* mesons arises in the same fashion as for the pseudoscalar kaons. The quark structure of the scalar mesons is more involved than those of the pseudo-scalars (16). Their quark content is still an open issue [17], but there are strong hints that some of these states are tetraquark states or molecular bound states of pions and kaons.

The approximate global $\mathrm{SU}(2)_F$ symmetry of QCD appears to be a very good approximation of the underlying theory. A mass-difference between states from the same multiplet has only been experimentally established for the pions where $m_{\pi^\pm} - m_{\pi^0} = 4.5$ MeV and the kaons $m_{K^0} - m_{K^\pm} = 3.9$ MeV. This indicates the presence of further symmetry breaking effects in the SM due to the different electric charges of the u and d quarks as well as a small mass difference between them [42].

A direct determination of the quark masses themselves is not possible. No quark has been observed in isolation due to colour confinement [33]. Within QCD, the masses of quarks can be calculated, however, they are not physical but scheme-dependent quantities. Quark masses are only comparable when they have been calculated in the same renormalization scheme at the same renormalization scale μ. The light quarks of QCD are commonly given in the $\overline{\mathrm{MS}}$ scheme at a scale of $\mu = 2$ GeV [17]. Within this scheme the u quark has a

$\mathrm{SU}(2)_F$	
π	triplet
K	four-plet
η	singlet
η'	singlet
ρ	triplet
K^*	four-plet
ω	singlet
ϕ	singlet
a_0	triplet
K_0^*	four-plet
$f_0(500)/\sigma$	singlet
$f_0(980)$	singlet

$\mathrm{SU}(3)_F$	
(π, K, η)	octet
η'	singlet
(ρ, K^*, ω)	octet
ϕ	singlet
$(a_0, K_0^*, f_0(980))$	octet
$f_0(500)/\sigma$	singlet

Figure 2: Multiplets of the light mesonic states of QCD under $\mathrm{SU}(2)_F$ and $\mathrm{SU}(3)_F$. In real-world QCD these symmetries are broken by the non-vanishing and distinct quark masses as well as electroweak interactions.

mass of $2.2^{+0.5}_{-0.3}$ MeV, while the d quark mass is $4.7^{+0.5}_{-0.2}$ MeV [17]. This is consistent with the expectation of small but non-vanishing masses based on the analysis of the light hadron spectrum. In contrast, the strange quark s has a mass of 94^{+9}_{-4} MeV at this scale in the $\overline{\mathrm{MS}}$ scheme.

Given that the strange mass (in this definition) is still lighter than the hadrons observed in the physical spectrum, some imprints of an approximate $\mathrm{SU}(3)_F$ symmetry and its spontaneous chiral symmetry breaking pattern remain. Under this symmetry group the mesons appear either as octets or singlets. In the pseudoscalar sector the pions, kaons and the η meson are the eight PNGBs of $\mathrm{SU}(3)_L \times \mathrm{SU}(3)_R \to \mathrm{SU}(3)_V$ and form an octet while the η' remains a singlet. In the vector sector the ρ's, K^*'s and the ω meson form the octet while the ϕ is a singlet and in the scalar sector the octet consists of the $a_0(980), K_0^*$ and the $f_0(980)$ mesons, while the $f_0(500)$ is a singlet.

The pattern of light mesonic states further provides a case for the existence of the $U(1)_A$ anomaly. The absence of the anomaly would lead to an additional Goldstone mode in the spectrum. In that sense, the anomaly provides mass to the η' prime which would otherwise be a Goldstone boson. This can be seen from considering the limit of large-N gauge groups, where the effect of the anomaly is suppressed by N and the η' has the same mass as the other PNGBs in the limit $N \to \infty$ [35, 36]. For later reference, the different mesonic multiplets of QCD under $\mathrm{SU}(2)_F$ and $\mathrm{SU}(3)_F$ are shown in figure 2.

1.2.7 Conformal Window and Banks-Zaks fixed point

In section 1.2.2, it was shown that non-Abelian gauge theories lose asymptotic freedom if the theory contains too many fermions, specifically more than N^{AF}. At this point the theory is no longer consistent up too arbitrarily high energies. It is no longer *UV complete*.

This poses constraints on possible non-Abelian extensions to the SM with fermions as long as UV completeness is required. For models based on relatively light PNGBs, then another constraint occurs. This can be seen by looking at the perturbative two-loop beta function of massless quarks [43]

$$\beta(g) = -\beta_0 \frac{g^3}{16\pi^2} + \beta_1 \frac{g^5}{16\pi^2} + \mathcal{O}(g^7), \tag{24}$$

$$\beta_0 = \left(\frac{11}{3} C_2(G) - \frac{4}{3} N_f T(R) \right), \tag{25}$$

$$\beta_1 = \left(-\frac{34}{3} C_2^2(G) + \frac{20}{3} C_2(G) N_f T(R) + 4 C_2(R) N_f T(R) \right), \tag{26}$$

where $C_2(R)$ is the second Casimir operator of the fermion representation R. The beta function contains another zero for a number of fermions smaller than N^{AF}. At this point the theory develops an infrared (IR) fixed point known as the Banks-Zaks fixed point and the theory is expected to go into a conformal phase in which chiral symmetry is no longer spontaneously broken [44]. In that case the Goldstone theorem no longer applies, and no PNGBs will appear in the spectrum. The range of N_f in which the theory is chirally symmetric and conformal but still asymptotically free is referred to as the *conformal window*.

The Banks-Zaks fixed point has also gained considerable interest as a model for extending the SM. Theories close to the conformal window have been investigated in the context of composite Higgs bosons. Depending on the specific model these theories can also provide additional Dark Matter candidates and/or contain a partially composite top quark [45].

For Dark Matter models based on PNGBS, the occurrence of the infrared fixed-point will set another limit on the allowed fermion content of such a Dark Matter model. Note, that the exact value of this limit cannot be determined from perturbation theory and non-perturbative determinations are required. These calculations have proven to be particularly challenging the exact number N_f^{crit} is still debated, see [46–48] for recent reviews. For a moderately small number of fermions the chirally broken phase is, however, extremely well established. For the remainder of this thesis only gauge theories with no more than $N_f = 2$ Dirac fermions in the fundamental representation of the gauge group will be considered.

1.2.8 Real and Pseudo-real Breaking Patterns and Diquarks

In Sect. 1.2.4 it was shown that in SU(3) gauge theory with N_f degenerate fundamentally charged fermions, the global symmetry is $\mathrm{SU}(N_f)_V \times U(1)$ and in case of massless fermions spontaneous chirally symmetry breaking from $\mathrm{SU}(N_f)_L \times \mathrm{SU}(N_f)_R \times U(1)_V \to \mathrm{SU}(N_f)_V \times U(1)_V$ occurs, leading to $N_f^2 - 1$ pseudo-Goldstone bosons. The derivation of this pattern in Sect. 1.2.4 only used the decomposition into right- and left-handed components of the Dirac spinors. Thus, this symmetry should be present for other gauge theories and fermion representations as well. However, it could still be larger if an additional symmetry between the different projections exists. This is indeed the case for $\mathrm{Sp}(2N)$ theories (see appendix A.2 for the defining properties of the gauge group) with fundamental fermions as there always exists a global constant transformation S that fulfils

$$(\tau^a)^* = (\tau^a)^T = -S\tau^a S^{-1}, \tag{27}$$

where τ^a are the generators of $\mathrm{Sp}(2N)$. The representation is said to be *pseudo-real* if $S^2 = -1$ which is the case here. The colour matrix S is explicitly given by

$$S = i\sigma_2 \otimes \mathbb{1}_N, \tag{28}$$

with σ_2 being the second Pauli matrix and $\mathbb{1}_N$ the $N \times N$ unit matrix. These equations relate the fundamental representation of $\mathrm{Sp}(2N)$ to its complex conjugate [49, 50]. This can be made explicit by rewriting the fermionic Lagrangian again in left- and right-handed chiral Weyl components of the Dirac spinors [4]

$$\psi^i = \begin{pmatrix} \psi_l^i \\ \psi_r^i \end{pmatrix}, \tag{29}$$

and subsequently grouping the left- and right-handed components in a vector of spinors with N_f Weyl components.

$$\psi_L = \begin{pmatrix} \psi_l^1 \\ \vdots \\ \psi_l^{N_f} \end{pmatrix}, \qquad \psi_R = \begin{pmatrix} \psi_r^1 \\ \vdots \\ \psi_r^{N_f} \end{pmatrix}. \tag{30}$$

[4] The left- and right-handed projections of the four-component Dirac spinors are denoted as ψ_L and ψ_R (17) and the corresponding two-component Weyl spinors as ψ_l and ψ_r

Making use of the chiral representation of the Dirac gamma matrices, they can be rewritten in the massless, fermionic Lagrangian as block matrices of Pauli matrices – see Appendix A.

$$\mathcal{L}_f = \bar{\Psi}\gamma_\mu D_\mu \Psi = i \begin{pmatrix} \psi_l^* \\ \psi_r^* \end{pmatrix}^T \begin{pmatrix} \bar{\sigma}_\mu D^\mu & 0 \\ 0 & \sigma_\mu D^\mu \end{pmatrix} \begin{pmatrix} \psi_l \\ \psi_r \end{pmatrix}. \tag{31}$$

Here, the four-component notation $\sigma_\mu = (1, \vec{\sigma})$ and $\bar{\sigma} = (1, -\vec{\sigma})$ where σ_j are the usual Pauli matrices was used. So far this is not different from the case of SU(3). Note that this equation is implicitly written in flavour space, i.e. $(\psi_l^\dagger, \psi_r^\dagger)$ is a vector of $2N_f$ Weyl components. Now, the pseudo-reality of the colour group (27) and $S^2 = -1$ are used, as well as the relation $\sigma_2\sigma_\mu\sigma_2 = \bar{\sigma}_\mu^T$ (which is just the pseudo-reality condition for the fundamental representation of $\mathrm{Sp}(N) = \mathrm{SU}(2)$). The fermionic kinetic term is rewritten as

$$\mathcal{L}_f = i \begin{pmatrix} \psi_l^* \\ \sigma_2 S \psi_r \end{pmatrix}^T \begin{pmatrix} \bar{\sigma}_\mu D^\mu & 0 \\ 0 & \bar{\sigma}_\mu D^\mu \end{pmatrix} \begin{pmatrix} \psi_l \\ \sigma_2 S \psi_r^* \end{pmatrix}. \tag{32}$$

Note, that the Dirac matrix term now has the same diagonal components. This implies that both ψ_L and $\sigma_2 S \psi_R^*$ have the same transformation properties. This is made explicit by introducing the notation

$$\tilde{\Psi} = \begin{pmatrix} \psi_l \\ \sigma_2 S \psi_r^* \end{pmatrix} \equiv \begin{pmatrix} \psi_l \\ \tilde{\psi}_r \end{pmatrix}. \tag{33}$$

The fermionic Lagrangian is rewritten as

$$\mathcal{L}_f = i\tilde{\Psi}^\dagger \bar{\sigma}_\mu D^\mu \tilde{\Psi}, \tag{34}$$

which makes it apparent that this Lagrangian is invariant under $\mathrm{SU}(2N_f)$ transformations of the extended spinors $\tilde{\Psi}$. The extended symmetry exists for any fermion representation that fulfils the pseudo-reality condition (27). In the case of SU(2) it is also known as the Pauli-Gürsey symmetry [51, 52]. The particular vector notation is known as the Nambu-Gorkov formalism and the object $\tilde{\Psi}$ is sometimes called the Nambu-Gorkov spinor [49]. A similar argument applies to fermions in the adjoint representation of any gauge group. There, the generators τ^a (where a labels the different generators) are given by the structure constants $(\tau^a)^{bc} = f^{abc}$ which are antisymmetric in its indices. In this case

$$(\tau^a)^T = -\tau^a \tag{35}$$

which is the same condition as in (27) with S being the identity matrix and subsequently $S^2 = +1$. The adjoint representation (and other representation fulfilling (27) with $S^2 = +1$) are called real representation. Rewriting the adjoint fermionic Lagrangian using the same Nambu-Gorkov spinor as before, makes it apparent that also in this case the massless Lagrangian is invariant under $\mathrm{SU}(2N_f)$ transformations. The global symmetry is enlarged from $\mathrm{SU}(N_f)_L \times \mathrm{SU}(N_f)_R$ to $\mathrm{SU}(2N_f)$ if the fermion representation is either real or pseudo-real. All other representations are referred to as complex, as there is no isomorphism between the fermion representation and its conjugate representation.

So far only the kinetic part of the fermionic Lagrangian was discussed. In a chirally broken phase, the fermion condensate will further break the global symmetry. This will then be the same global symmetry as for degenerate, massive fermions. The pattern of chiral symmetry breaking can be deduced by examining the symmetries of the mass term for degenerate fermions [53]. In terms of Nambu-Gorkov spinors for pseudo-real representations the mass term can be shown to be [50]

$$\bar{\Psi}\Psi = -\frac{1}{2}\tilde{\Psi}^T\sigma_2 S \begin{pmatrix} 0 & \mathbb{1}_{N_f} \\ -\mathbb{1}_{N_f} & 0 \end{pmatrix} \tilde{\Psi} + \frac{1}{2}\tilde{\Psi}^{*T}\sigma_2 S \begin{pmatrix} 0 & \mathbb{1}_{N_f} \\ -\mathbb{1}_{N_f} & 0 \end{pmatrix} \tilde{\Psi}^* \tag{36}$$

$$= -\frac{1}{2}\tilde{\Psi}^T\sigma_2 SE\tilde{\Psi} + \text{h.c.}, \tag{37}$$

and for the real, adjoint representations

$$\bar{\Psi}\Psi = -\frac{1}{2}\tilde{\Psi}^T\sigma_2 \begin{pmatrix} 0 & -\mathbb{1}_{N_f} \\ -\mathbb{1}_{N_f} & 0 \end{pmatrix} \tilde{\Psi} + \text{h.c.} = \frac{1}{2}\tilde{\Psi}^{\mathrm{T}}\sigma_2 \mathrm{F}\tilde{\Psi} + \text{h.c.} \quad . \tag{38}$$

After introduction of a degenerate mass term and/or after spontaneous chiral symmetry breaking the remaining symmetry is given by the subgroup of $\mathrm{SU}(2N_f)$ transformations that leave the mass term invariant.

In the case of pseudo-real representations, they are the transformations U for which

$$U^T E U = E, \tag{39}$$

holds. In equations (34),(36) and (38) the enlarged global symmetry has been made apparent by rewriting the Lagrangian in terms of two-component Weyl spinors. Equivalently, it can be rewritten in terms of the left- and right-handed projected Dirac spinors $P_R\psi$ and $P_L\psi$. In the case of Weyl spinors the (pseudo-)reality condition and $\sigma_2\sigma_\mu\sigma_2 = \bar{\sigma}_\mu^T$ were used. Expressing

everything in terms of Dirac spinors this relation is replaced by

$$-C\gamma_\mu C^{-1} = \gamma_\mu^T, \tag{40}$$

where C is the charge conjugation matrix. In the chiral representation it is explicitly given by $C = i\gamma_2\gamma_4$ and $C^{-1} = -C^*$ holds and the spinor (33) can be written as [54]

$$\hat{\Psi} = \begin{pmatrix} \psi_L \\ -SC\bar{\psi}_R^T \end{pmatrix} \equiv \begin{pmatrix} \psi_L \\ \tilde{\psi}_R \end{pmatrix}. \tag{41}$$

The role of the σ_2 in (33) is equivalent to charge conjugation of the Dirac spinor which ensures that ψ_L and $\tilde{\psi}_R$ transform under the same global group.

Note that the matrix E is the flavour space equivalent of the colour matrix S as defined in (28). It is the invariant tensor of Sp($2N$) groups. Thus, for pseudo-real representations remaining symmetry is Sp($2N_f$). In the real case, the mass-term is slightly different. It is invariant under all transformations that preserve

$$U^T F U = F, \tag{42}$$

which is the group of SO($2N_f$) transformations. Even though the massless Lagrangian has the same global symmetry for real and pseudo-real representations, the breaking pattern of chiral symmetry breaking is distinct. In summary, three distinct patterns occur [53, 55, 56]

$$\text{complex :} \qquad \mathrm{SU}(N_f)_L \times \mathrm{SU}(N_f)_R \to \mathrm{SU}(N_f)_V, \tag{43}$$

$$\text{real :} \qquad \mathrm{SU}(2N_f) \to \mathrm{SO}(2N_f), \tag{44}$$

$$\text{pseudo-real :} \qquad \mathrm{SU}(2N_f) \to \mathrm{Sp}(2N_f). \tag{45}$$

The number of associated PNGBs of chiral symmetry breaking is obtained by counting the number of broken generators. As noted earlier, complex representations have $N_f^2 - 1$ PNGBs, whereas for pseudo-real representations $(2N_f - 1)N_f - 1$ PNGBS and for real representations there are $(2N_f + 1)N_f - 1$ PNGBs occur. Not only the global symmetry is enlarged compared to a complex representation, but also the PNGBs and all other hadronic multiplets.

In the case of QCD the PNGBs are pseudoscalar mesonic bound states, i.e. bound states of a light anti-quark and a light quark. In the case of real and pseudo-real representations there are more Goldstone modes without increasing the number of fermion flavours in the theory. One obvious question is to ask what operators correspond to the additional PNGBs? In order to see this, it is instructive to consider the operator of a generic meson in terms of

its chiral components. For concreteness, let us consider the $\pi^{\pm}$ meson given by

$$\bar{u}\gamma_5 d = \bar{u}_L d_R + \bar{u}_R d_L. \tag{46}$$

Using (41), it follows that

$$\begin{pmatrix} \psi_L \\ \tilde{\psi}_R \end{pmatrix} \to U \begin{pmatrix} \psi_L \\ \tilde{\psi}_R \end{pmatrix} = \begin{pmatrix} A & B \\ C & D \end{pmatrix} \begin{pmatrix} \psi_L \\ \tilde{\psi}_R \end{pmatrix} = \begin{pmatrix} A\psi_L + B\tilde{\psi}_R \\ C\psi_L + D\tilde{\psi}_R \end{pmatrix} = \begin{pmatrix} A\psi_L - BSC\bar{\psi}_R^T \\ C\psi_L - DSC\bar{\psi}_R^T \end{pmatrix}, \tag{47}$$

where A, B, C, D are the $N_f \times N_f$ block matrices of the global $\mathrm{SO}(2N_f)$ or $\mathrm{Sp}(2N_f)$ (see [56] for more specific parametrizations). Under a global transformation of (33) a left-handed spinor component can transform into its adjoint right-handed counterpart. When performing such a transformation on a meson operator such as (46), new operators of a fermion and a fermion as well as an anti-fermion and another anti-fermion arise. These states are often referred to as *diquarks* and *anti-diquarks*. Contrary, to QCD where diquarks are colour non-singlet quantities, here these operators are colour singlets and correspond to physical states in the mesonic spectrum. Their overall structure is $\psi_i^T(\dots)\psi_j$ for diquarks and $\bar{\psi}_i(\dots)\bar{\psi}_j^T$ for anti-diquarks. The additional PNGBs are specifically of this form – as are the other states in the enlarged meson multiplets.

1.3 Effective Field Theories

In composite DM models, the low-energy physics of the underlying theory is of particular interest. This is especially the case if the DM candidate is the PNGB of a QCD-like theory.

A powerful tool, to make predictions in the low-energy, non-perturbative regimes of strongly interacting theories is provided through effective field theories (EFTs) [57–59]. They provide a simplified, non-renormalizable description of the underlying UV complete theory at low energies in terms of the low-lying bound-states and resonances. In an EFT description of confining theories the fermions and gluons are replaced as the degrees of freedom by the lowest lying hadrons which govern its dynamics up to some energy cutoff. EFTs can be constructed such that all global symmetries of the underlying UV complete theory are preserved.

1.3.1 Chiral Perturbation Theory

For theories close to chiral limit the PNGBs are the lightest states. The global symmetries are given by the global breaking pattern from a symmetry group G down to a subgroup H. The number of PNGBs is then identical to the number of broken generators in $G \to H$, i.e. the number of generators that span the coset G/H. Denoting the broken global generators by T^a, the PNGB fields are parameterized as

$$\pi = \pi^a T^a, \tag{48}$$

where the generators are normalized as $\mathrm{Tr}\left[T^a T^b\right] = \delta^{ab}/2$. The field Σ is introduced as

$$\Sigma = \exp\left(2i\pi/f_\pi\right) I, \qquad \text{(complex)} \tag{49}$$

$$\Sigma = \exp\left(2i\pi/f_\pi\right) E, \qquad \text{(pseudo-real)} \tag{50}$$

$$\Sigma = \exp\left(2i\pi/f_\pi\right) F, \qquad \text{(real)} \tag{51}$$

which is proportional to the chiral condensate (21) ensuring that the field has the correct breaking pattern under chiral symmetry breaking. By canonically normalizing the PNGB fields, the low-energy constant f_π can be identified as the PNGB *decay constant*. A low energy EFT at lowest order is provided by

$$\mathcal{L}_{\text{eff}} = \frac{f_\pi^2}{4} \mathrm{Tr}\left[\partial_\mu \Sigma \partial^\mu \Sigma^\dagger\right]. \tag{52}$$

This describes the true NGBs as the components of π while maintaining the breaking pattern since $\langle\Sigma\rangle \propto I/E/F$ depending on the fermion representation. In this description, the fields π^a are massless. This Lagrangian describes only the dynamics of the true Goldstone modes. An explicit mass term for sufficiently small fermion masses is added, which preserves the same symmetries as the one of the underlying UV complete theory as

$$\mathcal{L}_{\text{mass}} = -\frac{v^3}{2}\left(\mathrm{Tr}\left[M\Sigma\right] + \mathrm{Tr}\left[M^\dagger \Sigma^\dagger\right]\right), \tag{53}$$

where M is an appropriate mass matrix of the fermions and v^3 is the magnitude of the chiral condensate (21). In the mass-degenerate case it is $M = mI$ for complex representations, $M = mE$ for pseudo-real representations and $M = mF$ for real ones. This can be generalized to non-degenerate masses. In the complex case the matrix M is diagonal with entries m_i while in the pseudo-real and real case it requires correct assignment of the masses corresponding

to the individual Weyl components [27]. If combined with the kinetic term of the massless PNGBs this gives the effective Lagrangian of *chiral perturbation theory* (χPT) in the lowest order in Σ as

$$\mathcal{L}^{\mathrm{LO}}_{\chi\mathrm{PT}} = \frac{f_\pi^2}{4}\,\mathrm{Tr}\left[\partial_\mu\Sigma\partial^\mu\Sigma^\dagger\right] - \frac{v^3}{2}\left(\mathrm{Tr}\left[M\Sigma\right] + \mathrm{Tr}\left[M^\dagger\Sigma^\dagger\right]\right). \tag{54}$$

Since the EFT does not need to be renormalizable higher order terms such as $\mathrm{Tr}\left[\partial_\mu\Sigma\partial^\mu\Sigma^\dagger\right]^2$ could be included. For the purposes of this thesis, only the leading order contributions are taken into account. The field Σ can be expanded in terms of the PNGB fields as

$$\begin{aligned}\mathcal{L}^{\mathrm{LO}}_{\chi\mathrm{PT}} =& \,\mathrm{Tr}\left[\partial_\mu\pi\partial^\mu\pi\right] - \frac{2}{3f_\pi^2}\,\mathrm{Tr}\left[\pi^2\partial^\mu\pi\partial_\mu\pi - \pi\partial^\mu\pi\pi\partial_\mu\pi\right] \\ &- \frac{2v^3m}{f_\pi^2}\,\mathrm{Tr}\left[\pi^2\right] + \frac{2v^3m}{3f_\pi^4}\,\mathrm{Tr}\left[\pi^4\right] + \mathcal{O}\left(\frac{\pi^6}{f_\pi^4}\right)\end{aligned} \tag{55}$$

The product of the renormalization group dependent quantities, the renormalized chiral condensate v^3 and the renormalized quark masses m appearing in the mass matrix M is itself renormalization group invariant. From the term quadratic in the PNGB fields follows the universal PNGB mass. This relation can also be understood through the *partially conserved axial current* leading to the Gell-Mann–Oakes–Renner (GMOR) relation

$$f_\pi^2 m_\pi^2 = -mN_f v^3, \tag{56}$$

at this order in the expansion. This allows us to express the lowest-order expansion of chiral perturbation theory in terms of two physical quantities m_π and f_π that can be calculated on the lattice. Furthermore, the GMOR relation shows that the PNGB mass depends quadratically on the renormalized quark mass contrary to heavy fermion limit where the pseudoscalar meson mass will depend linearly on the fermion mass. The GMOR relation will be useful in testing the applicability of chiral perturbation theory, specifically it can be tested whether a PNGB mass squared is indeed linear with respect to the fermion mass. In this expansion the PNGB fields only occur in even powers. Thus, it cannot describe any process that involves an odd number, even though such processes occur in QCD and thus the symmetry $\pi \to -\pi$ is not present in the underlying theory. This can be remedied by noting an additional topological term of the action [60, 61] which can be written as the integral over the boundary of

a five dimensional disk which is identified as the four-dimensional spacetime

$$\mathcal{S}_{\text{WZW}} = \frac{-in}{240\pi^2} \int_{Q_5} \text{Tr}\left[\left(\Sigma^\dagger \frac{\partial \Sigma}{\partial x} dx\right)^5\right], \tag{57}$$

where the prefactor n has been shown to be an integer [60] and can be identified as $n = N_c$ in SM QCD. Expanding again in PNGB fields π and making use of Stokes' theorem reveals that this Wess-Zumino-Witten (WZW) term sources processes with an odd number of PNGB fields. At lowest order, this is the five-PNGB interaction

$$\mathcal{L}_{\text{WZW}} = \frac{2N_c}{15\pi^2 f_\pi^5} \epsilon^{\mu\nu\rho\sigma} \text{Tr}\left[\pi \partial_\mu \pi \partial_\nu \pi \partial_\rho \pi \partial_\sigma \pi\right] + \mathcal{O}\left(\pi^6/f_\pi^6\right). \tag{58}$$

This term does not always appear. It requires a sufficient amount of fermions in the gauge theory such that the fifth homotopy group of the coset G/H is non-trivial [62]. It is equivalent to the statement that at least five PNGB states under chiral symmetry breaking need to exist. This implies, that for the existence of a WZW it is required that

$$\text{complex :} \qquad N_f \geq 3 \quad \text{Dirac fermions} \tag{59}$$

$$\text{pseudo-real :} \qquad N_f \geq 2 \quad \text{Dirac fermions} \tag{60}$$

$$\text{real :} \qquad N_f \geq 3 \quad \text{Weyl fermions.} \tag{61}$$

This is now the full effective Lagrangian after both an expansion in the lowest order of Σ and a subsequent expansion of Σ in the PNGB fields. These expansions require that the overall energies of observables as well as the PNGB masses (and thus the fermion masses) are sufficiently small, i.e. $E \ll 4\pi f_\pi$ and $m_\pi \ll 4 f_\pi$ [63].

The EFT is formulated only in terms of PNGB and fully specified by their masses m_π and their decay constants f_π. These *low energy constants* (LECs) cannot be determined from within the EFT. In theories where experimental data is available such as SM QCD this can be used. Alternatively, they can be calculated from the underlying theory directly.

1.3.2 Beyond Chiral Perturbation Theory

As soon as the energies involved reach those of the next lowest state or resonance in the full theory, it no longer adequately describe the correct low-energy physics. At this point, the next-lowest states need to be included in the EFT to provide an adequate description at those energy scales. Again, this requires knowledge of the hadronic spectrum which needs to

be provided either through experimental observations or theoretical calculations. Once the relevant low-energy states have been identified, they can be included in the EFT.

The main goal of this thesis is to calculate the low-lying hadron masses of a candidate DM theory from first principles using lattice field theory and determine the relevant LECs in the lowest order.

Based on the observed hadrons in SM QCD and lattice calculations in QCD and related theories, the next relevant hadronic states are the vector mesons ρ, the pseudoscalar singlet η' and the scalar singlet f_0/σ.

The vector mesons (and the axial-vector mesons) can be included along the PNGBs using the framework of *hidden local symmetry* as in [63]. The vector and axial-vector mesons are introduced as the fields of an additional auxiliary local symmetry group G_A that has the same structure as the global unbroken group G. This choice will ensure that the vector and axial vector mesons appear in the correct multiplets under the broken, remaining global symmetries. Let T^a denote the generators of G_A, then the spin-1 mesons are parameterized as

$$\rho_\mu = \sum_a \rho_\mu^a T^a. \tag{62}$$

The vector mesons are identified as the ρ_μ^a corresponding to the unbroken generators under $G \to H$, and the axial-vector mesons as ρ_μ^a corresponding to the broken generators. The chiral perturbation theory can now be expanded by a kinetic term and a mass term for the spin-1 mesons

$$\mathcal{L}_\rho = -\frac{1}{2}\mathrm{Tr}\left[\rho_{\mu\nu}\rho^{\mu\nu}\right] + \frac{\mathrm{m}_\rho^2}{2}\mathrm{Tr}\left[\rho_\mu\rho^\mu\right], \tag{63}$$

$$\rho_{\mu\nu} = \partial_\mu\rho_\nu - \partial_\nu\rho_\mu - ig_\rho[\rho_\mu, \rho_\nu], \tag{64}$$

and the interaction between the spin-1 particles and the PNGBs can be introduced by a covariant derivative of Σ with respect to the auxiliary global G_A

$$D_\mu\Sigma = \partial_\mu\Sigma + ig_\rho\left(\rho_\mu\Sigma + \Sigma\rho_\mu^T\right). \tag{65}$$

This leads to an additional LEC g_ρ parametrizing the coupling of the spin-1 states to the PNGBs. At first glance it appears as if the vector and axial vector mesons would have the same mass in this framework which is in contradiction to experimental evidence. This is however not the case. The covariant derivative leads to non-diagonal kinetic terms for the

PNGBs and the axial vectors states

$$a_\mu = \sum_{T^a \text{ broken}} T^a \rho^a_\mu, \tag{66}$$

of the form

$$\mathcal{L}_{\text{kin}} = \frac{1}{2} \text{Tr} \left[\left(\partial_\mu \pi - f_\pi g_\rho a_\mu / \sqrt{2} \right) \left(\partial_\mu \pi - f_\pi g_\rho a_\mu / \sqrt{2} \right) \right]. \tag{67}$$

Diagonalizing these states leads to field redefinitions of a_μ and π as well as f_π and introduces a mass difference between axial-vector mesons a_1 and the vector mesons ρ given by

$$m^2_{a_1} = m^2_\rho / Z^2 \tag{68}$$

$$Z^2 = 1 - \frac{g^2_\rho f^2_\pi}{2 m^2_\rho}, \tag{69}$$

which is always positive, i.e. the axial-vector mesons are heavier than their vector counterparts. In total, two additional LECs were introduced, the vector meson mass m_ρ and the coupling constant g_ρ that need to be determined from the underlying theory. The latter can be determined from scattering processes such as $\pi\pi \to \rho$ [64–66]. An estimate of $g_\rho = m_\rho / f_\pi$ can be given through the KSRF relation [67,68] (see also [69] for an alternative derivation and a discussion of its assumptions). KSRF predicts $m_{a_1}/m_\rho = \sqrt{2}$ which in SM QCD is slightly below the experimental value of $m_{a_1}/m_\rho = 1.59(6)$ [17]. The inclusion modifies the WZW term and contributes to decays such as $\rho \to \pi\pi$, but it does not introduce any additional LECs [2, 70].

The pseudoscalar singlet is included in the EFT treatment by extending the unbroken global symmetry G to $G \times U(1)_A$, since the pseudoscalar singlet η' is associated with the $U(1)_A$. In the large-N_c expansion the mass difference $m_{\eta'} - m_\pi$ is suppressed by N_c and in the limit of $N_c \to \infty$ the mass of the η' becomes degenerate with the other PNGBs. This motivates the inclusion of this state as another would-be Goldstone mode in this limit which can be achieved by modifying the Σ field as

$$\Sigma \to \exp\left(\frac{2 i \eta'}{f_{\eta'}} \right) \Sigma, \tag{70}$$

where η' is a field in flavour space proportional to the appropriately normalized unit matrix. The explicit breaking of the $U(1)_A$ is introduced by giving the η' a distinct mass from the

other PNGBs

$$\mathcal{L}_{\eta'}^{\text{mass}} = m_{\eta'}^2 \eta'^2 = \left(m_\pi^2 + \Delta m_{\eta'}^2\right) \eta'^2, \tag{71}$$

at lowest order. These terms include an additional LEC in the form of the mass of the pseudoscalar singlet η'. Within this expansion at leading order its decay constant $f_{\eta'}$ is equal to the one of the PNGBs, i.e. $f_\pi = f_{\eta'}$ [2].

The inclusion of the scalar singlet f_0/σ is less straightforward. While it is comparatively light in SM QCD, it is also exceptionally broad and its hadronic composition is not yet fully understood. Close to the chiral limit it is expected to be dominated by tetraquark contributions [71]. Lattice studies have proven to be extremely challenging and an understanding of this state's fermion mass dependence in QCD is just emerging [72, 73]. There has been a particular interest in the effective description of the scalar singlet in theories close to the conformal window. Lattice investigations suggest a comparatively light scalar singlet [74–81] which is interpreted as the pseudo-Goldstone of approximate scale invariance. In this case the state is known as the *dilaton* [82] and an effective description in the form of the dilaton EFT has been proposed and tested against lattice results – see Ref. [83] for a review. While these theories are quite different from theories deep in the chirally broken phase, it provides an example of a theory with a phenomenologically highly relevant scalar singlet. Together with the surprisingly light and broad scalar singlet in SM QCD, this highlights the importance of dedicated lattice investigations of this hadron when attempting to construct an EFT. Specifically, the mass of this state as a function of the fermion masses is highly relevant.

1.4 Strongly Interacting Massive Particles from $\mathrm{Sp}(2N)$

Based on an effective theory, it is possible to construct well-motivated SIMP DM theories which naturally provide semi-annihilation 3DM $\to$ 2DM as a freeze-out process, as well as sizeable self-interactions. It was realized that theories with a Wess-Zumino-Witten term automatically provide $3 \to 2$ interaction that can set the DM relic density [26]. In this setup the PNGBs are the DM candidates and the PNGBs are often referred to as *dark pions*.

A minimal realization of SIMP DM are symplectic gauge theories $\mathrm{Sp}(2N)$ with two fermion flavours in the pseudo-real fundamental representation. For two fermion flavours the theory is deep in the chirally broken phase [84, 85] with exactly 5 PNGBs which is the minimal number of PNGBs needed to have a WZW term. The number of colours $N_c = 2N$ is always even which makes every bound state of this theory a boson. The stability of the PNGBs for

degenerate fermions is guaranteed by flavour symmetry.

SIMP models based on Sp($2N$) gauge theories have first been proposed in [26] and analysed within leading order (LO) chiral perturbation by solving the respective Boltzmann equations (1) and (2). It was shown that this model gives the correct order of magnitude self-scattering cross-section to address the cusp-vs-core and too-big-to-fail problem. The mass of the dark pions is then roughly in the regime of QCD hadrons, between a few MeV and below 1 GeV. Studies using chiral perturbation theory at LO [26] as well as next-to-leading-order (NLO) and next-to-next-to-leading-order (NNLO) [86] suggest that constraints are stronger at a lower number of colours N_c and in the presence of an unbroken global symmetry Sp($2N_f$).

This motivates a choice of a non-minimal number of colours $N_c > 2$. Since one main goal of this thesis is to provide lattice input for further phenomenological studies, large N_c are somewhat problematic. Firstly, the dimension of the all involved colour representations are larger and thus require substantial computing power. Secondly, at large N_c the standard lattice algorithms (see Sec. 2.3.3) experience topological freezing [87]. The sampling of the path integral can become non-ergodic, which might introduce unaccounted for systematic effects. This exploratory investigation starts with Sp(4) gauge theory which is the smallest non-SU(N) symplectic gauge group.

As noted before, an additional breaking of the global Sp($2N_f$) appears phenomenologically relevant. Apart from relaxing constraints derived from chiral perturbation a further breaking of this global symmetry leads to even richer dark sectors. This can have consequences for small-scale structure formation as it modifies DM self-scattering. In particular, it can provide inelastic scattering [88] as well as realizations of subcomponent DM [21]. Therefore, not only the case of two mass-degenerate fermions charged under the Sp(4) group is investigated, but also the non-degenerate case starting from small fermion mass differences up to sizeable splittings.

1.5 More Beyond the Standard Model Physics from Sp($2N$)

Section 1.4 motivated the choice of Sp(4) gauge theory with two fundamentally charged fermions as a realization of the SIMP DM model. Other models for physics beyond the standard model (BSM) exist, that are based on similar theories. Investigations of such a strongly-interacting theory produce useful information for other models.

The breaking pattern SU($2N_f$) $\to$ Sp($2N_f$) and in particular the $SU(4)$/Sp(4) coset have

gained significant attention in the context of composite Higgs models as well as in the context of partial top compositeness [63, 89–93]. Symplectic gauge theories have also been used in the construction of non-SIMP DM models. Since the system is expected to show chiral symmetry breaking, it can be a model of generic mesonic, Goldstone DM [94–100] where the DM relic abundance might be obtained through other mechanisms than the $3 \to 2$ interaction provided by the WZW terms or in scenarios where the SIMP mechanism is either modified or replaced through other scattering interactions within the dark sector [101, 102]. For heavy fermions these theories can also provide DM candidates in the form of glueballs [95].

The study of Sp(4) provides further insights into the generic structures of chirally broken, confining gauge theories. Being the smallest non-SU(N) group its study will help to identify commonalities and differences between Sp($2N$) and SU(N) gauge theories. Furthermore, it will provide insights into how these theories approach the limit of large-N.

1.6 The Case for Lattice Methods

The study of SIMP DM models based on confining gauge theories has currently been mostly based on chiral perturbation theory, i.e. based on dark pion dynamics alone [26]. NLO and NNLO calculations [86] have shown that sizeable corrections to LO can appear. However, these studies are plagued by a lacking knowledge of the low energy constants (LECs) of the underlying theory. The LECs cannot be computed within the EFT itself but require further input, e.g. in the form of first-principles lattice calculations. Additionally, the use of an EFT based purely on dark pions might be inappropriate. Given the moderately heavy fermions masses required to obtain the correct relic density [26], other light states such as the vector mesons ρ and the scalar and pseudoscalar singlets f_0/σ and η' might require inclusion in the EFT treatment as discussed in Sec. 1.3.

In order to test this, knowledge of the full low-energy spectrum of this theory is required as well as results on all relevant LECs. In principle, the LECs could be treated as free parameters of the EFT. However, not every possible combination of LECs corresponds to a UV microscopic complete theory. This is not surprising, given that at each order in the EFT expansion new LECs are introduced, whereas the UV complete theory is fully parameterized by the gauge coupling and the fermion masses.

In case of the theory at hand, the potentially relevant LECs are the masses of the mesons, their decay constants as well as the coupling between dark pions and vector mesons as noted in Sec. 1.3.2. The methods of lattice field theory allow us to determine them from first principles as a function of the free parameters of the theory, the gauge coupling and the

fermion masses. It can be calculated, which mesonic states are likely to provide relevant contributions to the EFT and which combination of LECs correspond to actual UV complete theories.

Additionally, other quantities beyond EFT LECs can be obtained directly on the lattice, such as scattering lengths and cross-sections for both 2DM $\to$ 2DM self-scattering and the 3DM $\to$ 2DM semi-annihilation; the spectrum of existed states and matrix elements relevant for coupling the strongly-interaction theory to a mediator. These results can then be used to further constrain the parameter space to phenomenologically relevant sub-spaces, to test the validity of the EFT by comparing its predictions to first-principles calculation and in further astrophysical and phenomenological investigations.

There are some lattice results available for symplectic gauge groups with fundamental fermions: The non-singlet spectrum for two-degenerate fermions has been studied for both SU(2) [54, 97, 103–105] and Sp(4) [29, 91] gauge theory. Scattering lengths as well as $\rho\pi\pi$ scattering and singlet channel scattering have been studied only in SU(2) thus far [64,106,107]. Little is known about the spectrum of singlet states in symplectic theories. An exploratory study in SU(2) [108,109] exists, indicating that these states might be light, but it was unable to resolve the respective mass hierarchies. Symplectic theories with non-degenerate fermions have so far never been studied on the lattice.

The main goal of this thesis is to fully resolve the low-energy spectrum of Sp(4) gauge theory with two fermions both for degenerate and non-degenerate masses. Additionally, all relevant LECs at LO in the EFT detailed in Sec. 1.3 will be determined. Since the scattering properties between DM candidates is of utmost importance for setting the relic density and for addressing the small-scale structure problems, an exploratory investigation of the dark pion scattering lengths in an appropriate channel will be provided. The relevant details of lattice gauge theory will be reviewed in Sec. 2. Both numerical and analytic results on the spectrum of such theories will be presented in Sec. 3.

Chapter 2

Lattice Gauge Theory

In this chapter the required techniques for performing non-perturbative calculations using lattice gauge theory will be reviewed. Sec. 2.1 deals with the effects of discretized spacetime and its relation to the continuum theory. In Sec. 2.2 the continuum action for non-Abelian gauge theories will be discretized. Sec. 2.3 and Sec. 2.4.1 examine the sampling algorithms for the path integral as well as statistical methods used in data analysis. The chapter closes by reviewing the details of hadron spectroscopy within lattice gauge theory. Most of the contents of this chapter can be found in dedicated lattice QFT textbooks [28, 110–113].

2.1 Finite and discrete spacetime

The starting point for lattice field theory is the Wick-rotated partition function Z of the QFT at hand, i.e. the Wick-rotated path-integral. In the case of a gauge theory with fermions fields ψ and their adjoint fields $\bar{\psi}$ it reads

$$Z = \int \mathcal{D}[A_\mu, \psi, \bar{\psi}] e^{-S[A_\mu, \psi, \bar{\psi}]}, \tag{72}$$

where A_μ denote the gauge field and $\mathcal{D}$ the measure of the path integral. Within this approach expectation values of operators O are

$$\langle O \rangle = \frac{1}{Z} \int \mathcal{D}[A_\mu, \psi, \bar{\psi}] e^{-S[A_\mu, \psi, \bar{\psi}]} O[A_\mu, \psi, \bar{\psi}], \tag{73}$$

where the operator can depend on any of the fields present in the theory. As long as the action is positive-definite the exponential $e^{-S[A_\mu, \psi, \bar{\psi}]}$ can be interpreted as a probability distribution.

This allows the use of numerical techniques in analogy to statistical mechanics. Discretizing spacetime to a grid of finite extent makes such a system potentially tractable for numerical investigation. Even more importantly, it provides genuinely non-perturbative UV and IR regulators.

In almost every case, spacetime is discretized to a hypercubic lattice with a lattice spacing a and $N_T \times N_L^3$ lattice sites. Here, N_T denotes the number of lattice sites in a "temporal" direction, whereas N_L denotes the number of lattice sites in the "spatial" direction. Because the lattice theory is formulated in a Euclidean metric there is no a priori distinction between temporal and spatial direction. However, in certain aspects of zero-temperature hadron spectroscopy it will be advantageous to have more lattice points in one of the four dimensions of the lattice and identify this dimension as the temporal one in the analysis [1].

The physics of the continuum theory corresponds to the limit of an infinite volume, and the limit of an infinitely small lattice spacing.

$$L \to \infty, \tag{74}$$

$$T \to \infty, \tag{75}$$

$$a \to 0. \tag{76}$$

When setting up a lattice calculation, the parameters are the bare gauge coupling g and the bare fermion masses m_0. The number of lattice sites is given by N_T and N_L. Once a lattice simulation is performed, the lattice spacing a can be determined in physical units by fixing an appropriate scale based on experimental input. For example, this could be a meson mass. The remaining free parameters can then be fixed from other distinct quantities.

This is problematic for BSM theories. Despite tremendous experimental effort, there are (currently) no experimental reference values for setting such a scale. In this case only dimensionless ratios that do not involve the lattice spacing a such as the ratio of hadron masses or decay constants can be obtained. The overall scale of the theory at a given lattice spacing is then unfixed.

The lattice spacing a is not an input parameter, and can only be determined once a lattice simulation with bare input parameters (g, m_0) has been performed. Which choices of the bare parameters corresponds then to the continuum limit $a \to 0$? It can be shown that,

[1] In the case of non-vanishing temperatures this direction can also be associated with temperature. In this case the T is usually smaller than L and the boundary conditions need to be chosen carefully.

due to asymptotic freedom, the continuum limit is reached as

$$g \to 0. \tag{77}$$

In a real-world simulation the continuum limit cannot be reached directly. As a decreases, the number of lattice sites in a given dimension N_L and N_T must increase in order to keep the physical volume fixed. This will quickly become infeasible as the required computing power grows rapidly as the number of lattice sites scales for a fixed volume with the fourth power of $1/a$. In practice, first the quantities of interest are determined at fixed spacing a (i.e. fixed bare parameters) for different lattice sizes. For theories with chiral symmetry breaking the leading finite volume contributions are derived from chiral perturbation theory at a fixed volume, allowing an extrapolation to infinite volumes $L, T \to \infty$ [114, 115].

$$m_\pi(L) = m_\pi^{\text{inf}} \left(1 + A(m_\pi L)^{-3/2} \exp\left(m_\pi L\right)\right), \tag{78}$$

where m_π in general denotes the PNGB mass, i.e. the mass of the dark pion in the DM model or the SM pion in QCD. Similar expressions can be derived for the decay constants and generalizations have been applied to extrapolate other meson masses to the infinite volume limit [91]. Due to this relation, the product $m_\pi L$ is often used to estimate the relevance of finite volume effects.

Then, the lattice spacing is decreased by lowering the bare coupling g while preserving all ratios of observables that are used to fix the remaining free parameters of the theory. Using this procedure the results obtained at different lattice spacings a can be compared. When a is smaller than all relevant hadronic scales, the effects of finite a should be small which can be explicitly checked. Other prescriptions of approaching the continuum limit are usually better motivated but are infeasible due to the associated computational cost [28].

2.2 Discretizing the continuum action

Once spacetime is restricted to a discrete lattice a discretization prescription for the gauge fields as well as the fermion fields is required. Formulating lattice gauge theory goes back to the seminal work of Wilson [116]. It is formulated in terms of the lattice sites and links between neighbouring sites. In this formulation the gauge fields are given by link variables $U_\mu(n)$, connecting a lattice site $n = (n_0, n_1, n_2, n_3)$ to a neighbouring site in the direction μ, denoted as $n + \hat{\mu} = (n_0 + \delta_{\mu 0}, n_1 + \delta_{\mu 1}, n_2 + \delta_{\mu 2}, n_3 + \delta_{\mu 3})$ with the Kronecker symbols $\delta_{\mu\nu}$. The link variables are related to the lattice gauge fields in the fundamental representation

$A_\mu(n)$ as

$$U_\mu(n) = \exp\left(iaA_\mu(n)\right). \tag{79}$$

Since the fields $A_\mu(n)$ are in the algebra of the gauge group, the link variables are elements of the gauge group itself. In the lattice formulation of the gauge theory the link variables U_μ replace A_μ in the path integral as the fundamental variables. In contrast, the fermion fields $\psi(n)$ live on the lattice site. Under a local gauge transformation specified by a group element $\Omega(n)$ they transform as

$$\psi(n) \to \Omega(n)\psi(n) \tag{80}$$
$$\bar{\psi}(n) \to \bar{\psi}(n)\Omega(n)^\dagger \tag{81}$$
$$U_\mu(n) \to \Omega(n)U_\mu(n)\Omega(n+\hat{\mu})^\dagger. \tag{82}$$

From the gauge transformation of the links, it can be seen that closed paths are gauge invariant due to the unitarity of $\Omega(n)$. The action of pure gauge theory can be expressed in terms of a sum of all shortest closed loops. The smallest loop $U_{\mu\nu}$ is a product of four links and referred to as *plaquette*

$$U_{\mu\nu} = U_\mu(n)U_\nu(m+\hat{\mu})U_{-\mu}(m+\hat{\mu}+\hat{\nu})U_{-\nu}(m+\hat{\nu}). \tag{83}$$

The *Wilson plaquette action* of pure Yang-Mills theory is then given by

$$S_G = \beta \sum_n \sum_{\mu<\nu} \left(\mathbb{1} - \frac{1}{N_c} \operatorname{Re}\left(\operatorname{Tr} U_{\mu\nu}(n)\right) \right). \tag{84}$$

Rewriting the plaquette action in terms of the lattice gauge fields (79) shows that this gives the correct continuum action in the limit of $a \to 0$. Then the coefficient β is identified as

$$\beta = \frac{2N_c}{g^2}, \tag{85}$$

and the continuum limit corresponds to

$$\beta \to \infty. \tag{86}$$

In practical lattice calculation β will be specified rather than the gauge coupling g. The quantity β is known as the *inverse gauge coupling*. The choice of the action is not unique

as many other formulations will produce the same continuum limit. This can be used to construct actions that minimize effects of the lattice spacing a. For the purposes of this thesis only standard plaquette action is used. The naively discretized fermion action is

$$S_F^{\text{naive}} = a^4 \sum_{n,m} \bar{\psi}(n) D^{\text{naive}}(n|m) \psi(m) \tag{87}$$

$$= a^4 \sum_n \sum_\mu \bar{\psi}(n) \gamma_\mu \frac{U_\mu(n)\psi(n+\hat{\mu}) - U_{-\mu}(n)\psi(n-\hat{\mu})}{2a} + a^4 \sum_n m\bar{\psi}(n)\psi(n), \tag{88}$$

where the discretized derivative has been introduced symmetrically and $D(n|m)$ denotes the Dirac operator from lattice site n to m. The gauge links U_μ ensure gauge invariance and provide the interactions arising between the fermions and gauge fields from the covariant derivative of the continuum. The case of free fermions is obtained by setting $U_\mu(n) = \mathbb{1}$. Careful inspection of this action shows, that the fermion propagator obtains additional (unphysical) poles on a finite lattice. In the case of massless, free fermions the physical pole at $p = (0,0,0,0)$ remains while additional poles at momenta $p_i = \pi/a$ occur. This is due to the term $\sin(p_\mu a)$ in the lattice Dirac operator in momentum space. In the formulation by Wilson [116] these poles are removed by introducing additional terms that vanish in the continuum limit. The discretized Wilson Dirac action is then

$$S_F = a^4 \sum_{n,m} \bar{\psi}(n) D(n|m) \psi(m) \tag{89}$$

$$= a^4 \sum_{n,\mu} \bar{\psi}(n) \frac{(1+\gamma_\mu)U_\mu(n)\psi(n+\hat{\mu}) - (1-\gamma_\mu)U_{-\mu}(n)\psi(n-\hat{\mu})}{2a}$$

$$+ a^4 \sum_n \left(m + \frac{4}{a}\right) \bar{\psi}(n)\psi(n), \tag{90}$$

where the Wilson Dirac operator $D(n|m)$ between lattice sites n and m with suppressed indices was implicitly defined in the first line. It can be shown that these additional terms give the additional poles a mass of $m + \frac{2l}{a}$, where l is the number of non-vanishing momentum components in the additional pole. In the continuum limit $a \to 0$ these poles acquire an infinite mass and decouple from the remaining theory while the physical pole approaches its correct continuum limit. This discretization comes at the cost of breaking chiral symmetry at finite lattice spacing a through the introduction of an additional mass term. For the purposes of this investigation this is sufficient since the theories of interest also have moderate fermion masses that break chiral symmetry explicitly. Combining the Wilson plaquette gauge action

(84) with the Wilson discretization of fermions(89), the full discretized action for the Wilson formulation of lattice gauge theory is

$$S[U,\psi,\bar{\psi}] = S_G[U] + S_F[U,\psi,\bar{\psi}], \tag{91}$$

and the partition function

$$Z = \int \mathcal{D}[\bar{\psi},\psi,U] \exp\left(-S[U,\psi,\bar{\psi}]\right). \tag{92}$$

The path integral measures are defined as a product of the individual measures at a single lattice site

$$\mathcal{D}[\bar{\psi},\psi] = \prod_{n,\alpha,c} \mathrm{d}\psi_{\alpha,\mathrm{c}}(\mathrm{n})\mathrm{d}\bar{\psi}_{\alpha,\mathrm{c}}(\mathrm{n}), \tag{93}$$

$$\mathcal{D}[U] = \prod_{n,\mu} \mathrm{dU}_{\mu}(\mathrm{n}), \tag{94}$$

where α and c are the spinor and colour index. Note that ψ and $\bar{\psi}$ are Grassmann valued fields and the partition function requires Grassmann integration. The integration over the group in $dU_\mu(n)$ is defined via the Haar measure which is unique given the requirements of invariance under group multiplication and normalization of the measure [110].

2.3 Sampling the Path Integral

2.3.1 Importance Sampling

By introducing a discretization the partition function is a high-dimensional finite integral. A numerical evaluation of the path integral is in principle feasible, but a direct evaluation of the integral is numerically intractable due to the number of degrees of freedom. Monte-Carlo methods can still be used to sample the integral, which in the case for pure Yang-Mills theory is

$$\langle O \rangle = \frac{\int \mathcal{D}[U] \exp\left(-S[U]\right) O[U]}{\int \mathcal{D}[U] \exp\left(-S[U]\right)}. \tag{95}$$

Furthermore, the factor $\exp\left(-S[U]\right)$ provides different weights to different gauge configurations. The method of *importance sampling* can be used to randomly generate new gauge

configurations according to the distribution

$$\rho(U) = \frac{\exp\left(-S[U]\right)}{\int \mathcal{D}[U] \exp\left(-S[U]\right)}. \tag{96}$$

By sampling gauge configuration U according to this distribution, the expectation value of O is approached as

$$\langle O \rangle = \lim_{N\to\infty} \frac{1}{N} \sum_{i=1}^{N} O[U_i]. \tag{97}$$

This approach hinges on the fact that $e^{-S[U]}$ is a positive definite quantity so that $\rho(U)$ can be interpreted as probability distribution. Already by including fermions this is no longer generically guaranteed.

2.3.2 Fermions and pseudofermions

Consider a generic observable in a gauge theory with fermions for a fixed gauge configuration U

$$\langle O \rangle = \frac{\int \mathcal{D}[U] \exp\left(-S_G[U]\right) \int \mathcal{D}[\psi,\bar{\psi}] \exp\left(-\bar{\psi} D[U] \psi\right) O[U,\bar{\psi},\psi]}{\int \mathcal{D}[U] \exp\left(-S_G[U]\right) \int \mathcal{D}[\psi,\bar{\psi}] \exp\left(-\bar{\psi} D[U] \psi\right)}, \tag{98}$$

where $D[U]$ is the (Wilson) Dirac operator for a fixed gauge configuration. The fermionic contributions can be integrated analytically because they are built from Grassmann variables. For one species of fermions ψ and its adjoint $\bar{\psi}$ an observable can be rewritten as

$$\langle O \rangle = \frac{\int \mathcal{D}[U] \exp\left(-S_G[U]\right) O_F[U]}{\int \mathcal{D}[U] \exp\left(-S_G[U]\right)}, \tag{99}$$

$$O_F[U] = \frac{1}{Z_F[U]} \int \mathcal{D}[\psi,\bar{\psi}] \exp\left(-\bar{\psi} D[U] \psi\right) O[U,\bar{\psi},\psi], \tag{100}$$

$$Z_F[U] = \int \mathcal{D}[\psi,\bar{\psi}] \exp\left(-\bar{\psi} D[U] \psi\right). \tag{101}$$

Interpreting $O_F[U]$ as a new observable with respect to the pure gauge theory this expression is rewritten as

$$\langle O \rangle = \frac{1}{Z} \int \mathcal{D}[U] \exp\left(-S_G[U]\right) O_F[U] Z_F[U], \tag{102}$$

where Z is the partition function of the full theory. For sampling the full path integral it suffices to generate gauge configurations as the fermionic integrations can be done analytically. The O independent quantity, $Z_F[U]$, can be shown to be proportional to the determinant of the Dirac operator

$$Z_F[U] = \int \mathcal{D}[\psi, \bar{\psi}] \exp\left(-\bar{\psi} D[U] \psi\right) = \int \prod_i \left(\mathrm{d}\bar{\psi}_\mathrm{i} \mathrm{d}\psi_\mathrm{i}\right) \exp\left(\sum_{ij} \bar{\psi}_i (-D_{ij}) \psi_j\right) = \det\left[-D\right]. \tag{103}$$

In the final step the Matthews-Salam formula for Gaussian integrals of Grassmann variables has been applied [28] and i, j are multi indices combining lattice site, spinor and colour indices. For multiple fermion species products of the *fermion determinant* occur. Similarly, expressions for the fermionic expectation value of spinors can be derived

$$\begin{aligned} \langle \prod_{l=1}^{n} \psi_{i_l} \bar{\psi}_{j_l} \rangle_F &= \frac{1}{Z_F} \int \prod_j \left(\mathrm{d}\bar{\psi}_\mathrm{j} \mathrm{d}\psi_\mathrm{j}\right) \prod_l \psi_{i_l} \bar{\psi}_{j_l} e^{\sum_{ij} \bar{\psi}_i (-D_{ij}) \psi_j} \\ &= (-1)^n \sum_{P(1,\ldots,n)} \mathrm{sign}(P) \prod_{l=1}^{n} (-D^{-1})_{i_l, j_{P(l)}}. \end{aligned} \tag{104}$$

The fermionic expectation value evaluates to the sum over all permutations of products of inverse Dirac operators. The relative signs are given by the permutation P of the n involved products of Grassmann variables.

In the case of the expectation value of fermion operators, the fermionic integrals are given by products the inverse Dirac operator from multi index $i = (n, \alpha, a)$ to multi index $j = (m, \beta, b)$. This inverse is known as the *fermion propagator*. $D^{-1}_{i,j}$ corresponds to the as the operator which propagates a fermion from lattice site x to y, from spinor index α to β and from colour index a to b. It will be useful to introduce a graphical notation for this as

$$D^{-1}_{i,j} = \left(D^{-1}\right)^{a,b}_{\alpha,\beta}(x|y) = \quad .$$

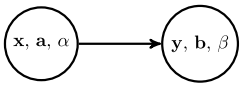

(105)

Equations (103) and (104) show that $O_F[U]$ and $Z_F[U]$ have a different structure with respect to the Dirac operator D. Typically, the determinant leads to large fluctuations and introduces numerical instabilities while being computationally expensive [28]. Including the fermion determinant as an observable has proven to be useless for most systems. Thus, it needs to be included as a weight together with $\exp\left(-S_G[U]\right)$. Setting the determinant to 1 is known as

the *quenched approximation*. This is equivalent to considering the effect of infinitely heavy fermions where the fields decouple from the gauge field dynamics in the generation of the gauge configurations. This is opposed to including the determinant in the generation of samples. In this case the fermions are said to *dynamical*. The Wilson fermion discretization is γ_5-hermitian, i.e.

$$\gamma_5 D \gamma_5 = D^\dagger \tag{106}$$

and thus the fermion determinant is always real. This further implies that for an even number of degenerate fermions, the product of the determinants is always positive definite and can safely be used as a probability distribution

$$\det[D] \det[D] = \det[D] \det\left[D^\dagger\right] = \det\left[DD^\dagger\right] \geq 0. \tag{107}$$

For odd numbers of degenerate fermions, this is not guaranteed. However, specifically for moderately heavy fermions, the determinant might remain positive due to the comparatively large diagonal term in the Dirac operator proportional to the fermion mass. One approach to including the fermion determinant is to rewrite it as an exponential of fictitious bosonic fields ϕ, known as *pseudofermions*. Using the bosonic version of (103) the fermion determinant can be written as

$$\det\left[DD^\dagger\right] = \pi^{-N} \int_{\mathbb{R}^{2N}} \mathcal{D}\left[\phi, \phi^\dagger\right] \exp\left(-\phi^\dagger \left(DD^\dagger\right)^{-1} \phi\right), \tag{108}$$

where N the number of real components of the complex field ϕ.

2.3.3 Markov Chain Monte-Carlo and (R)HMC algorithms

The algorithms used in this thesis start with an initial gauge configuration and randomly generate a new configuration based on the previous one. This step is then repeated and the succession of new, random configurations set up the so-called *Markov chain*. The configurations should be distributed according to the weight factor $\exp(-S[U])$. This can be achieved by requiring a suitable transition probability $T(U'|U)$ from one configuration U to the new one U' (which can be generalized in case more fields, such as the pseudofermions, are present). For a sufficiently long Markov chain the configurations will obey an equilibrium

distribution. In equilibrium the *balance equation*

$$\sum_U T(U'|U)P(U) = \sum_U T(U|U')P(U'), \tag{109}$$

holds. The *Metropolis* algorithm [117] provides such an update scheme. By first selecting a new candidate configuration according to a selection probability of $T_s(U'|U)$, but only accept the new configuration with an acceptance probability of

$$T_a(U'|U) = \min\left(1, \frac{T_s(U|U')\exp(-S[U'])}{T_s(U'|U)\exp(-S[U])}\right). \tag{110}$$

It can be shown that the combined probability $T = T_s T_a$ fulfils the balance equation elementwise and produces the correct equilibrium distribution. In case of symmetric T_s, the acceptance probability is proportional to $\exp(-\Delta S[U', U])$, i.e. this algorithm suppresses large changes to the action. For the generation of configurations with dynamical fermions the cost of evaluating the action is high, since it involves the inversion of Dirac operators (108). An effective algorithm should make a larger number of updates to the links in the configuration when selecting a candidate configuration to reduce the correlation between configurations, while keeping the change in the action small so that the acceptance rate of T_a remains sufficiently high. This can be achieved by using the *molecular dynamics* algorithm, which introduces conjugate variables to the gauge links $U_\mu(n)$ on each lattice site $\pi(n, \mu)$ as

$$\pi(n, \mu) = i\pi^a(x, \mu)\tau^a, \tag{111}$$

where τ^a are the generators of the colour group. Including the conjugate momenta in the expectation values, does not change anything, because the fictitious π cancel. This corresponds to a non-relativistic Hamiltonian (hence the name *molecular dynamics*) which can be evolved in Monte-Carlo time through its classical equations of motion.

$$H[\pi, U, \phi] = \frac{1}{2}\sum_{x,\mu} \pi(x, \mu)\pi(x, \mu) + S_G[U] + S_F[U, \phi, \phi^\dagger], \tag{112}$$

with $S_G[U]$ the gauge action and $S_F[U, \phi, \phi^\dagger]$ the pseudo-fermion action. The equations of motion in computer time t_{MC} are

$$\frac{d}{dt_{\mathrm{MC}}} U_\mu(n) = \pi(x, \mu) U_\mu(n), \tag{113}$$

$$\frac{d}{dt_{\mathrm{MC}}} \pi(x, \mu) = \delta S_G[U] + \delta S_F[U, \phi, \phi^\dagger], \tag{114}$$

where $\delta S_{G/F}$ denotes the change in the action upon an infinitesimal change in the link variables. An update in the gauge configurations can then be made by numerically evolving the equations of motion in Monte-Carlo time t_{MC}. First a pseudo-fermion field configuration is generated by solving $\phi = D\chi$, where χ are drawn from a multidimensional Gaussian distribution $\exp(-\chi^T \chi)$. Then the conjugated momenta are generated according to a Gaussian $\exp(-\operatorname{Tr}[\pi^2])$. After evolving the fields for some time Δt_{MC} the gauge field configuration is the new candidate configurations and an accept-reject step (110) is performed. The acceptance rate is given by the change in the Hamiltonian

$$T_a = \min\left(1, \exp\left(-\Delta H\right)\right) = \min\left(1, \exp\left(-\left[H[\pi', U', \phi'] - H[\pi, U, \phi]\right]\right)\right). \tag{115}$$

If the evolution of the equations of motion is perfect, then the change in H will always be vanishing. The accept-reject step thus accounts for numerical inaccuracies. The combination of a molecular dynamics algorithm with Gaussian distributed conjugate momenta and a Metropolis accept step is known as the *hybrid Monte Carlo* (HMC) algorithm.

Assuming a positive definite fermion determinant $\det[D]$, the HMC algorithm can be generalized to an arbitrary number of fermion species N_f. In this case, the pseudo-fermion action is written as

$$S_F[U, \phi, \phi^\dagger] = \exp\left(-\phi^\dagger \left(D[U] D[U]^\dagger\right)^{-N_f/2} \phi\right), \tag{116}$$

which is combined with an approximation of $DD^\dagger$ based on rational functions

$$\left(\frac{1}{DD^\dagger}\right)^{N_f/2} \approx \alpha_0 + \sum_n \frac{\alpha_n}{DD^\dagger - s_n}, \tag{117}$$

where the expansion coefficients can be pre-calculated using e.g. the Remez algorithm. This leaves the form of the pseudo-fermion action unchanged (up to a shift by the coefficient s_n) and the HMC is thus generalized to an arbitrary number of dynamical fermions which is known as the rational HMC (RHMC) algorithm. The (R)HMC algorithms can be generalized

to non-fundamental fermion representations [118].

2.4 Statistical analysis and autocorrelation

By generating gauge configurations using the (R)HMC algorithms, the expectation value of operator can be estimated as

$$\langle O \rangle = \frac{1}{N} \sum_{n=1}^{N} O[U_n] + \mathcal{O}\left(\frac{1}{\sqrt{N}}\right). \tag{118}$$

For a finite number N of samples O_i, the lattice result are given in terms of an estimator $\bar{O}$ and an estimation of the variance σ_O^2 defined using the usual definitions as

$$\bar{O} = \frac{1}{N} \sum_{i=1}^{N} O_i \tag{119}$$

$$\sigma_O^2 = \frac{1}{N-1} \sum_{i=1}^{N} \left(O_i - \bar{O}\right)^2. \tag{120}$$

The statistical uncertainty is given not by σ_O^2 but by the standard deviation of the mean $\bar{O}$. Assuming that individual measurements O_i are uncorrelated, the standard deviation of the mean $\sigma_{\bar{O}}^2$ is given by

$$\sigma_{\bar{O}}^2 = \frac{\sigma_O^2}{N}, \tag{121}$$

showing that the statistical uncertainty drops off with the factor $1/\sqrt{N}$ as a function of the number of MC measurements as in (118). The best estimator is then quoted with the uncertainty as $\langle O \rangle = \bar{O} \pm \sigma_O/\sqrt{N}$ assuming that the individual measurements in a Markov chain are fully uncorrelated. In practice individual elements in a Markov chain are correlated with the previous elements in the chain, which is known as *autocorrelation*. This can be quantified by explicitly studying the correlation between successive MC samples.

In equilibrium, it only depends on the separation in MC time

$$C_O(t) = C(O_i, O_{i+t}) = \left(O_i - \langle O_i \rangle\right)\left(O_{i+t} - \langle O_{i+t} \rangle\right). \tag{122}$$

If there is no auto-correlation between measurements then this quantity is compatible with

zero. In case they are present it can be parameterized by its leading exponentially decaying contribution

$$\frac{C_O(t)}{C_O(0)} \sim \exp\left(\frac{-t}{\tau_{\text{exp}}}\right), \tag{123}$$

which is parameterized by the *exponential auto-correlation time* τ_{exp}. For an auto-correlation time much smaller than one, this indicates that no autocorrelation between successive measurements exists. If $\tau_{\text{exp}} > 1$, this is taken into account by replacing the number of measurements N in (119) by an estimate of the number of uncorrelated measurements N/τ_{exp}. However, the determination of τ_{exp} comes with inherent uncertainties. It is difficult to judge, a priori, whether the extracted auto-correlation time is reliable. Thus, it is useful to recompute the auto-correlation time based on N/τ_{exp} blocked measurements.

2.4.1 Jackknife and bootstrap resampling techniques

Quite often, the determination of observables goes beyond taking a statistical average as in (119). This may include combining different quantities in non-linear expressions, performing fits and/or extrapolation and interpolation. This is even more pronounced when some quantities cannot be determined based only on a measurement of one or few configurations, e.g. in the case of fits the statistical fluctuations may make the fits unstable.

In these cases error propagation is far from straightforward. Resampling techniques provide ways of estimating uncertainties even for involved analysis setups. The *jackknife* and the *bootstrap* methods are standard procedures for performing such an analysis by constructing many new datasets based on the existing N measurements. The resampled sets are of comparable size to the initial ones, which ensures that fitting can remain stable.

In the jackknife method, from the existing dataset $\{O_i\}$ consisting of N samples in total, N new sets of size $N-1$ are created by removing the ith element in each set. Consider an observable θ, where the best estimator based on the original dataset is $\tilde{\theta}$. The resampled datasets are then used to calculate the observable of interest, leading to N resampled values of the observable denoted as θ_j. The best estimator $\hat{\theta}$ and jackknife uncertainty σ_θ are then

given by

$$\hat{\theta} = \frac{1}{N}\sum_{j=1}^{N}\theta_j, \tag{124}$$

$$\sigma_\theta = \frac{N-1}{N}\sum_{j=1}^{N}\left(\theta_j - \tilde{\theta}\right). \tag{125}$$

The bootstrap method similarly builds new datasets, but allows the construction of an arbitrary number of resampled datasets K. They are generated by randomly drawing N samples without replacement from the original datasets. In this case the estimators of the observable θ are given by

$$\hat{\theta} = \frac{1}{K}\sum_{j=1}^{K}\theta_j, \tag{126}$$

$$\sigma_\theta = \frac{1}{K}\sum_{j=1}^{K}\left(\theta_k - \tilde{\theta}\right). \tag{127}$$

A number of variations of these two methods exists [119]. The jackknife method can be generalized to variations where more than one sample is removed from the original dataset. Similarly, the bootstrap can be extended to an arbitrary number of the resample size, instead of generating samples of the same size as the original set.

2.5 Hadron Spectroscopy and Scattering

Within this thesis, spectroscopic properties are the most interesting observables. The ground state properties of mesons are of particular interest. This information can be extracted from the meson correlators at large Euclidean time separations.

2.5.1 Meson spectroscopy

A meson correlator can be constructed from interpolators which correspond to operators that create and annihilate the states of the desired quantum numbers. For the purposes of this thesis, the creation operators are denoted as $O^\dagger$ and the annihilating operators as O. For

	J^P	Γ
pseudoscalar	0^-	$\gamma_5, \gamma_0\gamma_5$
scalar	0^+	$\mathbb{1}$
vector	1^-	γ_i
axial vector	1^+	$\gamma_5\gamma_i$

Table 1: Spin and parity quantum number, corresponding to the different choices of Γ used in this thesis. Vector and axial vector mesons are sourced by the spatial γ-matrices γ_i, where $i = 1, 2, 3$.

mesons in two-flavour theories these operators are typically of the form

$$O_{\text{meson}} = \bar{\psi}_1(n)\Gamma\psi_2(n), \tag{128}$$

where Γ is a combination of γ-matrices, chosen such that the desired J^P quantum numbers of the meson are obtained. The spinor fields are denoted as ψ_1 and ψ_2. For notational simplicity and in analogy with QCD, they will be referred to as dark up quark $\psi_1 = u$ and dark down quark $\psi_2 = d$. The choices of Γ used throughout this thesis are given in Tab. 1. Note, that operators of the form (128) have open flavour indices. Additional non-flavoured states exist both in mesonic multiplets and in the form of singlets. In the two-flavour theory they are given by

$$O_{\text{meson}} = \frac{1}{\sqrt{2}}\left(\bar{\psi}_1(n)\Gamma\psi_1(n) \pm \bar{\psi}_2(n)\Gamma\psi_2(n)\right). \tag{129}$$

The corresponding interpolator that creates the flavoured meson is given by

$$\bar{O}_{\text{meson}} \equiv O^\dagger_{\text{meson}} = \left(\bar{\psi}_1(n)\Gamma\psi_2(n)\right)^\dagger = \pm\bar{\psi}_2\Gamma\psi_1, \tag{130}$$

where the overall sign is $(\pm)$ if $-\gamma_0\Gamma^\dagger\gamma_0 = \pm\Gamma$. This straightforwardly applies as well for the unflavoured meson interpolators. The ground state information dominates at large Euclidean times. This can be seen by formally expanding the time separated operators $O(t)$ and $\bar{O}(t')$ in the eigenstates of the theory.

$$\langle O(t)\bar{O}(t')\rangle = \sum_n \frac{1}{2E_n}\langle 0|O|n\rangle\langle n|O^\dagger|0\rangle e^{-|t-t'|E_n} \tag{131}$$

At large separations all states except for the states corresponding to the lowest energy E_0, i.e. the ground state, are strongly suppressed and negligible. The suppression of the next

highest state is governed by the energy difference to the first excited state, $\Delta E = E_1 - E_0$. On the lattice this quantity can be obtained by Fourier transformation and projecting to definite momentum of the state.

$$C(t-t',\vec{p}) = \frac{1}{L^3}\sum_{\vec{n},\vec{m}} e^{-i(\vec{n}-\vec{m})\cdot\vec{p}}\langle\bar{O}(t,\vec{n})O(t',\vec{m})\rangle, \tag{132}$$

where the possible momenta on a fixed lattice are discretized to multiples of $(2\pi)/L$ in every component. At large times the correlator $C(t-t',\vec{p})$ have the desired behaviour

$$C(t-t',\vec{p}) = Ae^{-|t-t'|E_0(\vec{p})} + \mathcal{O}\left(e^{-|t-t'|\Delta E(\vec{p})}\right), \tag{133}$$

and the ground state energy is obtained at vanishing momentum $E_0(\vec{p}=0)$. The right-hand side of (132) can be calculated directly on the lattice and the result can be fitted to the function (133) to extract E_0. The continuum mass can then be achieved by performing the continuum limit as discussed in Sec. 2.

2.5.2 Meson Scattering

In the case of multi-particle states, the finite volume effects are no longer expected to drop of exponentially, but they are expected to be only suppressed in inverse powers of L. For scattering of mesons this can be used to extract information of the infinite volume scattering properties as shown by Lüscher [120–122]. This allows investigations into the scattering properties of two dark pions which encode the information of the scattering cross-section $\langle\sigma_{\mathrm{2DM}\to\mathrm{2DM}}\rangle$. Lüscher derived relations between scattering phase shift $\delta(k)$ in the infinite volume limit, the finite lattice size L and momentum k. Thus, by calculating the one-particle and two-particle energies (and the associated momenta) on a finite lattice of spatial extent L, the infinite volume phase shift is determined.

The most accessible quantity is the s-wave scattering of two identical particles without any relative momenta. For the scattering of the PNGB the cleanest state on the lattice is given by the two-PNGB in the highest-dimensional representation of the global flavour symmetry, i.e. at maximal isospin in QCD [123,124]. For pseudo-real representations of a two-flavour theory the representations under the global Sp(4) have a one-to-one correspondence to the case of isospin $I = 0, 1, 2$ in two-flavour QCD [106]. The dark pions of $N_f = 2$ are in a five-dimensional representation and the product representation decomposes into $5 \otimes 5 = 1 \oplus 10 \oplus 14$ [2]. The singlet representation corresponds to the $I = 0$ case of QCD,

[2]See [105] for the decomposition of a three-pion state which can be classified in the multiplets $5 \otimes 5 \otimes 5 =$

the ten-dimensional representation corresponds to $I = 1$, and the fourteen-dimensional one corresponds to maximal isospin i.e. $I = 2$. In the limit of $\lim_{k\to 0} \delta(k)/k$ only the momentum independent term of scattering phase shift survives which is the scattering length a_0. For s-wave scattering of (dark) pions in the isospin channel I at vanishing relative momentum on a lattice of spatial extent L the relation

$$\frac{\delta E^I_{\pi\pi}}{m_\pi} \equiv \frac{E^I_{\pi\pi} - 2m_\pi}{m_\pi} = \frac{4\pi m_\pi a^I_0}{(m_\pi L)^3}\left(1 + c_1\frac{a^I_0}{L} + c_2\left(\frac{a^I_0}{L}\right)^2 + \mathcal{O}(L^{-6})\right) \tag{134}$$

holds. Here $E^I_{\pi\pi}$ is the energy of the two-PNGB state in the isospin channel I and a^I_0 the corresponding scattering length. The coefficients c_1 and c_2 can be calculated analytically [121]. Assuming that the PNGB mass is already known, only the energy of the two-PNGB state needs to be determined on the lattice to calculate the scattering length. For the isospin $I = 2$ channel a corresponding interpolator is

$$O_{\pi\pi}(n) = O_\pi(n)O_\pi(n), \tag{135}$$

where the PNGBs π need to correspond to identical off-diagonal PNGB fields, i.e. in the case of QCD the operator $O_{\pi^+\pi^+} = \bar{u}\gamma_5 d\bar{u}\gamma_5 d$ is interpolating the $I = 2$ channel. The energy can be extracted in the same way as for the mesonic one-particle operators discussed in Sec. 2.5.1

2.5.3 Fermionic integrals

The operators corresponding to mesonic one- and two-particle states of interest are given by Eqs. (128),(129) and (135). The fermionic Grassmann integrals according to (104) needs to be performed. The simplest case is given by the flavoured meson (128). There the fermionic integrals factorize for the different fermion species and

$$\langle O(n)\bar{O}(m)\rangle_F = -\langle\bar{u}(n)\Gamma d(n)\bar{d}(m)\Gamma u(m)\rangle_F = \pm\,\mathrm{Tr}\left[\Gamma D_u^{-1}(n|m)\Gamma D_d^{-1}(m|n)\right], \tag{136}$$

where the potential overall sign due to (130) has been assumed to be positive. The different fermions are labelled as u and d respectively. This trace can be expressed diagrammatically

$5 \oplus 5 \oplus 5 \oplus 10 \oplus 30 \oplus 35 \oplus 35$. Note that only the ten-dimensional representation - which happens to be the representation of the vector meson multiplet - appears in both decompositions.

following the notation introduced in Eq. (105) as

$$\langle O(n)\bar{O}(m)\rangle = -$$ 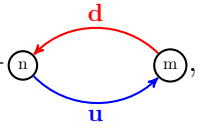

$$, \tag{137}$$

and it can be interpreted as a fermion u propagating from lattice site n to m and the other fermion d propagating from n to m. For the unflavoured mesons (129) the fermionic integral does not always factorize. Additional terms appear with fermions propagating from lattice site n back to the same lattice site known as *disconnected contributions* or *disconnected pieces*. In contrast, the other diagrams are known as *connected contributions*. Diagrammatically one obtains

$$2\langle O_{\pm}(n)\bar{O}_{\pm}(m)\rangle = -$$ 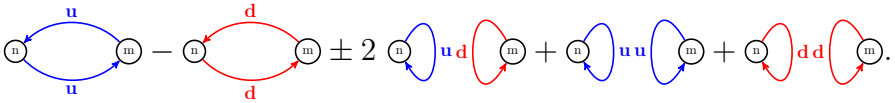

$$. \tag{138}$$

On the left-hand side the choice of sign in the interpolator (129) has been made explicit. The additional terms give rise to pure gluonic propagation of the meson. Thus, they can only correspond to operators that do not have a conserved quantum number arising due to flavour symmetry. These contributions can only be non-vanishing for singlets. In the case of the flavour-diagonal non-singlet states this becomes explicit when setting the fermion masses equal. Then $D_u^{-1} = D_d^{-1}$, the diagrams simplify to

$$\langle O_{-}(n)\bar{O}_{-}(m)\rangle = \langle O(n)\bar{O}(m)\rangle = -$$ 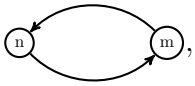

$$, \tag{139}$$

$$\langle O_{+}(n)\bar{O}_{+}(m)\rangle = -$$ 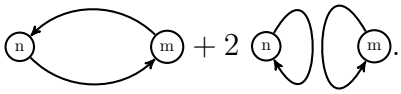

$$. \tag{140}$$

This makes it apparent that the operator O_- sources the flavour-diagonal non-singlet meson states. In the case of the two-PNGB operators the number of fermion fields increases even further. Due to the maximal isospin in the $I = 2$ only two distinct diagrams appear after setting $D_u^{-1} = D_d^{-1}$ which are both connected

$$\langle O_{\pi^+\pi^+}(n)\bar{O}_{\pi^+\pi^+}(m)\rangle =$$ 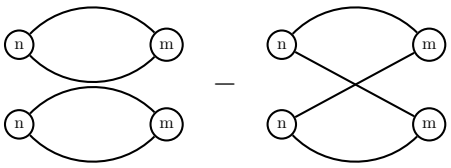

$$. \tag{141}$$

For other channels than the $I = 2$ case more diagrams contribute [107]. In order to evaluate the correlators on a given gauge configuration the inverse fermion propagator $D^{-1}(n|m)$ is needed. Since the Dirac operator $D[U]$ depends on the gauge configuration (89) this needs to be done for each configuration separately.

2.5.4 Calculating the fermion propagator

A straightforward inversion of the Dirac operator $D^{a,b}_{\alpha,\beta}(x|y)$ is unfeasible. On a given lattice of size $\Lambda = N_L^3 N_t$ with fermions in the fundamental representation it is a $(4N_c\Lambda) \times (4N_c\Lambda)$ matrix, where for even moderate lattices sizes studied in this thesis it has roughly $\mathcal{O}(10^7) - \mathcal{O}(10^8)$ rows and columns.

For connected diagrams involving two fermions the Dirac operator does not have to be fully inverted. When performing the lattice Fourier transform of (137), a sum over all lattice sites n and m occurs. Fixing one of the lattice sites when performing the average reduces the required computations substantially. In this context it is useful to make all indices in (136) explicit. After performing the Fourier transform to definite momentum $\vec{p}$ in (132) and dropping the normalization the correlator is obtained as

$$C(t - t') = \sum_{\vec{m},\vec{n}} e^{-i(\vec{n}-\vec{m})\cdot\vec{p}} \operatorname{Tr}\left[\Gamma D_u^{-1}(n|m)\Gamma D_d^{-1}(m|n)\right] \tag{142}$$

$$= \sum_{\vec{m},\vec{n},\alpha_i,a,b} e^{-i(\vec{n}-\vec{m})\cdot\vec{p}}\, \Gamma_{\alpha_1,\alpha_2} D_u^{-1}(n|m)^{ab}_{\alpha_2,\alpha_3} \Gamma_{\alpha_3,\alpha_4} D_d^{-1}(m|n)^{ba}_{\alpha_4,\alpha_1}. \tag{143}$$

Fixing one lattice site as $m = m_0 = (\vec{m}_0, t'_0)$ and dropping the sum over m is equivalent to inserting a Kronecker delta δ_{m,m_0}. Setting $m_0 = 0$ for concreteness leads to

$$C(t) = \sum_{\vec{n},\alpha_i,a,b} e^{-i\vec{n}\cdot\vec{p}}\, \Gamma_{\alpha_1\alpha_2} D_u^{-1}(n|0)^{ab}_{\alpha_2\alpha_3} \Gamma_{\alpha_3\alpha_4} D_d^{-1}(0|n)^{ba}_{\alpha_4\alpha_1}. \tag{144}$$

The inverse Dirac operator $D^{-1}(n|m_0)^{a_0 b}_{\alpha_0,\beta}$ with fixed lattice site m_0 and fixed colour a_0 and spinor α_0 index now corresponds to a single row of the full propagator D^{-1} and is known as a *one-to-all propagator*. For calculating $C(t)$ according (144) only $N_c \times 4$ rows of the full propagator are required [3]. This can be achieved by introducing *sources*. A source η can be understood as an object that projects out components of the fermion propagator. It allows us to relate the full propagator $D^{-1}(n|m)^{ab}_{\alpha\beta}$ to the propagator where (m_0, a_0, α_0) are fixed

[3] This is because the fundamental representation of the fermions which is N_c-dimensional. For a general representation N_c needs to be replaced by the dimension of the fermion representation.

$D^{-1}(n|m_0)^{a_0 b}_{\alpha_0\beta}$ as

$$\phi^{m_0 a_0 \alpha_0}(n,b,\beta) \equiv D^{-1}(n|m_0)^{a_0 b}_{\alpha_0\beta} = \sum_{m,a,\alpha} D^{-1}(n|m)^{ab}_{\alpha\beta}\eta^{m_0 a_0 \alpha_0}(m,a,\alpha), \tag{145}$$

$$\eta^{m_0 a_0 \alpha_0}(m,a,\alpha) = \delta_{m,m_0}\delta_{a,a_0}\delta_{\alpha,\alpha_0}. \tag{146}$$

Because this approach fixes a specific index the associated sources are known as *point sources*. This equation can now be solved for the vector ϕ iteratively. With ϕ for all required colour and spin indices, the meson propagator in (144) can be calculated. Rewriting the above equation in matrix notation $\phi = D^{-1}\eta$ leads to

$$D\phi = \eta, \tag{147}$$

where the right-hand side is a known source and the problem of finding ϕ is equivalent to solving the system of equations (147). The Dirac operator D is sparse in contrast to its inverse. This means that acting with it on a generic test vector ϕ_0 is comparatively cheap in computational cost. In practice, algorithms from the family of *Krylov* solvers are usually used to obtain ϕ (see e.g. [113] for a textbook treatment). At first glance, it appears as if (147) requires inversions for both $D^{-1}(n|0)$ and $D^{-1}(0|n)$. This can be avoided by making use of γ_5-hermiticity (106). This can be used for rewriting the propagator in terms of its hermitian conjugate which leads to

$$\left(\gamma_5 D^{-1}(0|n)\gamma_5\right)^{ab}_{\alpha\beta} = \left(D^{-1}(n|0)^{ba}_{\beta\alpha}\right)^*. \tag{148}$$

Thus, the entire meson correlator can be obtained by only calculating $N_c \times 4$ rows of the full fermion propagator. This is no longer possible when the relevant diagrams contain a propagator that connects a lattice site to itself such as the disconnected pieces appearing in the singlet mesons (140). In this case the disconnected contributions are given by

$$C^{\text{disc.}}(t-t') = \sum_{\vec{m},\vec{n}} e^{-i\vec{n}\cdot\vec{p}} e^{i\vec{m}\cdot\vec{p}} \operatorname{Tr}\left[\Gamma D^{-1}(n|n)\right] \operatorname{Tr}\left[\Gamma D^{-1}(m|m)\right] \tag{149}$$

$$= \sum_{\vec{n}} e^{-i\vec{n}\cdot\vec{p}} \operatorname{Tr}\left[\Gamma D^{-1}(n|n)\right] \sum_{\vec{m}} e^{i\vec{m}\cdot\vec{p}} \operatorname{Tr}\left[\Gamma D^{-1}(m|m)\right]. \tag{150}$$

In this situation, it is no longer possible to keep one lattice site fixed while still obtaining a signal for the disconnected diagram. This requires an estimate of the fermion *all-to-all propagator*. The notion of a source introduced earlier can be generalized to circumvent these

issues. In theory, the full propagator could be calculated by inverting D with a different point source for each row of the full propagator and then summing over all sources. By finding an approximation to summing over all point sources

$$\sum_{m_0,a_0,\alpha_0} \eta_{\text{point}}^{m_0 a_0 \alpha_0}(m,a,\alpha), \tag{151}$$

the all-to-all propagator can be estimated with reduced computational cost. Specifically, a set of N vectors containing random noise $\{\eta_i\}$ as sources for the inversion of the propagator can be used, given that they approximate the full propagator in the limit of infinitely many samples $N \to \infty$ [125]. This can be achieved by requiring

$$\lim_{N\to\infty} \sum_{i=1}^{N} (\eta_i)^{na\alpha} (\eta_i^*)^{mb\beta} = \delta_{m,n}\delta_{a,b}\delta_{\alpha,\beta}, \tag{152}$$

which includes an appropriate normalization of the source so that the product of the Kronecker deltas is recovered. For a suitable choice of noisy source vectors a finite number of N is sufficient to calculate the fermion propagator at the desired accuracy. Using complex $Z_2 \times Z_2$ noise (i.e. a random element of the set $Z_2 \times Z_2 = \left\{\frac{1+i}{\sqrt{2}}, \frac{-1+i}{\sqrt{2}}, \frac{1-i}{\sqrt{2}}, \frac{-1-i}{\sqrt{2}}\right\}$ is chosen for every element of the source η_i) has proven to be an adequate choice [125]. Using this approach the disconnected contributions are given by

$$\text{Tr}\left[\Gamma D^{-1}(n|n)\right] = \Gamma_{\alpha\beta} D^{-1}(n|n)^{\beta\alpha}_{a,a} = \lim_{N\to\infty} \sum_{i}^{N} \Gamma_{\alpha\beta}\phi^i(n,\beta,a)\,(\eta_i^*)^{n,\alpha,a}\,, \tag{153}$$

where ϕ^i denotes the solution vector after inverting the Dirac operator with the source η_i. Note, that the source appears explicitly in the estimate of the disconnected pieces. That this expression leads to the correct all-to-all propagator can be seen by inserting (145) into (153).

$$\lim_{N\to\infty} \sum_{i}^{N} \Gamma_{\alpha\beta}\phi^i(n,\beta,a)\,(\eta_i^*)^{n,\alpha,a} = \lim_{N\to\infty} \sum_{i}^{N} \Gamma_{\alpha\beta} \sum_{n',\beta',a'} D^{-1}(n'|n)^{\beta'\beta}_{a,a'}\,(\eta_i)^{n',\beta',a'}\,(\eta_i^*)^{n,\alpha,a} \tag{154}$$

$$= \Gamma_{\alpha\beta} \sum_{n',\beta',a'} D^{-1}(n'|n)^{\beta'\beta}_{a,a'} \lim_{N\to\infty} \sum_{i}^{N} (\eta_i)^{n',\beta',a'}\,(\eta_i^*)^{n,\alpha,a} \tag{155}$$

$$= \Gamma_{\alpha\beta} \sum_{n',\beta',a'} D^{-1}(n'|n)^{\beta'\beta}_{a,a'} \delta_{n,n'}\delta_{a,a'}\delta_{\beta',\alpha} = \text{Tr}\left[\Gamma D^{-1}(n|n)\right] \tag{156}$$

In general, the method of noisy sources can also be applied to one-to-all propagators. It was found that fewer inversions of the Dirac operator are needed to reach the same level of accuracy as with point sources [126]. In this case the sources can again be restricted to probing a subset of the entire fermion propagator by restricting them to be only non-vanishing on a specific timeslice t. These sources are known as *wall sources*. It was found that *diluting* the existing stochastic noise vectors provides additional computational advantage [127, 128]. In the dilution approach a given stochastic source η_i is split up into multiple sources

$$\eta_i = \sum_d^{N_d} \eta_i^{(d)}, \tag{157}$$

where every $\eta_i^{(d)}$ is non-vanishing for distinct entries. This was nicely illustrated in [129] as

$$\overset{\eta_i}{\begin{pmatrix} Z_1 \\ Z_2 \\ Z_3 \\ \vdots \\ Z_{N_\mathrm{d}} \end{pmatrix}} \longrightarrow \overset{\eta_i^{(1)}}{\begin{pmatrix} Z_1 \\ 0 \\ 0 \\ \vdots \\ 0 \end{pmatrix}} \overset{\eta_i^{(2)}}{\begin{pmatrix} 0 \\ Z_2 \\ 0 \\ \vdots \\ 0 \end{pmatrix}} \overset{\eta_i^{(3)}}{\begin{pmatrix} 0 \\ 0 \\ Z_3 \\ \vdots \\ 0 \end{pmatrix}} \cdots \overset{\eta_i^{(N_d)}}{\begin{pmatrix} 0 \\ 0 \\ 0 \\ \vdots \\ Z_{N_\mathrm{d}} \end{pmatrix}},$$

where Z_i label all non-vanishing entries to the noisy sources. Many possible choices of partitioning the diluted sources exist. Partitioning non-vanishing terms in the spin index (spin dilution), colour index (colour dilution), on even or odd lattice sites (even-odd dilution), or on fixed timeslices (time dilution) have all been used in the literature. Time dilution in particular, is widely used in the study of singlet mesons [129].

2.5.5 Correlator fitting

Once the correlator $C(t)$ has been calculated on the lattice, the ground state information according to (133) can be extracted from large Euclidean times t. The coefficient of the exponential A in (133) is related to the matrix element of the probed state and the vacuum state (131). For a meson state M interpolated by the operator O_M the asymptotic behaviour

is given by

$$C(t) = \frac{1}{2m_M}\langle 0|O_M|M\rangle\langle M|O_M^\dagger|0\rangle e^{-tm_M} + \mathcal{O}\left(e^{-t\Delta E}\right), \tag{158}$$

$$= \frac{1}{2m_M}|\langle 0|O_M|M\rangle|^2 e^{-tm_M} + \mathcal{O}\left(e^{-t\Delta E}\right). \tag{159}$$

In the limit of infinite Euclidean time t the correlator is given by a single exponential. The prefactor and the exponential decay can then be extracted using non-linear fitting, such as the Levenberg–Marquardt algorithm [130]. On a finite lattice the fit has to performed at sufficiently large times. Due to lattice periodicity an additional exponential term in (133) appears that corresponds to a backward propagating hadron. Depending on the relative sign between the exponential terms a cosh- or sinh-like behaviour emerges

$$Ae^{-mt} \pm Ae^{-m(T-t)} = \tilde{A}\begin{cases}\cosh\left[m\left(\frac{T}{2}-t\right)\right] \\ \sinh\left[m\left(\frac{T}{2}-t\right)\right]\end{cases}. \tag{160}$$

The cosh-term which is symmetric around $T/2$ corresponds to a positive sign in (160) and the antisymmetric sinh-term corresponds to a negative sign. Thus, the largest Euclidean time separation obtainable on a finite lattice is $T/2$. All larger separations are equivalent to smaller separations due to (anti-)periodic boundaries. The interval $[t_{\max}, t_{\min}]$ in which the correlator is dominated by the leading exponential terms can be found by considering the logarithm of the ratio of the correlator at neighbouring times

$$m_{\text{eff}}^{(1)}\left(t+\frac{1}{2}\right) = \log\left(\frac{C(t)}{C(t+1)}\right). \tag{161}$$

If the correlator is only given by a single exponential term, this reduces to

$$\log\left(\frac{C^{1\exp}(t)}{C^{1\exp}(t+1)}\right) = \log\left(\frac{e^{-mt}}{e^{-m(t+1)}}\right) = m. \tag{162}$$

In that case the effective mass is constant and equal to the mass of the hadron. This allows an identification of the interval $[t_{\max}, t_{\min}]$ by looking for a *plateau* in the effective mass. This definition does not take into account the (anti-)periodicity of the correlator on a finite lattice. A straightforward way of taking the periodicity into account is to use the inverse of

the hyperbolic functions as

$$m_{\text{eff}}^{(2)}\left(t+\frac{1}{2}\right)=\begin{cases}\operatorname{acosh}\left(\frac{C(t)}{C(T/2)}\right)\frac{1}{T/2-t}\\ \operatorname{asinh}\left(\frac{C(t)}{C(T/2)}\right)\frac{1}{T/2-t}\end{cases}. \tag{163}$$

This requires the correlator at the mid-point of the lattice for the effective mass at every $t+1/2$. This is unfortunate, as the relative errors at the largest at the midpoint [4]. An alternative, is to define the effective mass for a time $(t+1/2)$ implicitly as

$$\frac{C(t)}{C(t+1)}=\frac{e^{-tm_{\text{eff}}^{(3)}}\pm e^{-(T-t)m_{\text{eff}}^{(3)}}}{e^{-(t+1)m_{\text{eff}}^{(3)}}\pm e^{-(T-(t+1))m_{\text{eff}}^{(3)}}}, \tag{164}$$

and to numerically solve for m_{eff} at every timeslice t. For the purposes of this thesis, a simple secant method was sufficient. It needs to be stressed, that the effective mass should only be used for determining the fitting interval $[t_{\max}, t_{\min}]$. Once the interval is determined it is advantageous to directly fit the correlator instead of the effective mass. The fit interval of correlation functions corresponding to other states such as the dark two-PNGB states relevant for the study of scattering processes.

2.5.6 Decay constants

The decay constants can be extracted from the coefficients of the exponentially decaying terms in (158). The decay constant is defined as in [91] by the matrix elements involving the pseudoscalar $|\pi\rangle$ and vector meson $|\rho\rangle$ ground states

$$\langle 0|O_{\gamma_5\gamma_\mu}|\pi\rangle = f_\pi p_\mu \tag{165}$$

$$\langle 0|O_{\gamma_\mu}|\rho\rangle = f_\rho m_\rho \epsilon_\mu. \tag{166}$$

In this convention the decay constant of the π in QCD is approximately 93 MeV. This definition ensures that this quantity corresponds to the LEC of chiral perturbation theory defined in (52). Here ϵ_μ is the polarization vector for which $\epsilon_\mu p^\mu = 0$ and $\epsilon_\mu^* \epsilon^\mu = 1$ hold. In the rest frame the pseudoscalar matrix element is then

$$\langle 0|O_{\gamma_5\gamma_0}|\pi\rangle = f_\pi m_\pi. \tag{167}$$

[4] This is because at the mid-point the magnitude of the correlator is the smallest. For a roughly constant absolute error, the relative error is at its maximum there.

Note, that this definition corresponds to a choice of $\Gamma = \gamma_5\gamma_0$ in the interpolating operators (128) and (129). This choice also interpolates the pseudoscalar mesons - see Tab. 1. By replacing the dark pion interpolator with the singlet interpolator, the same relation for the singlet η' meson is obtained. Inserting this expression into the corresponding correlators at large times gives

$$C_{\pi,\gamma_5\gamma_0}(t) = \frac{m_\pi}{2} f_\pi^2 \exp\left(-m_\pi t\right) \tag{168}$$

$$C_\rho(t) = \frac{m_\rho}{2} f_\rho^2 \exp\left(-m_\rho t\right) \tag{169}$$

Alternatively, the decay constants can be extracted from correlators where the creating and annihilating operators have different structures in terms of γ matrices. Defining a generalized correlator as

$$C_{\Gamma_1,\Gamma_2}(t-t',\vec{p}) = \frac{1}{L^3}\sum_{\vec{n},\vec{m}} e^{-i(\vec{n}-\vec{m})\cdot\vec{p}} \langle \bar{O}_{\Gamma_1}(t,\vec{n}) O_{\Gamma_1}(t',\vec{m})\rangle, \tag{170}$$

where the choice of Γ in the individual operators has been made explicit. The mixed correlator with $\Gamma_1 = \gamma_5\gamma_0$ and $\Gamma_2 = \gamma_5$ can also be used for the pseudoscalars [91] by performing a simultaneous fit to this correlator and the standard dark pion correlator with $\Gamma_1 = \Gamma_2 = \gamma_5$.

Matrix elements calculated on the lattice need to be treated as unrenormalized, bare quantities. The lattice merely acts as a regulator [131]. The relevant renormalization constants that need to be introduced are

$$f_\pi^{\text{ren}} = Z_A f_\pi, \tag{171}$$

$$f_\rho^{\text{ren}} = Z_V f_\rho. \tag{172}$$

The non-perturbative determination of renormalization constants is highly involved. In light of the exploratory nature of this investigation the prescription from [91] for determining the renormalization constants is sufficient. They are obtained from leading order lattice perturbation theory. In this approach the renormalization constants are given [132] by

$$Z_A = 1 + C_F\left(\Delta_{\Sigma_1} + \Delta_{\gamma_5\gamma_\mu}\right)\frac{g^2}{16\pi^2\langle P\rangle}, \tag{173}$$

$$Z_V = 1 + C_F\left(\Delta_{\Sigma_1} + \Delta_{\gamma_\mu}\right)\frac{g^2}{16\pi^2\langle P\rangle}, \tag{174}$$

where C_F is the quadratic Casimir in the fundamental representation. For Sp(4) it is $C_F =$

5/4. The effective coupling is $\tilde{g}^2 = g^2/\langle P \rangle$, where $\langle P \rangle$ is the average value of the plaquette. By matching to the $\overline{\text{MS}}$ scheme in the continuum the coefficients are determined to be [132]

$$\Delta_{\Sigma_1} = -12.82, \tag{175}$$

$$\Delta_{\gamma_5\gamma_\mu} = -3.0, \tag{176}$$

$$\Delta_{\gamma_\mu} = -7.75. \tag{177}$$

It can be shown, that at this loop in the perturbative expansion the renormalization factors are the same for the singlet and the non-singlet mesons. The difference between the singlet and non-singlet factors only appears at order $\mathcal{O}(g^4)$ [133].

2.5.7 Fermion masses

For any lattice simulation the bare fermion masses are input parameters. These input masses are unrenormalized and thus regulator-dependent and unphysical. An obvious question is, therefore, if there is a way of calculating a "physical" quark mass. This is however *not* possible. Due to confinement there is no notion of a physical quark mass since no physical quark has ever been observed in experiment. Any definition of a quark mass is scheme-dependent and necessarily not unique. In the context of Standard Model QCD several ways of a defining a quark mass are being used. See for example the current PDG review [134] for a detailed discussion of quark masses in the SM.

The scheme-dependence of any quark mass implies that quark masses are comparable only in the same scheme at the same energy scale μ. This requires a determination of the renormalization constants associated with the bare quark masses m_u and m_d in order to obtain the renormalized quark masses $m_u^{(r)}$ and $m_d^{(r)}$. The discretization of the fermion fields on the lattice makes this even more challenging: The Wilson action of fermions breaks chiral symmetry explicitly on the lattice and results in both a multiplicative *and* additive renormalization of the bare quark mass as long as the lattice spacing is non-vanishing, i.e. $a > 0$ [113]. It is not uncommon for bare Wilson fermion masses to be negative. This is another example highlighting the unphysical nature of bare parameters.

A quark mass can be defined based on the *partially conserved axial current* (PCAC) equation (see e.g. [28] for a textbook discussion) which relates the axial current to the pion field and the *axial Ward identity* (AWI) which connects the axial current J_A^μ to the renormalized

quark mass $m^{(r)}$. The AWI for the flavoured π PNGB reads

$$J_A^\mu = \bar{d}\gamma_0\gamma_5 u \tag{178}$$

$$\partial_\mu J_A^\mu = (m_u^{(r)} + m_d^{(r)})\bar{d}\gamma_5 u \tag{179}$$

The unrenormalized quark mass can be defined through correlation functions $C_\Gamma(t)$ of the unrenormalized axial currents $\bar{u}\gamma_0\gamma_5 d$ and $\bar{u}\gamma_5 d$

$$m^{\mathrm{PCAC}} = \lim_{t\to\infty} \frac{1}{2}\frac{\partial_t C_{\gamma_0\gamma_5,\gamma_5}(t)}{C_{\gamma_5}(t)} = \lim_{t\to\infty} \frac{1}{2}\frac{\partial_t \int d^3\vec{x}\langle(\bar{u}(\vec{x},t)\gamma_0\gamma_5 d(\vec{x},t))^\dagger\, \bar{u}(0)\gamma_5 d(0)\rangle}{\int d^3\vec{x}\langle(\bar{u}(\vec{x},t)\gamma_5 d(\vec{x},t))^\dagger\, \bar{u}(0)\gamma_5 d(0)\rangle}. \tag{180}$$

Here the notation introduced in (170) is used, for correlators with mixed Γ structures. A number of alternative ways exist to obtain the renormalized mass through appropriate combinations of correlators – see e.g. [135] for a detailed discussion. At large times t the ratio of the two correlation functions in Eq. (180) tends to the constant PCAC-mass. In the mass-non-degenerate case this expression gives the average mass of up-type quarks and down-type quarks $m^{\mathrm{PCAC}} = (m_u^{\mathrm{PCAC}} + m_d^{\mathrm{PCAC}})/2$. The PCAC-mass is related to the renormalized (average) mass by a multiplicative factor

$$m^{(r)} = \frac{Z_A}{Z_P} m^{\mathrm{PCAC}}, \tag{181}$$

and is therefore an unrenormalized quantity. In order to obtain the renormalized mass the factor Z_A/Z_P needs to be determined and a scheme to be chosen. This is however quite involved and in addition a matching to other commonly used renormalization scheme is needed in order for this mass to be used in perturbative calculations (see e.g. [136]). Therefore, this calculation is skipped in this thesis for degenerate fermions. In the non-degenerate case, however, the renormalization factors cancel for of PCAC-masses such as $m_u^{\mathrm{PCAC}}/m_d^{\mathrm{PCAC}}$ since only multiplicative renormalization occurs. The PCAC relation allows to quantify the non-degeneracy in ratios of fermion masses. While this ratio is still unphysical, it corresponds to commonly used definitions in the continuum.

Note that the PCAC relation is closely linked to chiral perturbation theory and the Gell-Mann-Oakes-Renner (GMOR) relation in particular (56). It appears as if chiral perturbation theory can be tested by calculating both the chiral condensate v^3 and the PCAC mass. However, the calculation of the PCAC mass uses the PCAC relation which connects to the GMOR relation which is usually used to define the chiral condensate. Thus, calculating the PCAC masses and the chiral condensate and comparing this to the GMOR relation

cannot be considered to be a truly independent and quantitative test of chiral perturbation theory. It can still be used as a qualitative test by examining the dependence of square of the Goldstone masses on the PCAC-masses and comparing the results to the expected linear behaviour $m_\pi^2 \propto m^{(r)} \propto m^{\mathrm{PCAC}}$. This was done (although with a differently defined unrenormalized quark mass) in [91].

Chapter 3

The Spectrum of Two-Flavour Sp(4) Gauge Theory

In this chapter results obtained from explicit lattice simulations of Sp(4) gauge theory with two fermions are presented.

First, the explicit structure of the meson states under the global symmetries is discussed in Sec. 3.1.1. For non-degenerate fermions their explicit structure under the global transformations of the remaining SU(2) × SU(2) is derived. The parity assignment of diquark states is discussed in Sec. 3.1.3 and the simulation details are described in Sec. 3.2.

In Sec. 3.3 the results on the non-singlet spectrum in $N_f = 1 + 1$ are presented, including the masses and decay constant of the non-singlet mesons, as well as the fermion mass defined through the PCAC relation. Lattice systematics are studied and a consistency check with the chiral effective theory for non-degenerate fermions of [2] is performed. In Sec. 3.4 the singlet spectrum for both degenerate and non-degenerate is presented. This includes the singlet states η' and σ, as well as the π^0 state for non-degenerate fermions. Finally, in Sec. 2.5.2 an exploratory determination of the isospin 2 scattering length on a single ensemble is performed.

3.1 Breaking Patterns, Global Symmetries and Parity

3.1.1 Meson multiplets for degenerate fermions

The flavour symmetry of the Sp(4) gauge theory is enlarged compared to a theory with a complex fermion representation such as QCD due to the pseudo-reality of the fundamental representation of Sp(4) – see Sec. 1.2.8. Specifically, for $N_f = 2$ the global symmetry of the massless Lagrangian neglecting the anomalous $U(1)_A$ is $SU(4)$. It is broken both by non-

vanishing degenerate fermion masses and the chiral condensate down to Sp(4). This entails that also the meson multiplets are enlarged in both the *degenerate* and *non-degenerate* case, e.g. there are now five instead of three Goldstone bosons of two-flavour QCD. This can be seen by rewriting the generic fermion bilinears (128) and (129) in Minkowski space in terms of the Nambu-Gorkov spinors (41). The PNGBs in this theory are denoted as π^N, the pseudoscalar singlet as η', the scalar non-singlets as a_0^N, the scalar singlet as σ, the axial-vector non-singlets as a_1^N and the vector mesons as ρ^N, such that

$$\pi^N = -\hat{\Psi}^T SCT^N E\hat{\Psi} + \bar{\hat{\Psi}} ET^N SC\bar{\hat{\Psi}}^T \qquad (N = A, B, C, D, E), \tag{182}$$

$$\eta' = -\hat{\Psi}^T SCE\hat{\Psi} + \bar{\hat{\Psi}} ESC\bar{\hat{\Psi}}^T, \tag{183}$$

$$a_0^N = \hat{\Psi}^T SCT^N E\hat{\Psi} + \bar{\hat{\Psi}} ET^N SC\bar{\hat{\Psi}}^T \qquad (N = A, B, C, D, E), \tag{184}$$

$$\sigma = \hat{\Psi}^T SCE\hat{\Psi} + \bar{\hat{\Psi}} ESC\bar{\hat{\Psi}}^T, \tag{185}$$

$$a_1^N = \bar{\hat{\Psi}} T^N \gamma_\mu \hat{\Psi} \qquad (N = A, B, C, D, E), \tag{186}$$

$$\rho^N = \bar{\hat{\Psi}} T^N \gamma_\mu \hat{\Psi} \qquad (N = F, G, H, \ldots, O). \tag{187}$$

Among the non-singlets the PNGB π, scalars a_0 and the axial vectors a_1 appear in 5-plets, while the vector mesons appear in a 10-plet. The generators of the unbroken SU($2N$) global symmetry are denoted by $T^{A\ldots N}$, where the generators $A \ldots E$ correspond to the broken generators under chiral symmetry breaking, while the remaining ones are the unbroken generators of the global Sp(4). It is also possible to express the operators (182)-(187) in terms of their Weyl components (33) as was done in Ref. [29].

The meson multiplets are enlarged by quark-quark and antiquark-antiquark operators. In appendix B the meson sources in terms of the spinors u and d are listed. The extra states are quark-quark and antiquark-antiquark states. The extra operators corresponding to the Goldstone bosons are given by [54, 94]

$$\pi^D = \bar{d}\gamma_5 SC\bar{u}^T \tag{188}$$

$$\pi^E = d^T SC\gamma_5 u, \tag{189}$$

which are known as *diquark* states. In this case, only diquarks of differing flavour are possible for scalar, pseudoscalar and axial vector states. Other operators of this form vanish identically for spin-0 composite states, i.e. the ones corresponding to (182) and (184) with unbroken generators. They can occur, however, for other spin states such as $J = 1$. In the case of the axial vectors, replacing a broken generator by an unbroken one leads to the resulting state

to be in the vector meson multiplet. This highlights the non-trivial relation between flavour symmetries and parities – see also Sec. 3.1.3

The multiplet structure of mesons for *mass-degenerate* fermions is discussed in [29,63,91]. It is the same structure as in two-flavour $\mathrm{SU}(2)_c$ gauge theory – see e.g. [108]. The pattern in Eqs. (182)-(187) is consistent with the one found for one-flavour $\mathrm{SU}(2)_c$ gauge theory [137]. There, scalar, pseudoscalar and axial vector states exist only as singlets as there are no broken generators. The vector multiplet is larger than the other multiplets and corresponds to the unbroken generators of the global symmetry.

3.1.2 Meson multiplets for non-degenerate fermions

For *non-degenerate fermions*, the Sp(4) flavour symmetry is broken to $\mathrm{SU}(2)_u \times \mathrm{SU}(2)_d$, one for each fermion flavour u and d. In general for any non-degenerate fermion in a pseudo-real theory, there will be a global SU(2) symmetry. It will be shown that the 5-plet splits into a degenerate 4-plet and a singlet. The 10-plet of the vector mesons ρ decomposes into a 4-plet of similar structure as the 4-plet of Goldstones and two degenerate triplets under each of the SU(2) groups, i.e., the remaining 6 states will have identical properties. The 4-plets contain in both cases the flavoured mesons of the form (128).

Because SU(2) exponentials are easily calculated analytically, general analytic expressions for $\mathrm{SU}(2)_d \times \mathrm{SU}(2)_u$ transformations of mesonic states are obtainable. This provides a straightforward classification of the individual states under the remaining global symmetry. In the basis given by (249), the transformation is in block diagonal form

$$V = \begin{pmatrix} a & -b^* & 0 & 0 \\ b & a^* & 0 & 0 \\ 0 & 0 & e & -c^* \\ 0 & 0 & c & e^* \end{pmatrix}, \tag{190}$$

where the diagonal matrix blocks are elements of SU(2). Denoting the complex coefficients of the individual SU(2) by (a, b) and (e, c); they fulfil $|a|^2 + |b|^2 = 1$ and $|c|^2 + |e|^2 = 1$, respectively. It is convenient to rewrite the Dirac spinors in terms of their left- and right-handed projections (17). Under an $\mathrm{SU}(2)_d \times \mathrm{SU}(2)_u$ transformation the components of $\hat{\Psi}$

transform as $\hat{\Psi} \to V\hat{\Psi}$, or, explicitly,

$$\begin{pmatrix} u_L \\ \tilde{u}_R \\ d_L \\ \tilde{d}_R \end{pmatrix} = \begin{pmatrix} u_L \\ -SC\bar{u}_R^T \\ d_L \\ -SC\bar{d}_R^T \end{pmatrix} \to \begin{pmatrix} au_L - b^*\tilde{u}_R \\ bu_L + a^*\tilde{u}_R \\ ed_L - c^*\tilde{d}_R \\ cd_L + e^*\tilde{d}_R \end{pmatrix}. \tag{191}$$

Note, that the change of basis also reflects in the way the Nambu-Gorkov spinor (41) is written. It corresponds to an exchange between the second and third element. For completeness, I give the following useful relations for the colour matrix S as well as the charge conjugation operator C in Minkowski space.

$$C^\dagger = C^{-1} = C^T = -C, \quad C^2 = -\mathbb{1}, \quad C\gamma_\mu C^{-1} = -\gamma_\mu^T, \tag{192}$$

$$(SC)^\dagger = (SC)^{-1} = (SC)^T = SC, \quad (SC)^2 = \mathbb{1}, \quad SC\gamma_\mu SC = -\gamma_\mu^T, \tag{193}$$

For the individual left- and right-handed spinors $\tilde{u}_R$ and $\tilde{d}_R$, the following relations hold

$$q_R = SC\bar{\tilde{q}}_R^T, \qquad q_R^T = \bar{\tilde{q}}_R SC, \tag{194}$$

$$\bar{q}_R = -\tilde{q}_R^T SC, \qquad \bar{q}_R^T = -SC\tilde{q}_R. \tag{195}$$

The scalar $\bar{u}d$ and vectors $\bar{u}\gamma_\mu d$ transform under $\mathrm{SU}(2)_d \times \mathrm{SU}(2)_u$ as

$$\begin{aligned} \bar{u}d = \bar{u}_L d_R + \bar{u}_R d_L \to\ & a^*c^*\left(\bar{u}_L SC\bar{d}_L^T + \bar{u}_R SC\bar{d}_R^T\right) - be\left(u_L^T SCd_L + u_R^T SCd_R\right) && (196)\\ & + a^*e\left(\bar{u}_L d_R + \bar{u}_R d_L\right) - bc^*\left(u_L^T\bar{d}_R^T + u_R^T\bar{d}_L^T\right) \\ & = a^*c^*\left(\bar{u}SC\bar{d}^T\right) - be\left(u^T SCd\right) + a^*e\left(\bar{u}d\right) + bc^*\left(\bar{d}u\right), && (197)\\ \bar{u}\gamma_\mu d = \bar{u}_L\gamma_\mu d_L + \bar{u}_R\gamma_\mu d_R \to\ & a^*e\left(\bar{u}_L\gamma_\mu d_L + \bar{u}_R\gamma_\mu d_R\right) + bc^*\left(u_L^T\gamma_\mu^T\bar{d}_L^T + u_R^T\gamma_\mu^T\bar{d}_R^T\right) \\ & + a^*c^*\left(\bar{u}_L\gamma_\mu SC\bar{d}_R^T + \bar{u}_R\gamma_\mu SC\bar{d}_L^T\right) \\ & + be\left(u_L^T\gamma_\mu^T SCd_R + u_R^T\gamma_\mu^T SCd_L\right) && (198)\\ & = a^*e\left(\bar{u}\gamma_\mu d\right) - bc^*\left(\bar{d}\gamma_\mu u\right) + a^*c^*\left(\bar{u}\gamma_\mu SC\bar{d}^T\right) - be\left(u^T SC\gamma_\mu d\right). && (199) \end{aligned}$$

Here, the property $\left(\phi^T\Gamma\chi\right)^T = -\chi^T\Gamma^T\phi$ for Grassmann variables ϕ, χ was used. The pseu-

doscalars and axial-vectors transform similarly since they only differ by γ_5.

$$\begin{aligned}\bar{u}\gamma_5 d &= \bar{u}_L d_R - \bar{u}_R d_L \\ &\to a^* c^* \left(\bar{u} SC\gamma_5 \bar{d}^T\right) - be\left(u^T SC\gamma_5 d\right) + a^* e\left(\bar{u}\gamma_5 d\right) + bc^*\left(\bar{d}\gamma_5 u\right) \qquad (200)\\ \bar{u}\gamma_\mu\gamma_5 d &= \bar{u}_R\gamma_\mu d_R - \bar{u}_L\gamma_\mu d_L \\ &\to a^* e\left(\bar{u}\gamma_\mu\gamma_5 d\right) - bc^*\left(\bar{d}\gamma_\mu\gamma_5 u\right) + a^* c^*\left(\bar{u}\gamma_\mu\gamma_5 SC\bar{d}^T\right) - be\left(u^T SC\gamma_\mu\gamma_5 d\right) \qquad (201)\end{aligned}$$

These states form a quadruplet under $\mathrm{SU}(2)_d \times \mathrm{SU}(2)_u$. The remaining pseudo-scalars and scalars transform as singlets. The associated operators have the form $\bar{u}\Gamma u \pm \bar{d}\Gamma d$ and the individual $\mathrm{SU}(2)_{d,u}$ only change one of the terms, so it is sufficient to look at the transformation property of, say, $\bar{u}\Gamma u$,

$$\begin{aligned}\bar{u}u &= \bar{u}_L u_R + \bar{u}_R u_L \to \bar{u}_L u_R + \bar{u}_R u_L = \bar{u}u, \qquad (202)\\ \bar{u}\gamma_5 u &= \bar{u}_L u_R - \bar{u}_R u_L \to \bar{u}_L u_R + \bar{u}_R u_L = \bar{u}\gamma_5 u, \qquad (203)\\ \bar{u}\gamma_\mu u &= \bar{u}_L\gamma_\mu u_L + \bar{u}_R\gamma_\mu u_R \\ &\to \left(|a|^2 - |b|^2\right)\left(\bar{u}\gamma_\mu u\right) + 2a^* b^*\left(\bar{u}\gamma_\mu SCP_L\bar{u}^T\right) - 2ab\left(u^T SC\gamma_\mu P_L u\right), \qquad (204)\\ \bar{u}\gamma_\mu\gamma_5 u &= \bar{u}_R\gamma_\mu u_R - \bar{u}_L\gamma_\mu u_L \to \bar{u}\gamma_\mu\gamma_5 u. \qquad (205)\end{aligned}$$

Similar expressions for $\bar{d}\Gamma d$ are obtained by replacing $u \to d, a \to e$ and $b \to c$. The scalar, pseudoscalar and axial vector states transform as singlets under the remaining symmetry. Thus, the associated flavour-neutral states are all singlets. The situation is different for the unflavoured vectors where each unflavoured bilinear transforms as a triplet under the corresponding global SU(2). The same pattern has previously been found in SU(2) gauge theory with one fermion [137].

Figure 3 groups mesons into degenerate and non-degenerate sets and compares them to QCD with two degenerate fundamental fermions. In the case of different UV fermion masses $m_u \neq m_d$, π^C becomes a singlet under the global flavour symmetry, whereas before it was part of a multiplet. This has consequences for its viability as a dark matter candidate: it is no longer protected by a flavour symmetry and, equipped with further interactions, may in principle decay. Even after breaking the global symmetry, no vector singlet meson appears in the spectrum due to the additional unflavoured diquark states. This will occur in every 10-plet of mesons that has the same structure as the vector mesons. For the 5-plet states this does not happen, as the unflavoured diquark states are identically zero.

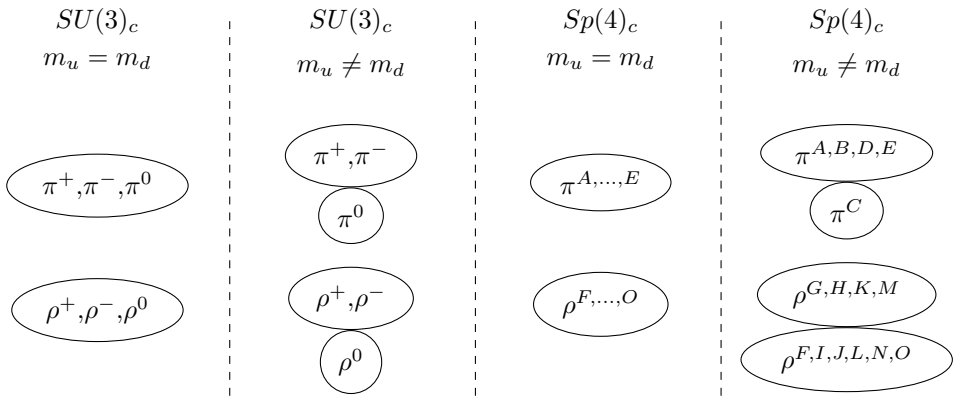

Figure 3: The flavour structure of the meson multiplets for an Sp(4) gauge theory with $N_f = 2$, compared to QCD with the same number of quarks. The multiplets of Sp(4) are enlarged due to additional diquark states. When the flavour symmetry is explicitly broken by non-degenerate fermion masses, $m_u \neq m_d$, the pseudoscalar and vector multiplets split further into smaller flavour-multiplets under the flavour group. The unflavoured π^C becomes a singlet.

3.1.3 Parity and diquarks

Since the global flavour transformation acts on combinations of the left- and right-handed Dirac components, the relation between flavour symmetries and parity is non-trivial. Conventionally, the transformation of a Dirac fermion under parity is defined as [138]

$$P : \psi(\mathbf{x}, t) \to \gamma_0 \psi(-\mathbf{x}, t). \tag{206}$$

This implies that parity mixes left-handed and right-handed components. This can be made explicit by going to the chiral representation of the γ-matrices,

$$P : \quad \begin{aligned} &\psi_L(\mathbf{x}, t) \to \psi_R(-\mathbf{x}, t), \\ &\psi_R(\mathbf{x}, t) \to \psi_L(-\mathbf{x}, t). \end{aligned} \tag{207}$$

The discrete ordinary parity transformation P leaves the Lagrangian invariant and is thus a symmetry. However, it is important to note that the global flavour symmetry mixes left-handed and right-handed components. In general, such transformations do not commute with parity as defined above. In other words, the flavour eigenstates are not eigenstates of P. This has the consequence that a diquark Goldstone state is a scalar rather than a

	J^P	J^D
π^A, π^B, π^C	0^-	0^-
π^D, π^E	0^+	0^-
$\rho^H, \rho^M, \rho^N, \rho^O$	1^-	1^-
$\rho^F, \rho^G, \rho^I, \ldots, \rho^L$	1^+	1^-

Table 2: Parity assignments of the quark-antiquark bound-states and the additional diquark states. Under ordinary P-parity different parity-eigenstates occur in the same meson multiplet. Only under D-parity all Goldstones can be classified as pseudoscalars and all particles in the ρ-multiplets as vectors. An extension of this table is given in App. B.

pseudoscalar under P:

$$\begin{aligned}\pi^E(\mathbf{x},t) = d^T(\mathbf{x},t)SC\gamma_5 u(\mathbf{x},t) &\xrightarrow{P} d^T(-\mathbf{x},t)\gamma_0^T SC\gamma_5\gamma^0 u(-\mathbf{x},t)\\ &= d^T(-\mathbf{x},t)SC\gamma_5 u(-\mathbf{x},t) = +\pi^E(-\mathbf{x},t).\end{aligned} \tag{208}$$

The different sign is caused by the charge conjugation matrix C in the diquark states for which $\gamma_0^T C\gamma_0 = -C$ holds. Concretely, the multiplet of the Goldstones bosons consists of 3 pseudoscalar mesons and 2 scalar diquarks and the multiplet containing the ρ is made up of 4 vectors and 6 axialvectors under P; these states may then change their ordinary parity under flavour transformations.

A "better" definition of parity is obtained by combining it with any other internal symmetry present in the Lagrangian, see e.g. [40]. Introducing an additional phase in the transformation properties of the spinors (206). A new parity D can be chosen so that it now commutes with all flavour transformations [105]. It is given by

$$D : \psi(\mathbf{x},t) \to \pm i\gamma_0\psi(-x,t). \tag{209}$$

The extra phase cancels in all operators of the form $\bar{u}\Gamma d$ but produces an extra minus sign in the diquark operators. The new parity D is again a symmetry of the Lagrangian introduced below and all members of a meson multiplet share the same parity assignment under D. In this way, all Goldstones become pseudoscalars and all members of the ρ-multiplet become vectors under D; see Tab. 2 for an overview of P- and D-parity of the mesons considered in this work. The detailed flavour structure of these mesons - including the vector meson multiplet - can be found in appendix B. For concreteness consider the diquark π^E and its

transformation under the parity assignment D. It transforms as

$$\begin{aligned}\pi^E(\mathbf{x},t) = d^T(\mathbf{x},t)SC\gamma_5 u(\mathbf{x},t) &\xrightarrow{D} i^2 d^T(-\mathbf{x},t)\gamma_0^T SC\gamma_5\gamma^0 u(-\mathbf{x},t) \\ &= -d^T(-\mathbf{x},t)SC\gamma_5 u(-\mathbf{x},t) = -\pi^E(-\mathbf{x},t),\end{aligned} \tag{210}$$

and thus remains a pseudoscalar under D. For the remainder of the thesis, the definition (209) will be used, when referring to parity. This assignment is identical for all quark-antiquark states appearing in QCD and general theories with complex representations. The multiplet of the flavoured PNGBs $\pi^{A\ldots E}$ is the generalization of the $\pi^{\pm}$ states of QCD, and the flavour diagonal π^C is the equivalent of the π^0. Similarly, the flavoured vector mesons are the generalization of the $\rho^{\pm}$ states and the unflavoured multiplet as the generalization of the flavour diagonal ρ^0 and ω states. In order to highlight the correspondence between the enlarged multiplets and its QCD counterpart, they will occasionally be referred to by the name of their QCD counterparts.

3.2 Lattice setup and technicalities

Gauge configurations are generated with two dynamical fermions using the HiRep code [118, 139] extended for Sp($2N$) gauge theories [63, 91, 140]. For two degenerate fermions the HMC algorithm was used to include them dynamically and for non-degenerate fermions the RHMC algorithm was employed. This gives rise to a potential sign problem as the determinant is not guaranteed to be positive. The studied masses were moderately heavy and the lowest eigenvalues of the Dirac operator were monitored and no signs of a negative eigenvalue and thus a potentially negative determinant was found. No $\mathcal{O}(a)$ improvement was used for the gauge and the fermion action.

The theory has three free parameters, the gauge coupling g and the two bare fermion masses m_u and m_d. In the context of lattice calculations, it is convenient to express the gauge coupling as $\beta = 8/g^2$. Note that both the coupling and the fermion masses are the unrenormalized bare parameters and thus unphysical. For degenerate fermions $m_u = m_d$ only two free parameters remain.

In the continuum theory, the overall scale would be set by one of the dimensionful parameters, but in a lattice calculation it is convenient to use instead the finite lattice spacing a. Masses are then measured in units of the inverse lattice spacing a^{-1}. Only once some dimensionful quantity is fixed, e.g., by experimental input, explicit units become possible. Fixing the scale, and thus the lattice spacing, implies that also one of the bare lattice parameters is

fixed. It is convenient to choose the gauge coupling for this fixing of the scale, leaving two dimensionless quark masses to uniquely characterize the physics. These two free parameters can be used to fix two observable quantities, e.g. properties of the dark hadrons such as masses or scattering cross-sections. All other results are then predictions.

For degenerate fermions the quantity used to relate the bare parameters to physical quantity is the ratio between the PNGB mass and the vector meson mass m_π/m_ρ. In the limit of vanishing mass it approaches $m_\pi/m_\rho \to 0$ as the PNGBs become massless. In the limit of infinite fermion mass all masses are dominated by the quark masses and the effects of dynamical mass generation becomes negligible and the ratio approaches unity $m_\pi/m_\rho \to 1$.

For non-degenerate fermions, I always start from degenerate dark quark masses, and then incrementally increase one of them, breaking the flavour symmetry from Sp(4) down to $\mathrm{SU}(2)_u \times \mathrm{SU}(2)_d$ explicitly. In terms of physical units $m_{\pi^\pm}/m_{\pi^0}$ is used to monitor the strength of strong isospin breaking. In SM QCD a relatively large change in the fermion mass (usually defined in the $\overline{MS}$ scheme) can lead to only small changes in the pion ratio. Thus, the PCAC mass ratio of the fermions is additionally monitored.

Fig. 4 depicts the previously outlined workflow. All bare input parameters are unrenormalized and thus unphysical (this includes the bare quark masses.)

The data analysis was performed using the Julia programming language [141]. For least-squares fitting the package LsqFit.jl [142] was used. Plots were generated using the Plots.jl [143] package using the PGFPlotsX backend. Error estimates quoted in this thesis were obtained using the standard jackknife method discussed in Sec. 2.4.1. When comparing the jackknife errors to the ones obtained using the statistical bootstrap, no appreciable differences were found.

3.3 Non-Singlet states in $N_f = 1 + 1$

3.3.1 Parameter choice and interpolators

In this section, the light non-singlet spectrum of Sp(4) gauge theory with two fundamental non-degenerate Dirac fermions are considered. The mass degenerate case was already studied in [91]. The scalar and axial-vector singlet mesons were found to be substantially heavier than the vector and pseudoscalar non-singlets.

In this work ensembles with $m_\rho/m_\pi \approx 1.15, 1.25$ and 1.4 or equivalently $m_\pi/m_\rho \approx 0.87, 0.8$ and 0.72 in the mass degenerate limits[1] have been studied. These values are slightly smaller

[1]For the degenerate case, if possible, results from [91] are used, since these have been obtained on larger

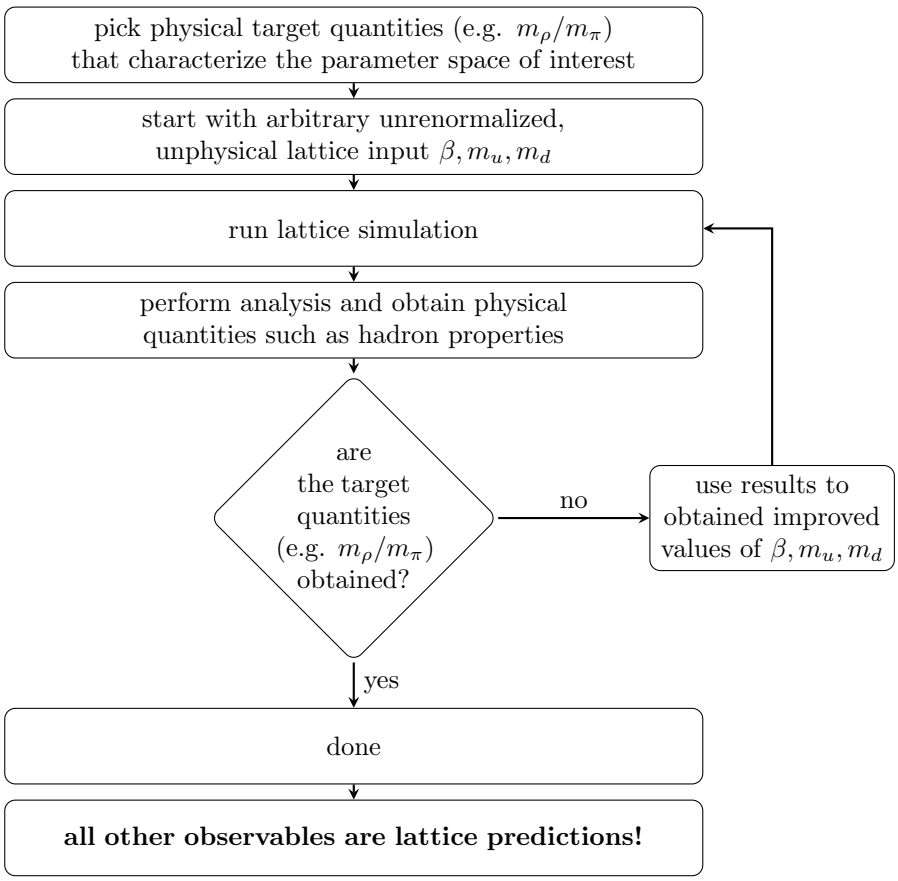

Figure 4: Workflow for choosing suitable input parameters m_u, m_d and β. These input parameters are unrenormalized and thus unphysical. They are chosen such that a set of observables has a prescribed value (in this case the ratio m_ρ/m_π and m_{π^+}/m_{π^0}). All other observables are then predictions from the lattice. No overall scale of the observables has been fixed.

than those suggested by existing phenomenological investigations of such theories as dark matter candidates [144]. Ensembles with $m_\pi/m_\rho < 0.7$ come at a significantly increased computational cost and will not be studied within this thesis. For the bare inverse coupling values of $\beta > 6.8$ are used. It was shown in [63], that for smaller values the system can enter a lattice phase with no connection to the continuum physics. A bulk phase transition as a function of the fermion mass was observed. Ensembles with $\beta > 6.8$ are thought to be in the same phase as the continuum limit of $\beta \to \infty$. The fermions studied here are more akin to the strange quark in SM QCD. Note that in all cases the aforementioned ratio m_ρ/m_π is smaller than 2 and the ρ at rest cannot decay into two Goldstone bosons.

Only quark-antiquark interpolators (129), (128) are used. The HiRep code has been modified to perform simultaneous measurements of the diagrams depicted in Eq. (137), i.e. a connected meson diagram with unequal fermion masses, and the degenerate counterparts of Eq. (138). This is sufficient to probe every meson multiplet in this theory. All diquark states are related to conventional meson states by flavour transformations. This has also been numerically checked using the HiRep code in [54]. Stochastic $Z_2 \times Z_2$ wall sources [126] with spin dilution [128] with three stochastic samples per configuration have been used.

3.3.2 Disconnected diagrams and expansion in the mass difference

In principle the flavour neutral operators give rise to disconnected diagrams, as can be seen in (138). In the isospin symmetric limit the disconnected contributions cancel for states that are degenerate with other flavoured states such as the ones appearing for the flavour-neutral pion.

For states where no singlet contribution can arise due to flavour symmetry such as the dark vector mesons ρ and ω in pseudo-real representations, the disconnected contributions need to vanish. However, for the true singlets of the theory they do not generically vanish. These states include the dark η' and f_0/σ mesons as well as the flavour-neutral pion π^0 for non-degenerate masses.

For the latter state the relevance of disconnected contributions is expected to be suppressed by two mechanisms. Firstly, by the mass of the fermions which suppress disconnected diagrams in general. Additionally, for states such as the π^0 cancellations between the two distinct disconnected contributions will arise – see Eq. (129). Thus, in Sec. 3.3 the π^0 is included in the study of "non-singlet" states assuming that disconnected contributions will be negligible. This will be shown to be a good approximation for the fermion masses studied in this thesis. Results on the π^0 and the other non-singlet states will be presented in Sec. 3.4

lattices with better statistics in comparison to ours.

For small mass differences it appears reasonable to first study the theory in the mass-degenerate limit and then introduce the strong isospin-breaking corrections perturbatively. This approach was employed in the study of the pion mass difference of QCD [145] allowing an extrapolation to small differences. On the lattice this requires the calculation of additional diagrams where in the usual diagrams (137) and (138) correlators are replaced with insertions on every spacetime point.

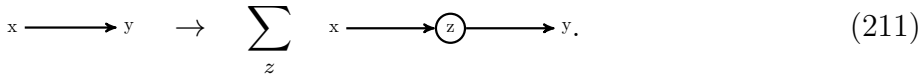

(211)

This has to be done for both the connected and disconnected diagrams irrespective of the details of the isospin breaking expansion. This would require additional operators to be measured on the lattice which require additional all-to-all propagators. Thus, they are not studied in this work. The derivation the relevant diagrams for different methods of expanding in the isospin breaking terms are derived in appendix D.

3.3.3 Masses and decay constants

The masses and decay constants of both the Goldstones and the vector mesons as well as the previously outlined unrenormalized PCAC masses were calculated. The tabulated results can be found in appendix C. The non-singlet meson masses and their decay constant for the ensembles with varying m_ρ/m_π at degeneracy are shown in Fig. 5 as a function of the PCAC mass ratio. Both for the Goldstone and vector mesons, the flavour-neutral states are the lighter states once strong isospin breaking is introduced. This makes the π^C (which is the equivalent of the QCD state π^0) the lightest state in the theory. The remaining four Goldstones are heavier and remain degenerate. This is the same pattern as observed in the SM where the neutral pion is the lightest bound state of the strong sector. The mass difference between the flavoured and unflavoured vector mesons is less pronounced. Again, the situation is similar in the SM where the mass difference between the charged and neutral vector mesons currently cannot be resolved [17]. The overall pattern is observed for all ensembles on all lattice spacing considered $\beta = 6.9, 7.05$ and 7.2, as well as for all values of m_π/m_ρ at degeneracy.

At some point the six lighter unflavoured vector mesons — corresponding to the unflavoured vector mesons ρ^0 and ω of QCD — become even lighter than the heavier pseudoscalars. The inversion of the mass hierarchy depends more strongly on the overall mass of the involved fermions. For generally lighter quarks it occurs at a higher ratio of the PCAC masses than for the heavier fermions. For large mass splittings the system resembles more

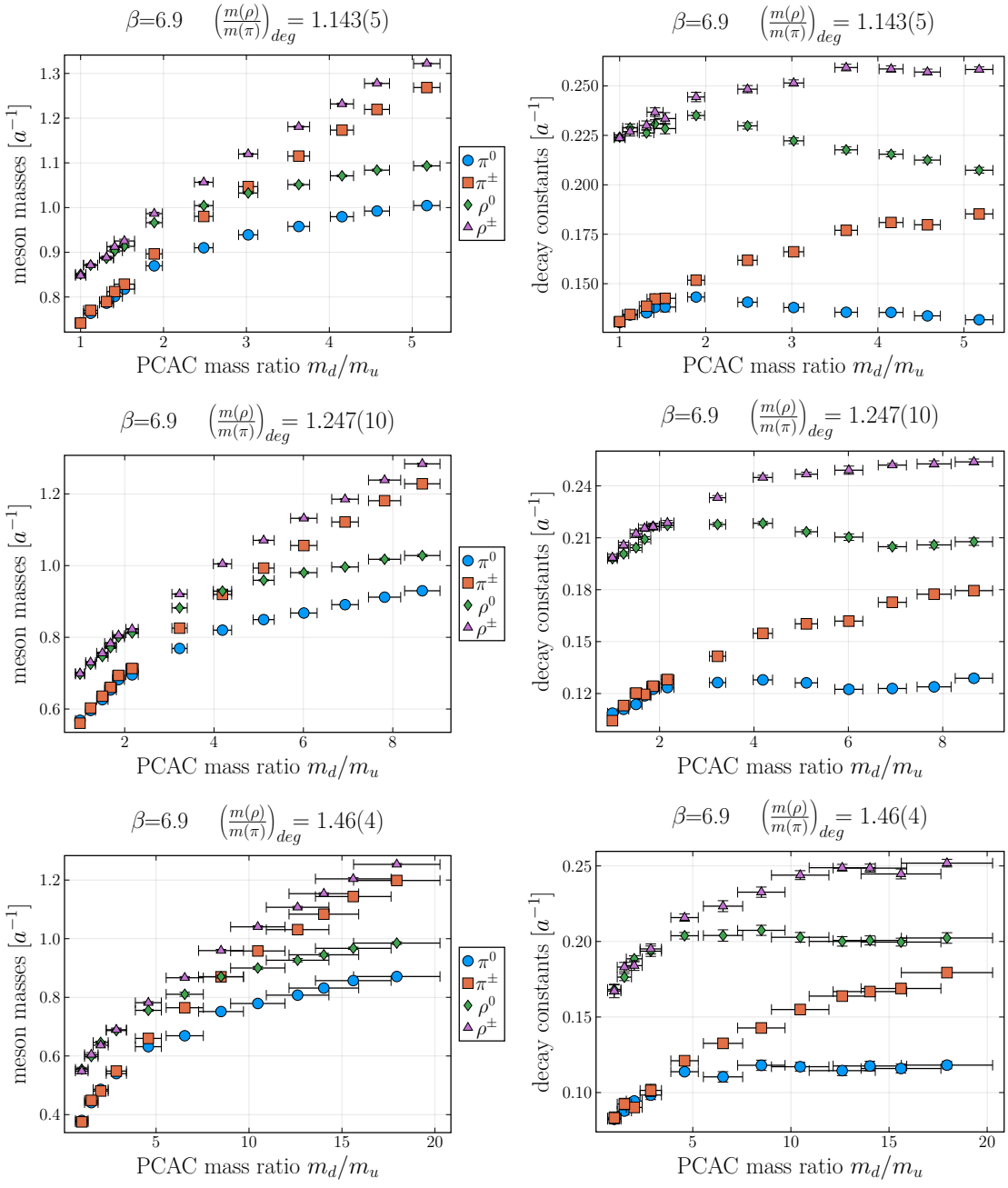

Figure 5: Masses and decay constants of the pseudo-Goldstone mesons and the vector mesons for different non-degenerate fermion masses against the ratio of the unrenormalized PCAC masses. One fermion mass is kept fixed while the other is incrementally increased. The unflavoured pseudo-Goldstone is the lightest particle in the spectrum of the isolated theory. For a larger mass difference between the fermions the unflavoured vector mesons get lighter than the flavoured pseudo-Goldstones.

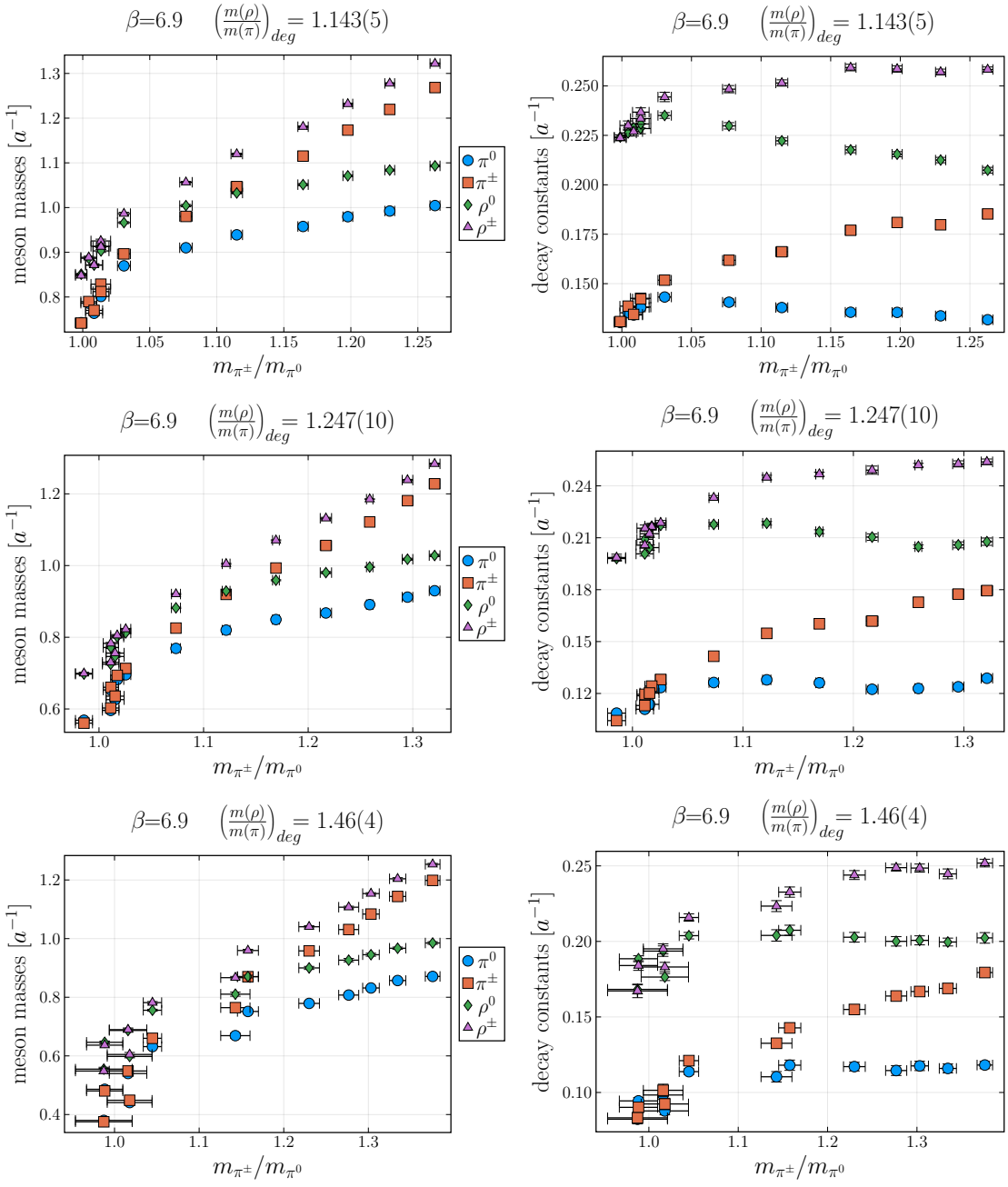

Figure 6: Same plot as Fig. 5 but plotted against the dark pion mass ratio. Even for large mass fermion mass differences the relative splitting between the dark pions never exceeds 50%.

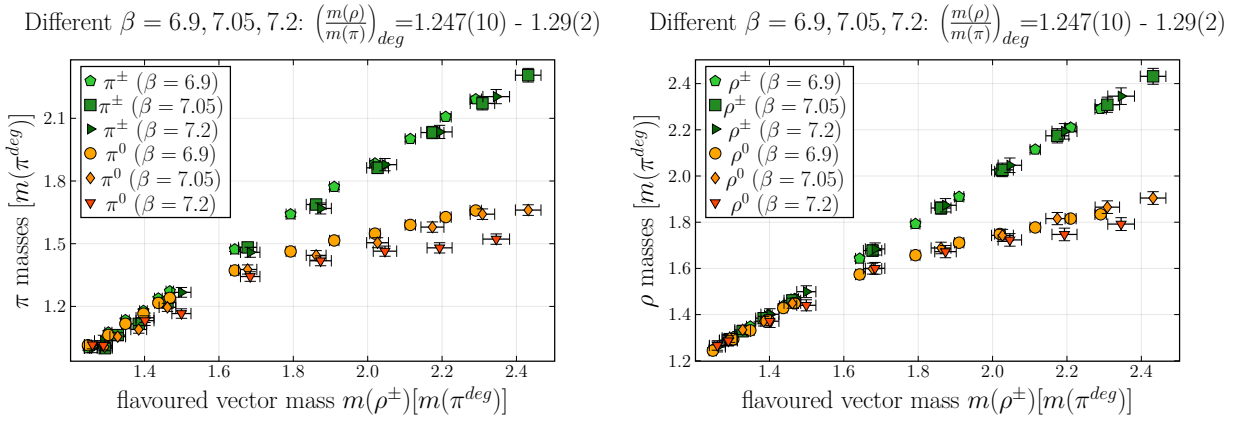

Figure 7: Masses of the pseudo-Goldstones (upper) and vector mesons (lower) for different values of the inverse coupling β in units of the pseudo-Goldstone mass degeneracy. The results at different β agree within errors except for the $\beta = 7.2$ ensembles with one relatively heavy fermion . Overall, the finite spacing effects for the meson masses are small.

closely a heavy-light system where the unflavoured mesons are the lightest hadronic states. At some point the mass of the second dark quark is so heavy that it decouples and the low-energy part of this theory is effectively an $N_f = 1$ theory which contains three vector mesons and one (massive) pseudoscalar [137]. In this case the theory develops a hierarchy of scales.

A similar pattern is observed for the decay constants of those dark mesons shown. The unflavoured decay constants are smaller than their flavoured counterparts. This is seen for both the Goldstone and the vector mesons, although the difference is less pronounced as in the case of the meson masses. No change in the hierarchy of decay constants is observed. The decay constant depicted in Fig. 5 are the renormalized using lattice perturbation theory at one loop – see Sec. 2.5.6. Furthermore, for the heavier ensembles the unflavoured decay constants shows a non-monotonic behaviour at intermediate values of the dark fermion mass splitting. This is less pronounced for lighter fermion masses. Fig. 6 shows the same meson masses against the mass ratio of the distinct dark pion species. Comparing these results to those of the PCAC mass ratio shows, that a rather large change in the fermion masses only leads to a moderate mass difference between the dark pions which never exceeds 50%, whereas PCAC mass ratios up to 10 were obtained.

Different lattice spacings

Figs. 7, 8 and 9 depict the masses and decay constants at different values of the inverse coupling and thus at different lattice spacings for the set of ensembles with intermediate

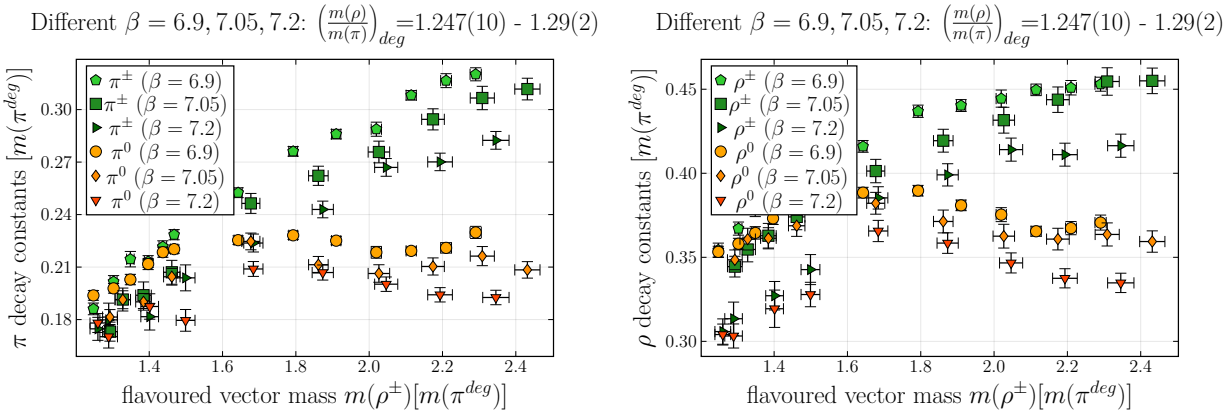

Figure 8: Decay constants of the pseudo-Goldstones (upper) and vector mesons (lower) for different values of the inverse coupling β in units of the pseudo-Goldstone mass degeneracy. The results at different β show stronger deviations than the meson masses even at very light fermion masses. For the pseudo-Goldstones the deviations are approximately 10% or smaller whereas for the vector mesons they can be as large as 20%.

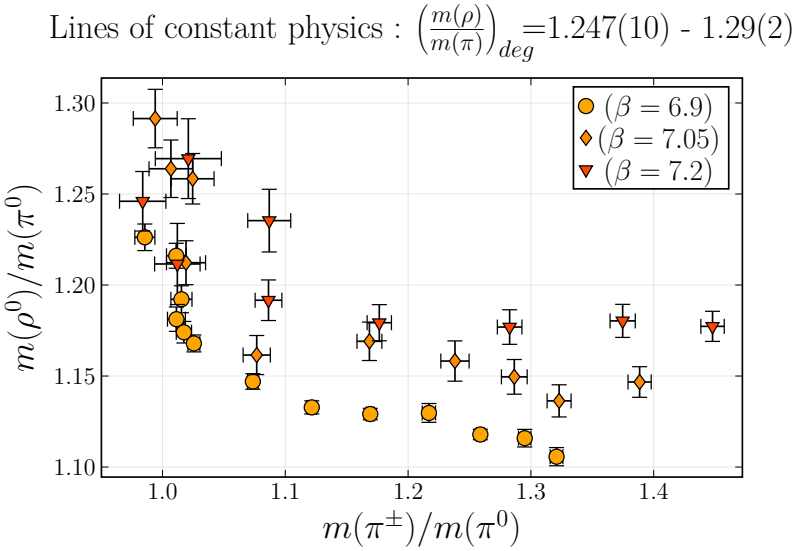

Figure 9: Ratio of the flavour-neutral vector and pseudoscalar mesons against the pseudoscalar mesons' mass ratio. Since the theory has only two free mass parameters, two coinciding points on this plot are defined describe the same physical system even at different lattice spacing. It can be seen that the different ensembles at distinct β are not exactly on constant lines oh physics. However, here they deviate by no more than 5%.

fermion masses. The same plots for the ensembles with lighter and heavier fermions can be found in appendix C. They show the same qualitative behaviour. Due to the different lattice spacings a, the lines of constant physics need to be defined through dimensionless quantities. Here, the masses were tuned so that at fermion masses a comparable value of m_π/m_ρ at degeneracy is obtained for the different values of β. Then the mass of one fermion was subsequently increased while the other was kept fixed. This is motivated by the observation that in $\mathrm{SU}(3)_c$ gauge theory with fermions, the lattice spacing a depends strongly on the value of the inverse coupling β and only weakly on the masses of the fermions m_f [28].

Two dimensionless quantities are needed to fix the two free fermion mass parameters this theory. A choice of such quantities then defines point or lines of constant physics. In this theory the chosen quantities are the mass ratio of the neutral pseudoscalar and vector meson and the ratio of the distinct pseudoscalar mesons. These quantities are plotted in figure 9. While the individual simulations at distinct β are not exactly on constant lines of physics, they never deviate by more than 5%.

It can be seen that the other mass ratios depicted in Figs. 7, 8 are mostly consistent across the different lattice spacings. Comparing the values of m_π at degeneracy, one concludes that the finest lattice at $\beta = 7.2$ is roughly 40% finer than the coarsest one at $\beta = 6.9$. Only for the finer lattice a statistically significant deviation for the flavour-neutral mesons is observed. The situation is different for the decay constants. The PNGB decay constants deviate at different lattice spacings by roughly 10% and the vector mesons show deviations of up to 20%.

Generically, the spacing effects become more pronounced for larger fermion mass differences. This can be understood by the relatively heavy mass of the mesons in lattice units. Tabulated results can be found in appendix C. On the coarsest lattice the meson masses are heavier than 1.0 in lattice units and discretization artefacts are expected to be sizeable. For a better control of these systematic issues on a quantitative level further investigations are certainly needed. At the level of $10\% - 20\%$ the results presented here appear to be reliable. The same hierarchies are observed in all sets of ensembles irrespective of the overall mass of the fermions and the lattice spacing.

Finite volume effects

As discussed in Sec. 2.1, the finite volume of a lattice can introduce additional artefacts. To quantify the effects of the finite spatial extent L the expression (78) for PNGBs in chiral

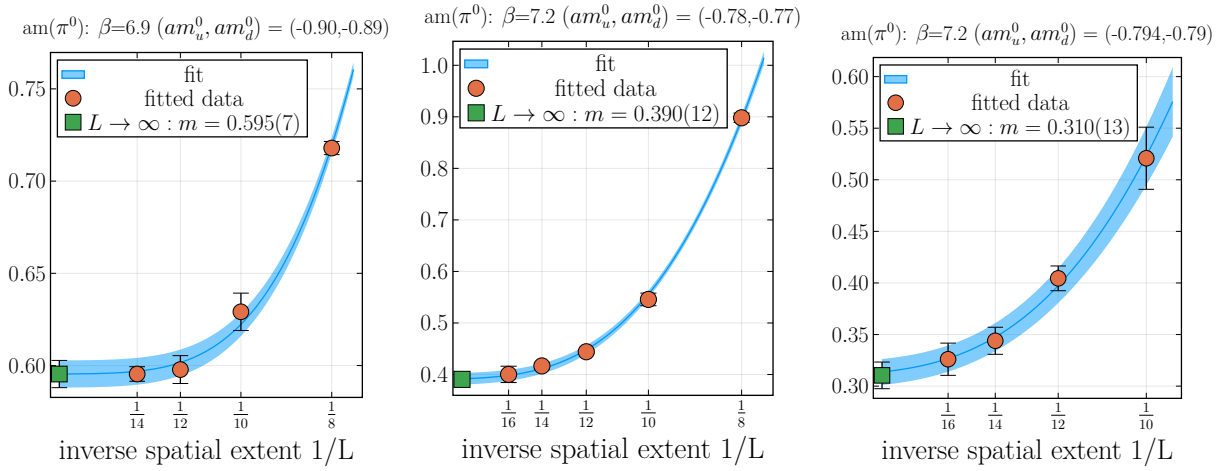

Figure 10: Finite volume extrapolation for the lighter, flavour-neutral Goldstone mass in the almost mass-degenerate limit. Only in the lightest ensembles on the finest lattices studied here, the finite volume effects become apparent.

perturbation theory in a finite box is generalized to other mesons as

$$m_{\text{meson}}(L) = m_{\text{meson}}^{\text{inf.}} \left(1 + A \frac{\exp(-m_\pi^{\text{inf}} L)}{(m_\pi^{\text{inf}} L)^{(3/2)}}\right), \tag{212}$$

and the coefficient A – which can be calculated within chiral perturbation theory – is taken to be a free parameter to account for deviations from the chiral theory as in [91]. By calculating the meson mass at different L, a fit to Eq.(212) can be performed and the infinite volume mass can be extracted. If the physical volume in relation to the PNGB mass $m_\pi L$ is sufficiently large, the deviations at a finite volume will be negligible. In [91] the finite volume effects were found to be below the level of 0.3% for $m_\pi^{\text{inf}} L < 7.5$. For smaller volumes at roughly $m_\pi^{\text{inf}} L \approx 6$ the finite volume effects were of the order $1-2\%$ and even at volumes of $m_\pi^{\text{inf}} L \approx 5$ they typically did not exceed 5%.

In Figs. 10 and 11 a selection of infinite volume extrapolations in the almost mass-degenerate limit are shown. They include the lightest ensemble on the finest lattice where the finite volume effects will be most pronounced. Only in the latter ensembles finite volume effects become apparent and generally the deviation from the infinite volume extrapolation stays well below 10%. On the coarser lattices the finite volume effects are less pronounced and mostly negligible compared to the statistical uncertainties.

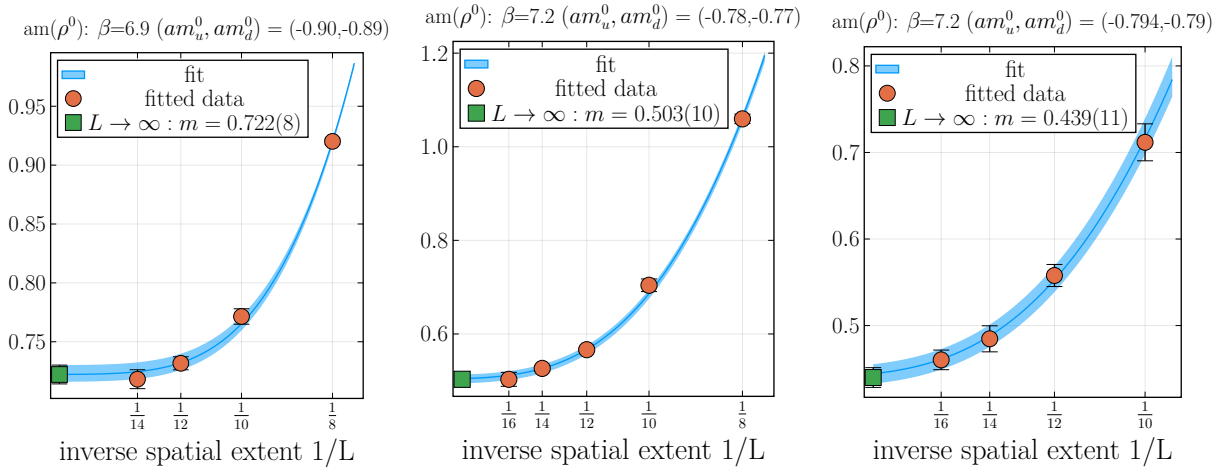

Figure 11: Finite volume extrapolation for the lighter, flavour-neutral vector meson mass in the almost mass-degenerate limit.

Lattice asymmetry

In this analysis the masses and decay constants are extracted from the behaviour of correlation functions at large Euclidean time t. For convenience, the lattices have a larger temporal extent than spatial extent, i.e. lattices of dimensions $L^3 \times T$ with $T > L$ are used. This allows a calculation of the correlation functions at large t while avoiding significantly increased computation time.

It is, however, still possible, that this introduces systematic error. Comparing meson masses on symmetric lattices of size L^4 to the masses obtained for asymmetric lattices can provide an estimate of such effects. On the symmetric lattices the time extent is substantially smaller. Even at the largest Euclidean times effects of excited state contamination are present. I therefore take the second-lightest state into account and extract the mass from the effective mass of the correlator.

This allows us to extract the masses from a three-parameter fit while simultaneously minimizing the effects of contamination of higher states. This comes at the cost of larger errors, since the effective mass defined this way discards some information because it as a local quantity around Euclidean time $\left(t + \frac{1}{2}\right)$. As can be seen in table 3, no systematic effects from the use of asymmetric lattice appear within the errors reported. However, the errors on the symmetric lattice are substantially larger.

$(-am_1^0, -am_2^0)$	$am(\pi^{\pm})(24 \times 12^3)$	$am(\pi^{\pm})(12^4)$	$am(\pi^0)(24 \times 12^3)$	$am(\pi^0)(12^4)$
(0.90,0.70)	0.993(7)	0.994(15)	0.83(1)	0.85(4)
(0.90,0.75)	0.917(14)	0.92(2)	0.80(2)	0.81(5)
(0.90,0.80)	0.826(11)	0.83(5)	0.76(2)	0.77(7)
(0.90,0.85)	0.712(15)	0.7(2)	0.69(2)	0.7(2)
(0.90,0.90)	0.56(4)	0.58(9)	0.56(4)	0.58(9)
$(-am_1^0, -am_2^0)$	$am(\rho^{\pm})(24 \times 12^3)$	$am(\rho^{\pm})(12^4)$	$am(\rho^0)(24 \times 12^3)$	$am(\rho^0)(12^4)$
(0.90,0.70)	1.070(9)	1.071(15)	0.951(14)	0.97(3)
(0.90,0.75)	1.001(14)	1.00(2)	0.92(2)	0.94(3)
(0.90,0.80)	0.921(15)	0.93(3)	0.88(2)	0.90(3)
(0.90,0.85)	0.82(2)	0.82(4)	0.81(2)	0.82(4)
(0.90,0.90)	0.70(2)	0.72(4)	0.70(2)	0.72(4

Table 3: Comparison of meson masses extracted from both symmetric and asymmetric lattices for an inverse coupling of $\beta = 6.9$. The other two input parameters are m_1^0 and m_2^0 - the unrenormalized bare quark masses. They agree within errors albeit with significantly larger uncertainties. There are no relevant systematic effects due to the asymmetric lattices used throughout this work at the level of the uncertainties of the masses on the symmetric lattices.

3.3.4 Validity of the Chiral Lagrangian

The chiral theory of Secs. 1.3 is based on the dynamics of the lightest hadronic states, which in this case are the pseudo-Goldstone bosons π. In the chiral limit, i.e., in the limit of massless dark fermions, the flavour symmetry is broken only spontaneously and the π's become massless themselves. Close to the chiral limit for degenerate quarks the GMOR relation gives the dependence of the product of Goldstone masses on the renormalized quark masses $m_q^{(r)}$ and the magnitude of the chiral condensate $(v^3)^{(r)}$

$$(f_\pi m_\pi)^2 = 2m^{(r)}(v^3)^{(r)}. \tag{213}$$

It can be seen that the square of the pseudo-Goldstone mass depends linearly on the average renormalized quark mass and in the chiral limit the equation is trivially fulfilled. As pointed out in section 2.5.7 the renormalized quark mass and the condensate are scheme-dependent. However, their product is scheme-independent since the involved renormalization constants cancel. For simplicity, the unrenormalized PCAC mass m_{PCAC} is used and the chiral condensate is defined through the GMOR relation. This entails that also the condensate is then unrenormalized and regulator-dependent. The superscript $^{(r)}$ is dropped in the following.

For non-degenerate quarks GMOR relations have been constructed in [2]. It is conveniently rewritten as

$$\begin{aligned}\mathrm{GMOR}_{\pi^\pm}(m_u, m_d, \mu_u, \mu_d) &= (m_{\pi^\pm} f_{\pi^\pm})^2 - \frac{2v_u^6(m_u + m_d)}{v_u^3 + v_d^3} = 0 \\ \mathrm{GMOR}_{\pi^0}(m_u, m_d, \mu_u, \mu_d) &= (m_{\pi^0} f_{\pi^0})^2 - \frac{2v_u^6(m_u v_u^3 + m_d v_d^3)}{v_u^6 + v_d^6} = 0. \end{aligned} \tag{214}$$

For sufficiently large UV mass difference in the dark fermions, the mass hierarchy in the mesonic spectrum changes qualitatively: the multiplet of vector mesons containing the ρ^0 becomes lighter than the multiplet of flavoured pseudoscalars containing the $\pi^\pm$. The set of π's are then no longer the lightest hadronic states and an inclusion of the relevant vector states becomes necessary. This provides an upper limit on the amount of strong isospin breaking.

Using the GMOR relations a potentially even stronger bound can be set on the amount of strong isospin breaking. The validity of the GMOR relation was already studied for degenerate fermions in [91]. It was found that dependence of the square of the pseudo-Goldstone mass on a (differently defined) unrenormalized quark mass is linear for ensembles with $m_\rho/m_\pi > 1.4$. Due to the increased computational cost of non-degenerate fermions no results on ensembles that fulfil $m_\rho/m_\pi \gg 1.4$ are currently available. Nevertheless, consistency tests can be performed using the GMOR relations in (214) around the threshold $m_\rho/m_\pi \approx 1.4$ and below, see table 4. The fact that in the non-degenerate simulations one bare quark mass has been kept fixed is exploited:

At degenerate fermion masses, the degenerate GMOR relation (213) is taken for granted, and it is used to determine the chiral condensate $(\mu_u^3)^{\mathrm{PCAC}}$ from the fixed quark mass m_u^{PCAC} [2]. Since these quantities are regulator-dependent, only results at the same value of the (bare) inverse gauge coupling β are compared. This determines three out of the four quantities that enter the non-degenerate GMOR relations in (214). Both equations in (214) can be used to determine $(v_d^3)^{\mathrm{PCAC}}$. If the non-degenerate GMOR relation holds, the functions $\mathrm{GMOR}_{\pi^{\pm,0}}(m_u, m_d, \mu_u, x)$ have common roots at $x = \mu_d^{\mathrm{PCAC}}$. This is shown in Fig. 12 for specific ensembles $\mathrm{GMOR}_{\pi^{\pm,0}}(m_u, m_d, \mu_u, x)$ as a function of x. It can be seen that at larger quark-mass-ratios the functions do not share a common root. In particular GMOR_{π^0} no longer has root in this region of x.

This is a sign that at this point the description provided by the leading order chiral

[2] From [91] it follows that the dependence of the squared Goldstone mass on the quark mass only becomes linear for $m_\rho/m_\pi \gtrsim 1.4$. However, this approach allows testing whether the explicit introduction of isospin breaking effects cause a breakdown.

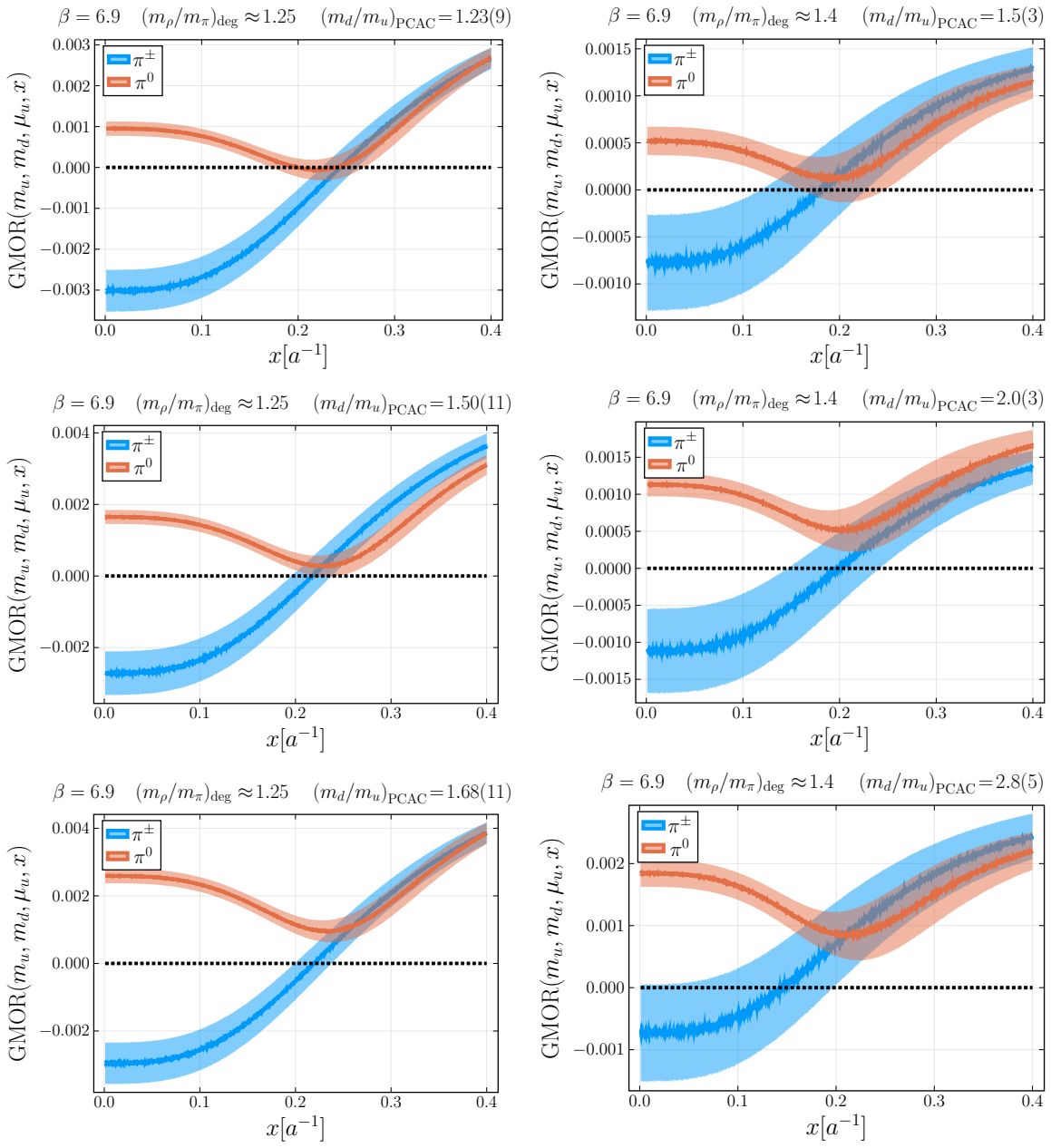

Figure 12: $\text{GMOR}_{\pi^{0,\pm}}(m_u, m_d, \mu_u, x)$ as a function of x for an inverse gauge coupling of $\beta = 6.9$ and values of $m_\rho/m_\pi \approx 1.24$ and $m_\rho/m_\pi \approx 1.46$ at degeneracy. If the non-degenerate GMOR relation holds, the condensate μ_d is given by the common root of the two functions. For small isospin breaking a common root exists. Starting at around $m_d/m_u \approx 1.5$ in both cases a tension develops. At around $m_d/m_u \approx 1.7$ for the heavier ensemble and at around $m_d/m_u \approx 2$ for the lighter ensemble the non-existence of a common root is more than one-sigma significant.

β	$\left(\frac{m_\rho}{m_\pi}\right)_{\text{deg}}$	$\left(\frac{m_u}{m_d}\right)$ where $m_{\rho^0} \approx m_{\pi^\pm}$	$\left(\frac{m_u}{m_d}\right)$ where non-deg. GMOR breaks down
6.9	1.144(5)	2.8(3)	3.0(2)
6.9	1.25(1)	4.4(4)	1.5(1)
6.9	1.46(4)	8(1)	1.8(5)
7.05	1.16(1)	2.7(3)	2.2(2)
7.05	1.29(2)	4.7(5)	1.7(2)
7.05	1.46(4)	6.8(8)	1.7(2)
7.2	1.17(1)	2.7(4)	4(1)
7.2	1.26(2)	4.4(7)	1.7(4)
7.2	1.37(4)	6(2)	4(2)

Table 4: The point at which a change in the meson mass hierarchy occurs and the point at which the non-degenerate GMOR relation breaks down at one-sigma significance. In general, this breakdown sets a stronger bound. Note that with increased statistics the breakdown of the non-degenerate GMOR can occur at even smaller PCAC-mass-ratios.

Lagrangian that lead to (214) no longer captures the underlying theory. This sets another upper bound on the validity of the non-degenerate GMOR relation. The non-degenerate GMOR relation holds true and the leading order Lagrangian might be an adequate description of strong isospin breaking in this theory at fixed $m_\rho/m_\pi \gtrsim 1.4$ at degeneracy. The tabulated upper limits can be found in table 4. Note that this is only an *upper bound* and the EFT might break down even earlier.

There are two reasons why the non-degenerate GMOR relation can break down: 1) The quark-mass-difference is too large in order for the system to be treated at leading order. In this case the next step would be to investigate this chiral Lagrangian at next-to-leading order in strong isospin breaking. 2) The average pseudo-Goldstone masses are in general too large to reliably use the GMOR relation at leading order even close to the mass-degenerate limit.

In any case, for small isospin breaking the non-degenerate GMOR relations do not break down immediately even for significantly heavier quarks than those used in the chiral extrapolation of [91]. It will be therefore already worthwhile to study this UV complete theory and the chiral Lagrangian at leading order in this region of parameter space.

3.4 Singlet Mesons in Symplectic Gauge Theories

In the context of SIMP DM models, singlet mesons can be of particular interest as they can decay into SM particles. The singlet meson spectrum of Sp(4) has never been studied previously. Most studies of singlet mesons have been performed in SU(3) gauge theory. Both

QCD like models with dynamically broken chiral symmetry and near-conformal theories have been studied in great detail. The pseudoscalar singlet has been studied in Refs. [71,146–157]. The determination of the mass (and width) of the lightest scalar singlet has proven to be particularly challenging and a number of studies in SU(3) with dynamical fermions exist both in the context of real-world QCD [73, 158–166] and more general field content [74, 77, 79, 81, 167–169].

Interpolating operators and singlet correlators

Two-quark operators are used for sourcing both singlet and non-singlet mesons. Due to the focus on moderately heavy fermions only quark-antiquark operators are used and for now no other operators are considered such as $\pi\pi$ operators, glueballs or even tetraquarks. In order to determine the mesonic spectrum both the connected and disconnected pieces need to be calculated and then fitted to the zero momentum correlator

$$C(t) = \sum_{\vec{n}} \langle O(\vec{n}, t) \bar{O}(\vec{0}, 0) \rangle \tag{215}$$

on a Euclidean time interval $(t_{\min}, t_{\max})$, where the ground state dominates and its energy and thus the mass can be extracted. The different components of $C(t)$ drop off exponentially with their energy as $\propto \exp(-E_n t)$ and thus at sufficiently large t only the ground state remains as all other states are exponentially suppressed. However, an additional constant term arises for both the η' and the σ meson. In the former case this is due to an insufficient topological sampling of the path integral and this constant vanishes in the continuum limit [170, 171]. For the scalar singlet σ it arises due to the fermion condensate and persists in the continuum limit for vanishing momenta. At large times the correlator $C(t)$ is then given by

$$\lim_{t\to\infty} C(t) = A\left(e^{-mt} + e^{-m(T-t)}\right) + \langle 0|O|0\rangle^2 \tag{216}$$

where the second exponential term is due to the lattice periodicity. While in the case of the η' this constant is small compared to the signal and only affects the correlator at large t this is not the case for the σ meson. This constant is multiple orders of magnitudes larger than the signal and its removal is a significant challenge. A numerical derivative as proposed in [172] is performed. Alternatively, the constant term $\langle 0|O|0\rangle^2$ could have been calculated directly and subsequently subtracted. A comparison with this method is performed in Sec. 3.4.4 [3].

[3]Other ways of subtracting the constant have been proposed recently. Specifically, the configuration-wise subtraction of the constant term to the scalar singlet by averaging over all Euclidean times t was used for

Ensemble	group	β	m_0	L	T	n_{conf}	n_{src}	$I_{\eta'}$	I_π	I_σ	$I_{\sigma^{\text{conn.}}}$	I_ρ	$\langle P \rangle$
SU2B1L1M8	SU(2)	2.0	-0.947	20	32	1020	300	-	(10, 16)	(5, 8)	(7, 10)	(10, 16)	0.56734(2)
SU2B1L1M7	SU(2)	2.0	-0.94	14	24	1851	192	(8, 12)	(8, 12)	-	-	(9, 12)	0.56516(3)
SU2B1L1M6	SU(2)	2.0	-0.935	16	32	951	256	(7, 11)	(9, 16)	-	-	(9, 16)	0.563654(28)
SU2B1L1M5	SU(2)	2.0	-0.93	14	24	1481	256	(7, 12)	(8, 12)	-	-	(9, 12)	0.56245(3)
SU2B1L1M4	SU(2)	2.0	-0.925	14	24	1206	192	(6, 10)	(8, 12)	-	-	(9, 12)	0.56119(3)
SU2B1L1M3	SU(2)	2.0	-0.92	12	24	2401	192	(6, 9)	(7, 12)	-	(6, 11)	(8, 12)	0.559983(29)
SU2B1L1M2	SU(2)	2.0	-0.9	12	24	500	128	(6, 9)	(7, 12)	-	-	(8, 12)	0.55571(6)
SU2B1L1M1	SU(2)	2.0	-0.88	10	20	2582	128	(5, 8)	(8, 10)	-	-	(9, 10)	0.55225(4)
Sp4B3L1M8	Sp(4)	7.2	-0.799	32	40	451	224	-	(15, 20)	(5, 9)	(11, 19)	(15, 20)	0.590862(5)
Sp4B3L1M7	Sp(4)	7.2	-0.794	28	36	504	288	(7, 12)	(10, 18)	-	(11, 16)	(11, 18)	0.590452(7)
Sp4B3L1M6	Sp(4)	7.2	-0.79	24	36	500	320	(7, 12)	(12, 18)	(5, 8)	(10, 16)	(13, 18)	0.590127(9)
Sp4B3L1M5	Sp(4)	7.2	-0.78	24	36	508	384	(6, 12)	(12, 18)	-	(11, 15)	(13, 18)	0.589278(8)
Sp4B3L1M4	Sp(4)	7.2	-0.77	24	36	200	384	(6, 11)	(11, 18)	-	(10, 15)	(12, 18)	0.588460(12)
Sp4B3L1M3	Sp(4)	7.2	-0.76	16	36	200	384	-	(11, 18)	(5, 8)	(9, 14)	(12, 18)	0.587666(25)
Sp4B1L1M7	Sp(4)	6.9	-0.924	24	32	492	320	-	(9, 16)	(4, 7)	(7, 10)	(10, 16)	0.56317(2)
Sp4B1L1M6	Sp(4)	6.9	-0.92	24	32	503	484	-	(7, 16)	(4, 9)	(8, 12)	(8, 16)	0.562075(13)
Sp4B1L2M6	Sp(4)	6.9	-0.92	16	32	176	128	(6, 10)	(9, 16)	(4, 10)	(7, 10)	(9, 16)	0.56212(5)
Sp4B1L1M5	Sp(4)	6.9	-0.91	16	32	435	256	(6, 11)	(8, 16)	-	(7, 9)	(9, 16)	0.55935(3)
Sp4B1L2M5	Sp(4)	6.9	-0.91	14	24	513	256	(5, 10)	(8, 12)	(4, 7)	(9, 12)	(9, 12)	0.55941(3)
Sp4B1L1M4	Sp(4)	6.9	-0.9	16	32	547	512	(6, 10)	(9, 16)	-	(7, 10)	(10, 16)	0.556921(25)
Sp4B1L2M4	Sp(4)	6.9	-0.9	14	24	942	128	(7, 10)	(8, 12)	(4, 9)	(7, 9)	(9, 12)	0.556981(26)
Sp4B1L3M4	Sp(4)	6.9	-0.9	12	24	2904	128	(6, 10)	(8, 12)	(4, 8)	(8, 10)	(9, 12)	0.557009(18)
Sp4B1L2M3	Sp(4)	6.9	-0.89	14	24	461	128	(7, 10)	(8, 12)	(5, 9)	(8, 11)	(9, 12)	0.55468(4)
Sp4B1L3M3	Sp(4)	6.9	-0.89	12	24	1019	320	(6, 10)	(8, 12)	(3, 6)	(7, 11)	(9, 12)	0.55467(3)
Sp4B1L2M2	Sp(4)	6.9	-0.87	12	24	1457	128	(7, 11)	(8, 12)	(5, 8)	(8, 10)	(9, 12)	0.550497(27)
Sp4B1L2M3	Sp(4)	6.9	-0.87	10	20	976	128	(6, 9)	(8, 10)	-	(6, 10)	(8, 10)	0.55068(5)

Table 5: List of all ensembles with degenerate fermion masses used in this work including the number of configurations n_{conf}, the number of the stochastic sources used in the approximation of the all-to-all quark propagator n_{src}, the intervals for fitting the resulting meson correlators I_{meson} and the average value of the plaquette $\langle P \rangle$. In some cases no clear plateau was identified in the effective masses and could not determine the singlet masses. In these cases no fit interval is reported. For the singlet mesons the interval quoted here was used to fit the correlators after subtracting the excited state contributions in the connected pieces and after performing a numerical derivative.

Ensemble	β	m_0^1	m_0^2	L	T	n_{conf}	n_{src}	$I_{\eta'}$	I_{π^0}	$I_{\pi^\pm}$	I_σ	$I_{\sigma^{\text{conn.}}}$	I_ρ	$\langle P \rangle$
Sp4B1L2M4ND1	6.9	-0.9	-0.89	14	24	300	64	(6, 9)	(2, 9)	(8, 14)	(4, 8)	(8, 14)	(8, 14)	0.55583(5)
Sp4B1L2M4ND2	6.9	-0.9	-0.88	14	24	191	128	(5, 9)	(3, 9)	(8, 14)	(4, 8)	(8, 14)	(8, 14)	0.55474(5)
Sp4B1L2M4ND3	6.9	-0.9	-0.87	14	24	400	128	-	(5, 8)	(8, 14)	(5, 8)	(8, 14)	(8, 14)	0.55361(4)
Sp4B1L2M4ND4	6.9	-0.9	-0.85	14	24	300	64	(5, 9)	(2, 9)	(8, 14)	(5, 8)	(8, 14)	(8, 14)	0.55163(4)
Sp4B1L2M4ND5	6.9	-0.9	-0.8	14	24	400	128	(5, 8)	(5, 9)	(8, 14)	-	(8, 14)	(8, 14)	0.54735(4)
Sp4B1L2M4ND6	6.9	-0.9	-0.75	12	24	264	64	(4, 7)	(3, 9)	(8, 12)	-	(8, 12)	(8, 12)	0.54395(6)
Sp4B1L2M4ND7	6.9	-0.9	-0.7	12	24	249	128	(5, 8)	(5, 9)	(8, 12)	-	(8, 12)	(8, 12)	0.54104(6)

Table 6: Same data as in table 5 for the non-degenerate ensembles.

The resulting correlator is the anti-periodic with respect to the midpoint $T/2$.

$$\tilde{C}(t) = \frac{1}{2}\left(C(t-1) - C(t+1)\right) \xrightarrow{t\to\infty} A \sinh(m)\left(e^{-mt} - e^{-m(T-t)}\right) \tag{217}$$

In order to determine the Euclidean time interval for fitting the effective mass $m_{\text{eff}}(t)$ defined in (164) is used. The interval $(t_{\min}, t_{\max})$ is determined by visually inspecting the effective mass and identifying a plateau at large times t. Restricting ourselves to ensembles where the plateau persists over four or more time slices, a fit of a single exponential term to the correlator $\tilde{C}(t)$ is performed. In Sec. 3.4.2 this method is compared to computing the additional constant $\langle 0|O|0\rangle^2$ directly without the use of a numerical derivative.

3.4.1 Variance reduction techniques

Both the connected and disconnected pieces in Eq. (138) need to be measured. The disconnected diagrams in particular are very noisy, and the signal is already lost at small to intermediate t where contaminations from excited states are non-negligible. A direct determination of the ground state mass at large t is thus not possible. This problem can be circumvented by removing the contributions of excited states in the singlet correlators manually. This is straightforward for the connected pieces. There, the signal for the connected pseudoscalar and vector mesons persists for all time slices t and in the case of the connected piece of the scalar meson a signal persists up to large t. At large times the correlator fit is performed (see Tabs. 5 and 6 for the choices of fit intervals) to a single exponential

$$C_{\text{conn}}^{1\text{exp}}(t) = A_0\left(e^{-m_{\text{conn}}t} + e^{-m_{\text{conn}}(T-t)}\right), \tag{218}$$

studying SU(3) close to the conformal window where the scalar singlet is expected to be light. This method was used on a particularly large and fine lattice and did not produce useful results for this use-case. [173]

and replace the full connected piece by the ground state correlator [174], where A_0 and $m_{\rm conn}$ are the fit parameters. The new singlet correlators are then

$$C^{\rm 1exp}_{\eta'}(t) = C^{\rm 1exp}_{\pi,\rm conn}(t) + C_{\eta',\rm disc.}(t)\,, \tag{219}$$
$$C^{\rm 1exp}_{\pi^0}(t) = C^{\rm 1exp}_{\pi,\rm conn}(t) + C_{\pi^0,\rm disc.}(t)\,, \tag{220}$$
$$C^{\rm 1exp}_{\sigma}(t) = C^{\rm 1exp}_{\sigma,\rm conn}(t) + C_{\sigma,\rm disc.}(t)\,. \tag{221}$$

The excited state contributions in the connected pieces are the dominant ones, and removing them shows a much earlier onset of a plateau in the effective masses. Sec. 3.4.5 shows that the results obtained by subtracting the connected excited state contributions through a fit at larger times produce the same results as using smeared operators, for the connected pieces with more overlap with the ground state.

The evaluation of disconnected pieces requires all-to-all propagators. In this thesis $Z_2 \times Z_2$ noisy sources with spin and even-odd dilution [128] were used. The connected pieces are evaluated using stochastic wall sources as discussed in Sec. 2.5.4. Uncertainties are estimated using the jackknife method – see Sec. 2.4.1.

3.4.2 Constant contributions to the correlators

In the beginning of section 3.4 the occurrence of constant terms in the propagators was noted of both the pseudoscalar singlet η' meson and the scalar singlet σ meson. This makes it difficult to determine when the excited states in the meson correlator are sufficiently suppressed and a fit can be performed. As shown in equations (216), this can be circumvented either by direct calculation of $\langle 0|O|0\rangle$ or by performing a numerical derivative. Once the interval $[t_i, t_f]$ where only the ground state contributes is known, a fit of the correlator to an exponentially decaying term plus a constant can be performed. In figure 13 an example of the correlator for the η' meson and the pseudo-Goldstone π are given. The flavour-singlet correlator shows a constant term at large Euclidean times while such a contribution is absent for the π meson. This is expected to occur for the disconnected pieces in a finite volume and at finite statistics if the topological sampling is insufficient [156, 170]. Then, the constant takes the form

$$\text{const} \propto \frac{1}{\mathrm{V}}\left(\frac{\mathrm{Q}^2}{\mathrm{V}} - \chi_{\mathrm{t}} - \frac{\mathrm{c}_4}{2\chi_{\mathrm{t}}\mathrm{V}}\right) + \mathcal{O}(\mathrm{V}^{-3}) + \mathcal{O}(\mathrm{e}^{-\mathrm{m}_\pi|\mathrm{x}|}). \tag{222}$$

A test of this relation was attempted by taking the ensemble with the largest statistics (corresponding to the bare parameters $m_0 = -0.90$, $\beta = 6.9$ on a 24×12^3 lattice) and measuring the topological charge Q using the same approach as in [91] and smooth the gauge

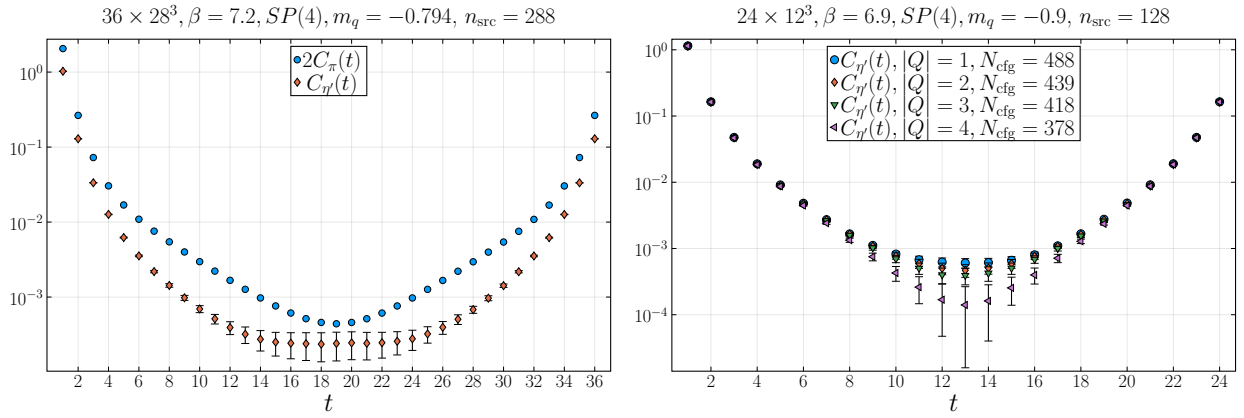

Figure 13: (left) Correlator of the pseudoscalar non-singlet π and the pseudoscalar singlet η'. At large times the singlet correlator shows a constant term, while this is absent for the non-singlet case. For visual clarity, twice the pion correlator is plotted. (right) Correlators of the pseudoscalar singlet for fixed values of the topological charge Q. The constant term shows signs of a dependence on Q. While the constant is not significantly different for any two examples shown here, the magnitude of the constant appears to be increasing with $|Q|$.

fields using the gradient flow. The test is performed by dividing the full statistics into sets of equal topological charge [4] and computing the pseudoscalar singlet η' correlator at fixed $|Q|$. Examples of the correlators for fixed Q with sufficient statistics are depicted in fig. 13. The constant term arising is sometimes statistically different for any pair of Q's present in this ensemble. A trend towards a constant with larger magnitudes for larger $|Q|$ as expected from Eq. (222) is observed.

3.4.3 Singlet Masses

The excited state contributions in the connected pieces were subtracted by fitting the connected diagram at large Euclidean times. A numerical derivative was performed to remove the constant term present both in the pseudoscalar and scalar singlet channels.

Pseudoscalar singlet in SU(2) and Sp(4) with $N_f = 2$

The results for the pseudoscalar singlet η' for degenerate fermions are tabulated in table 7. Plots are shown in figure 14. Only ensembles where $m_\pi L > 6$ were considered. In [91] it was found that for $m_\pi L \approx 6$ the finite volume effects are in the order of $1 - 2\%$ which is

[4] In practice, the topological charge is not strictly an integer on a finite lattice. Q is rounded to the closest integer.

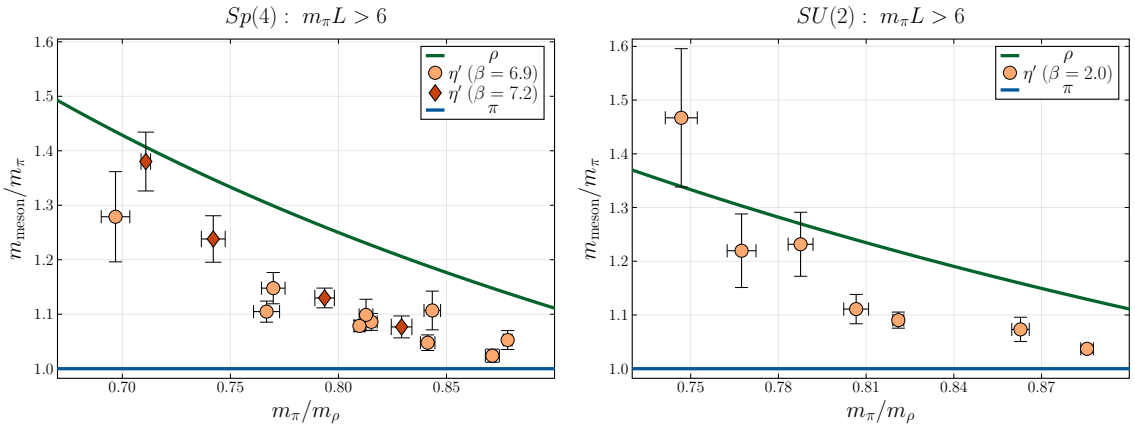

Figure 14: (left panel) Masses of the η' in Sp(4) gauge theory for two different lattice spacings corresponding to the two values of the inverse coupling $\beta = 6.9$ and 7.2. The pseudoscalar singlet is lighter than the vector mesons. For ensembles with lighter fermions no sufficiently good signal was found as to extract the mass of the pseudo-scalar singlet. The pseudoscalar singlet does not show significant spacing effects when expressed in units of the pseudo-Goldstone boson mass. (right panel) The same plot as above but in SU(2) gauge theory for a single lattice spacing. The same pattern is observed as in Sp(4). The green solid lines $m_\rho/m_\pi = 1/x$ are displayed for reference.

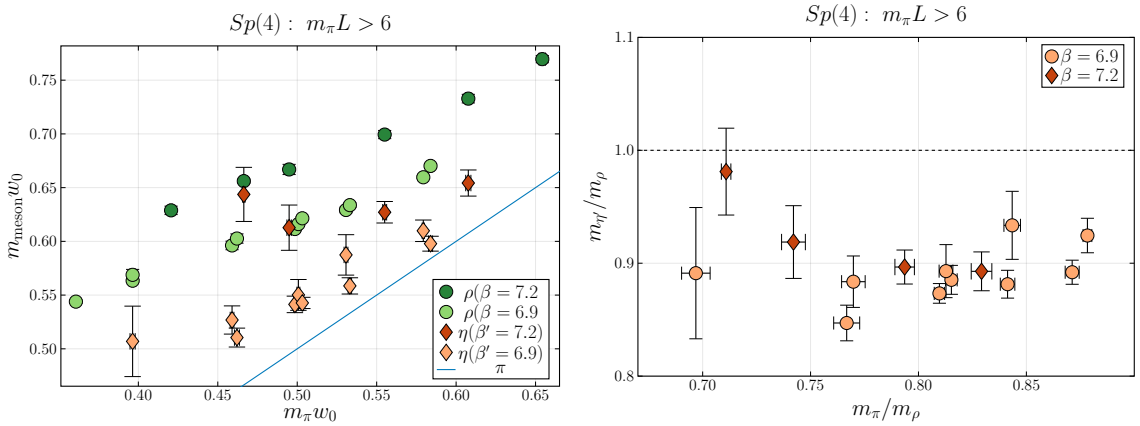

Figure 15: (left) Same data as in figure 14 but with the overall scale set using the gradient flow scale w_0 for two different values of the inverse coupling β. The larger value $\beta = 7.2$ corresponds to a lattice with a roughly 40% smaller lattice spacing than the ensembles at $\beta = 6.9$. Contrary to figure 14 clear finite spacing effects are visible. The absolute values quoted in this work are likely contaminated by finite spacing systematics while this is less pronounced for ratios of meson masses such as $m_{\eta'}/m_\pi$. The blue solid line $w_0 m_\pi = x$ is displayed for reference. (right) Mass ratio between of the vector mesons ρ and the scalar singlet η'.

significantly smaller than the uncertainties of the singlet meson masses in almost all cases. For a few ensembles the mass of the η' was determined to an accuracy of roughly 2%. In all these cases the considered volumes large enough to fulfil $m_\pi L > 7$ where the finite volume effects have been estimated to be at the sub-percent level [91]. The pseudoscalar singlet is always lighter than or compatible with the mass of the vector mesons. The results of the lightest ensembles is associated with larger statistical errors and the hierarchies between the pseudoscalar singlet and the vector mesons are not clearly resolved. For $\beta = 7.2$ the lattice spacing is approximately 40% smaller than for the coarser $\beta = 6.9$ ensembles [91]. The masses of the η' at different spacings agree within the quoted one sigma error bars when expressed in units of the pseudo-Goldstone mass. In [91] it was shown that the spacing effects can be generally large when the scale is set by employing the gradient flow scale. This indicates that some spacing effects cancel when considering only ratios of hadron masses. Figure 15 shows the results where an overall scale was set using a gradient flow scale w_0 and confirms that this behaviour persists for the η' meson. The spacing effects in the masses of the η' meson are not severe when expressed as a multiple of another meson mass, but the absolute values can still have sizeable finite spacing effects when expressed in terms of gradient flow scales. This suggests that leading finite size effects are similar for all mesons and thus cancel to some extent. For SU(2) the same mass hierarchy is seen both for the heavier and the lighter fermions. Only a single fairly coarse lattice is spacing considered here and the relevance of finite spacing effects is unclear.

Pseudoscalar singlets in Sp(4) with $N_f = 1 + 1$

For non-degenerate fermions the theory contains two singlet pseudoscalar mesons, the η' as before as well as the flavour-diagonal pseudo-Goldstone π^0. In the limit of degenerate quarks the π^0 becomes again a non-singlet which is degenerate with the other pseudo-Goldstone bosons as can be seen in (139). The meson masses are given in figure 16 and the tabulated results in table 8 which includes the mass of the neutral pion in a connected-only approximation obtained by dropping the last two terms in (138) denoted by $m_{\pi^0_c}$. For the $N_f = 1 + 1$ theory this approximation was already used in Sec. 3.3 and the results of the full π^0 allows a check of this approximation.

Consistent masses for the π^0 and η' are recovered as the degenerate limit is approached. As one fermion mass is increased the η' becomes lighter while the flavoured pseudo-Goldstones get heavier relative to the π^0 which is the lightest meson. This leads to an inversion of their hierarchy already at small relative pion mass differences $< 5\%$. When the mass of the heavier fermion is increased further the regime of a heavy-light system is approached and the mass

	β	m_0	L	T	$m_\pi L$	m_π/m_ρ	m_π	m_ρ	$m_{\eta'}$	m_σ
SU(2)	2.0	-0.947	20	32	7.47(3)	0.690(7)	0.3735(13)	0.540(5)	-	0.53(4)
SU(2)	2.0	-0.94	14	24	6.40(2)	0.746(6)	0.4576(14)	0.612(4)	0.67(6)	-
SU(2)	2.0	-0.935	16	32	7.91(2)	0.767(5)	0.4946(14)	0.644(4)	0.60(3)	-
SU(2)	2.0	-0.93	14	24	7.491(19)	0.787(4)	0.5350(14)	0.679(3)	0.65(3)	-
SU(2)	2.0	-0.925	14	24	7.999(19)	0.806(4)	0.5713(14)	0.708(3)	0.634(16)	-
SU(2)	2.0	-0.92	12	24	7.323(10)	0.8210(19)	0.6102(8)	0.7432(14)	0.665(9)	-
SU(2)	2.0	-0.9	12	24	8.620(17)	0.862(3)	0.7183(14)	0.832(2)	0.770(16)	-
SU(2)	2.0	-0.88	10	20	8.120(11)	0.885(2)	0.8120(11)	0.9169(19)	0.842(5)	-
Sp(4)	7.2	-0.799	32	40	8.087(16)	0.668(4)	0.2527(5)	0.377(2)	-	0.36(5)
Sp(4)	7.2	-0.794	28	36	8.072(11)	0.710(2)	0.2882(4)	0.4055(11)	0.397(16)	-
Sp(4)	7.2	-0.79	24	36	7.505(19)	0.742(6)	0.3127(8)	0.421(3)	0.387(13)	0.56(6)
Sp(4)	7.2	-0.78	24	36	8.882(17)	0.793(4)	0.3700(7)	0.466(2)	0.418(7)	-
Sp(4)	7.2	-0.77	24	36	10.16(2)	0.829(5)	0.4236(10)	0.510(3)	0.456(8)	-
Sp(4)	7.2	-0.76	16	36	7.544(17)	0.850(4)	0.4715(10)	0.554(2)	-	0.64(12)
Sp(4)	6.9	-0.924	24	32	8.208(12)	0.663(2)	0.3420(5)	0.5157(17)	-	0.46(3)
Sp(4)	6.9	-0.92	24	32	9.356(12)	0.7036(17)	0.3898(5)	0.5540(12)	-	0.42(2)
Sp(4)	6.9	-0.92	16	32	6.22(2)	0.696(7)	0.3889(14)	0.558(5)	0.49(3)	0.45(6)
Sp(4)	6.9	-0.91	16	32	7.817(19)	0.769(5)	0.4885(12)	0.634(4)	0.560(14)	-
Sp(4)	6.9	-0.91	14	24	6.86(2)	0.766(6)	0.4902(16)	0.639(5)	0.541(9)	0.41(3)
Sp(4)	6.9	-0.9	16	32	9.006(13)	0.815(3)	0.5629(8)	0.690(2)	0.611(9)	-
Sp(4)	6.9	-0.9	14	24	7.897(14)	0.812(3)	0.5641(10)	0.694(2)	0.619(16)	0.57(4)
Sp(4)	6.9	-0.9	12	24	6.796(9)	0.809(2)	0.5663(8)	0.6994(18)	0.610(6)	0.55(2)
Sp(4)	6.9	-0.89	14	24	8.813(19)	0.843(4)	0.6295(13)	0.746(3)	0.69(2)	0.57(9)
Sp(4)	6.9	-0.89	12	24	7.581(15)	0.841(3)	0.6318(12)	0.751(3)	0.661(9)	0.62(7)
Sp(4)	6.9	-0.87	12	24	8.925(10)	0.878(2)	0.7437(9)	0.8468(17)	0.782(13)	0.80(15)
Sp(4)	6.9	-0.87	10	20	7.470(16)	0.871(3)	0.7470(16)	0.857(3)	0.764(9)	-

Table 7: Results on the light spectrum with degenerate fermions including the singlet mesons. All dimensionful quantities are given in appropriate powers of the lattice spacing a. For the singlets a numerical derivative to subtract the constant term in the propagator was used. For the scalar singlet both a direct calculation of the term $\langle 0|O|0\rangle$ and a numerical derivative were performed. This produces equivalent result in almost all cases, while providing a better quality of fit for the rest of the ensembles. For details on the specific methods see appendix 3.4.2.

β	$m_0^{(1)}$	$m_0^{(2)}$	L	T	m_{π^0}	$m_{\pi^0_c}$	$m_{\pi^\pm}$	m_{ρ^0}	$m_{\rho^\pm}$	$m_{\eta'}$	m_σ
6.9	-0.9	-0.89	14	24	0.55583(5)	0.5968(18)	0.597(2)	0.596(2)	0.723(3)	0.45(6)	0.719(4)
6.9	-0.9	-0.88	14	24	0.55474(5)	0.6267(16)	0.6261(18)	0.628(2)	0.749(2)	0.51(8)	0.745(3)
6.9	-0.9	-0.87	14	24	0.55361(4)	0.6535(16)	0.6510(14)	0.6606(17)	0.7731(19)	0.69(14)	0.775(2)
6.9	-0.9	-0.85	14	24	0.55163(4)	0.6900(18)	0.6889(19)	0.709(2)	0.813(3)	0.51(12)	0.813(4)
6.9	-0.9	-0.8	14	24	0.54735(4)	0.761(2)	0.7563(16)	0.8277(18)	0.879(2)	-	0.922(3)
6.9	-0.9	-0.75	12	24	0.54395(6)	0.805(3)	0.803(4)	0.921(4)	0.927(6)	-	1.005(5)
6.9	-0.9	-0.7	12	24	0.54104(6)	0.840(4)	0.833(4)	0.996(3)	0.954(5)	-	1.073(5)

Table 8: Results on the light spectrum with non-degenerate fermions including the singlet mesons. All dimensionful quantities are given in appropriate powers of the lattice spacing a. The same methods for subtraction of the constant contributions as in the degenerate case are used. The mass of the neutral pseudo-Goldstone without the disconnected pieces $m_{\pi^0_c}$ is reported. This does not impact the results significantly.

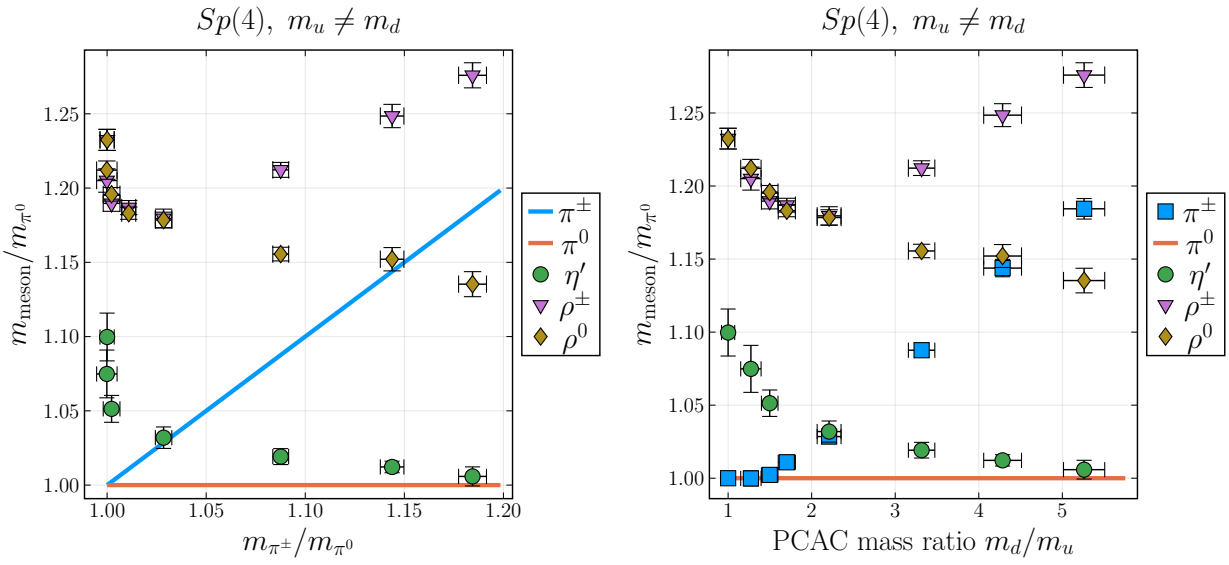

Figure 16: Masses of the η' with non-degenerate fermions at a fixed inverse coupling $\beta = 6.9$. The left panel shows the results as a function of the pion mass ratio and in the right panel as a function of the PCAC mass ratio. The solid blue line $m_{\pi^\pm}/m_{\pi^0} = x$ is displayed for reference. For quasi-degenerate fermions the results from the degenerate case are recovered. Already for small isospin breaking a change in hierarchy is observed where the η' meson gets lighter than the non-singlet pseudoscalars and the η' and π^0 become the lightest mesons. They become near-degenerate as the fermion masses is increased.

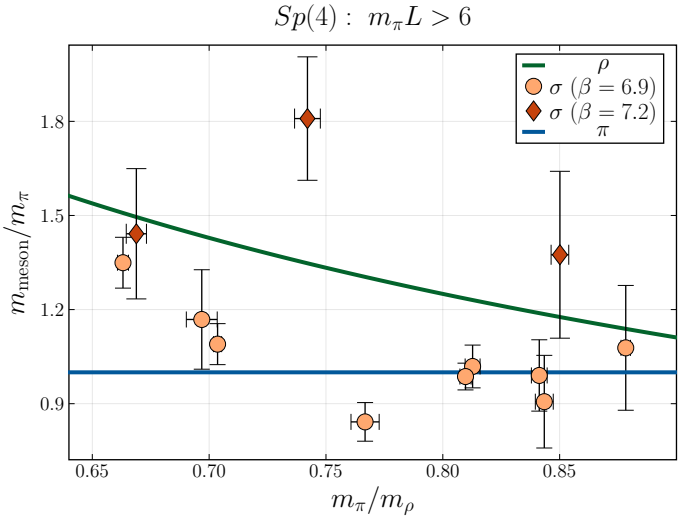

Figure 17: Masses of the σ with degenerate fermions in the Sp(4) theory. Strong signs of finite spacing effects are observed even when expressed as a ration of hadrons. On the coarser lattice the scalar singlet appears to be extremely light, in some cases even lighter than the pseudo-Goldstones. For the finer lattice this changes drastically and the scalar singlet σ is usually heavier than the vector meson but still below the two-pseudo-Goldstone threshold. The green solid lines $m_\rho/m_\pi = 1/x$ are displayed for reference.

difference between the η' and the π^0 decreases. They are then the lightest states of this theory (with the caveat being the unclear nature of the scalar singlet as discussed in sec. 3.4.3). This is consistent with the limit of an infinitely heavy fermion mass where only one light fermion remains and the employed operators of the π^0 and the η' source the same state [137].

Scalar singlet in Sp(4) with $N_f = 2$

In the case of the scalar singlet σ the signal is consistently worse even for different subtraction techniques. Furthermore, clear signs of finite spacing effects emerge – as shown in figure 17. For Sp(4) an extremely light state is observed on the coarse $\beta = 6.9$ lattices which is often even lighter than the pseudo-Goldstones. This pattern persists over the entire mass range considered here. On the finer lattices at $\beta = 7.2$ the mass of the σ increases and is consistently heavier than the pseudo-Goldstones and the vector meson. This suggests the existence of larger finite spacing effects that suppress the mass of the scalar singlet. Still, even for the finer lattice the state is lighter than its non-singlet counterpart. This signals that further studies are still needed, specifically on finer lattices or with (chirally) improved fermion actions. The scalar singlet might be a light meson at moderately heavy fermions well below the $2m_\pi$

threshold.

Comparison to SU(3) with $N_f = 2$

Figure 18 shows the available data published on the pseudoscalar singlet in SU(3) with $N_f = 2$. In some cases the measurement has been performed using different methods in the analysis or different operators have been used to study the same mesons (e.g. the mass of the η' has been obtained from pure gluonic operators as well as the usual fermionic operators or in the case of twisted mass fermions the non-singlet mesons include isospin breaking effects) and different sets of analysis results are available. The results that are closest to the standard determination of directly fitting the correlator of a pure fermionic operator have been used in this comparison. When this was not possible the largest and smallest values of the masses are quoted as $m_i \pm \Delta m_i$ for all measurements i and the uncertainties Δm_i are chosen to be symmetric. The data depicted in figure 18 has been taken from the UKQCD collaborations denoted by UKQCD1 [146, 147] and UKQCD2 [151]; the SESAM/TχL collaboration [148, 149]; the CP-PACS collaboration [150]; the RBC collaboration using domain-wall fermions [154]; the CLQCD collaboration using Wilson clover fermions on anisotropic lattices [155]; the ETMC collaboration denoted by ETMC1 [152, 153] and ETMC2 [71, 156] and from the analysis of $\eta'-$glueball mixing denoted by *Beijing* [157]. In all but the very lightest ensemble (and one obvious outlier at heavy fermions) the vector meson ρ was found to be lighter than the pseudoscalar singlet η'. The authors of [71] point out that in the lightest ensemble the ρ might be unusually light due to the small number of energy levels below the inelastic threshold in the determination of the $\pi\pi$ phase shift. It is lighter than their extrapolation to the physical point at which $m_\rho = 786(20)$ and even lighter than their extrapolation to the chiral limit. The mass dependence of the η' meson was found to be flat and an extrapolation in [156] to the physical point gave $m_{\eta'} = 772(18)$MeV. This is in contrast to SM QCD where the η' is significantly heavier – the current PDG lists $m_{\eta'}^{\mathrm{PDG}} = 957.78(6)$ MeV [17] which is in agreement with recent SU(3), $N_f = 2+1$ lattice results of $m_{\eta'} = 929.9\,(^{47.5}_{21.0})$ MeV [175]. The contribution of the s-quark that leads to the heavier mass. A quark model of the pseudoscalar singlet mesons based on approximate $\mathrm{SU}(3)_F$ flavour symmetry [176–178] was applied to early lattice results in [147]. In the regime of moderate and heavy fermion masses the SU(3) results are in agreement with the new Sp(4) and SU(2) lattice results, as depicted in the lower right panel in Fig. 18.

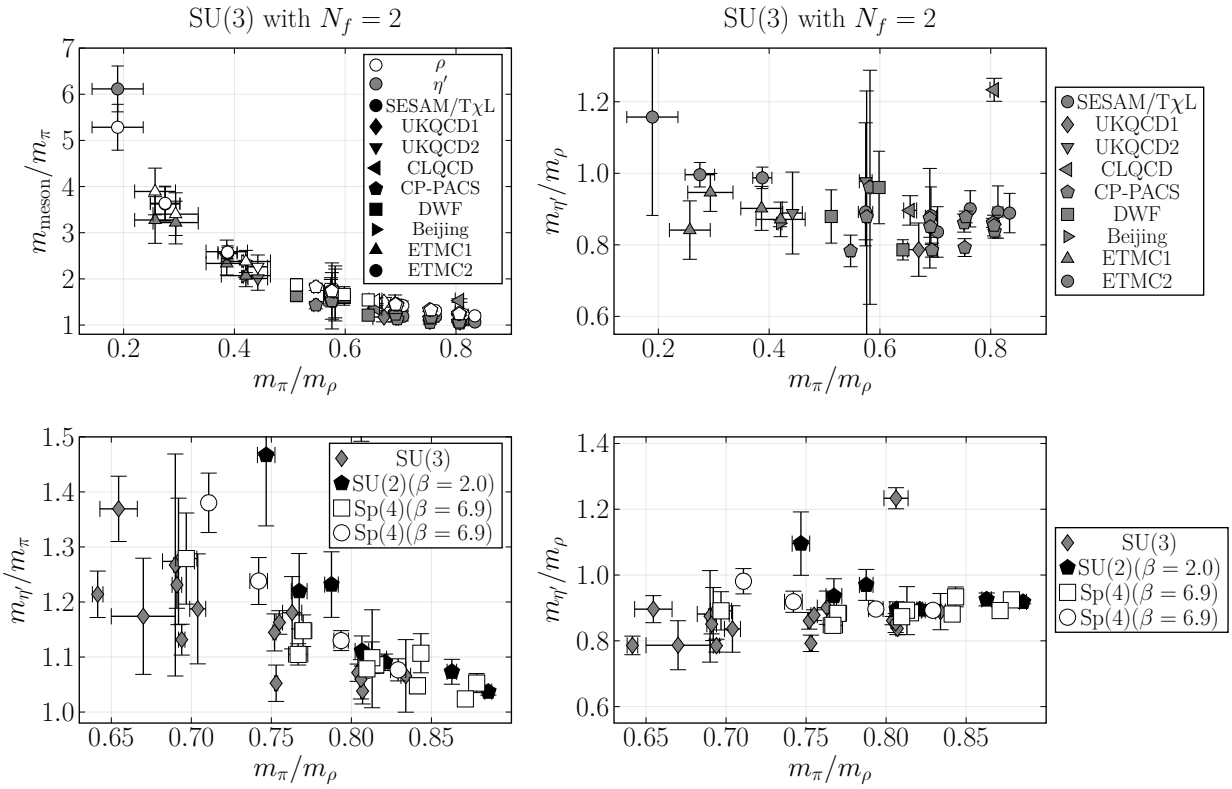

Figure 18: Comparison to the available lattice data in SU(3) with two fundamental fermions. The upper panels depict all available lattice results in SU(3). In the upper left panel the white markers denote the vector meson ρ and the grey ones the pseudoscalar singlet η'. The different marker shapes denote the different collaborations. The η' is lighter than the vector mesons almost everywhere. In the upper right panel the ratio $m_{\eta'}/m_\rho$ is plotted. The lower panels show the SU(3) results compared to the Sp(4) and SU(2) data. The lower left panel shows the ratio $m_{\eta'}/m_\pi$ as a function of m_π/m_ρ for values of $m_\pi/m_\rho \approx 0.7$ and larger. Different results of the ratio $m_{\eta'}/m_\rho$ are compared in the lower right plot.

3.4.4 Masses from different subtraction methods

In order to test the robustness of the subtraction choice, the mass of the pseudoscalar singlet η' for various techniques is reported. The results reported in section 3.4.3 are based on correlators where the connected part was modelled by a single sum of exponentials (216) taking lattice periodicity into account and removing the constant by a numerical derivative. In table 9 this is compared to four alternative methods: i) Direct calculation and subtraction of $\langle 0|O_{\eta'}|0\rangle$ ii) Ignoring the constant and restricting the fit to early time-slices iii) Performing a three-parameter fit of the decaying exponential plus a term modelling the constant. This procedure gives the numerical value of the constant as a by-product. As a check the constant was subtracted from the correlator a posteriori and the effective mass was examined for signs of a plateau. iv) Removing the constant using a numerical derivative but without any modelling of the connected part.

Whenever a signal without an explicit modelling of the connected pieces is obtained, the results agree within errors. The removal of excited state contamination leads to masses that are generally slightly lighter. The same pattern has been observed in SU(3) theory [156]. The explicit calculation of the constant $\langle 0|O_{\eta'}|0\rangle$ does not quantitatively capture the constant in the correlator. The results are almost indistinguishable from not taking the constant into account. For some ensembles (e.g. Sp(4) with $\beta = 7.2$) these methods appear to underestimate the meson's mass. This is a result from combining the modelling of the connected piece with an insufficient subtraction of the constant. Due to the absence of connected excited states in the correlator the effective mass is increasing at small t while for large t the constant leads to a decrease of the effective masses. This can lead to the formation of an apparent plateau in the effective mass and thus to a possibly severe underestimation of the meson's mass. The methods (*ii*) and (*iii*) do not appear sufficiently reliable. Modelling the constant as an additional fit parameter did not lead to any significant improvements. In most cases no reliable signal can be extracted. In the few cases where this is possible the constant term is quantitatively small and this method agrees with the others while providing no improvement at the cost of an additional fit parameter.

The method used throughout the main part of this work has proven to be the most reliable approach among the options considered here. Its results are always consistent with forgoing the explicit removal of subtracted states and the removal of the additional constant through derivative avoids any further estimations of the topological constant terms at the expense of a shorter plateau in the effective masses and thus, a smaller interval for fitting the correlator.

For the scalar singlet it is vastly different. The constant term is not related to an insufficient sampling of all topological sectors but arises due to the vacuum quantum numbers of

the scalar singlet. In addition, the modelling of the connected pieces is less important since the non-singlet state appears generally heavier than the singlet states and the connected pieces show a stronger exponential decay. In this case the direct estimation of the constant term $\langle 0|O_\sigma|0\rangle$ appears to be quantitatively reliable. Still, in some cases the modelling of the connected pieces can extend the plateau in the effective mass to lower timeslices t. Since the constant is several order of magnitude larger than the actual signal of the σ state a direct modelling of it as a fit parameter is infeasible and the constant can also not be ignored in the analysis. In table 10 approach used in the main part of this paper is compared to (i) using only a direct calculation of and (ii) using a numerical derivative without any modelling of the connected pieces.

3.4.5 Comparison between excited state subtraction and smeared connected diagrams

In Sect. 3.4.1 it was remarked that the signal of the singlet mesons can be extended to smaller time separations, t, if its connected contribution is replaced by approximating it with a single exponential term. Because the connected part corresponds to the flavoured mesons, the exponential is decaying with the energy of the non-singlet meson. This removes all the excited state contaminations of the connected piece.

A similar effect can be obtained by using smearing techniques on the connected piece. This can increase the overlap of the source operator with the ground state of the non-singlet and reduce the contribution of excited states. Recently, this approach has been implemented, tested, and shown to work in Sp(4) gauge theories [179]. These developments allow us to compare the excited-state subtraction technique.[5]

In order to compare the two techniques smearing was applied to only the connected piece. However, the use of smearing techniques leads to an overall change of normalization. Applying Wuppertal smearing [181] with N_1 steps at the source and N_2 steps at the sink leads to an asymptotic correlator of the form

$$C_{N_1,N_2}(t \to \infty) = \alpha_{N_1}\alpha_{N_2} e^{-m_{\mathrm{conn}} t}\,, \tag{223}$$

where the normalization of unsmeared point sources is recovered for the choice of the parameters $\alpha_{N_1} = \alpha_{N_2} = \alpha_0$. Two sets of correlators with the smearing steps $(N_1, N_2) = (N, 0)$ and $(N_1, N_2) = (N, N)$ were considered, to restore the normalization as the point source. A new

[5] I thank the authors of [179,180] for performing smeared measurements on a set of our configurations for comparison prior to publication.

	β	m_0	L	T	$m_{\eta'}$	$m_{\eta'}^{(\mathrm{i})}$	$m_{\eta'}^{(\mathrm{ii})}$	$m_{\eta'}^{(\mathrm{iii})}$	$m_{\eta'}^{(\mathrm{iv})}$
SU(2)	2.0	-0.947	20	32	-	-	-	-	-
SU(2)	2.0	-0.94	14	24	0.67(6)	0.699(14)	0.572(14)	-	0.67(6)
SU(2)	2.0	-0.935	16	32	0.60(3)	0.67(3)	0.61(5)	0.60(3)	-
SU(2)	2.0	-0.93	14	24	0.65(3)	-	-	-	0.68(5)
SU(2)	2.0	-0.925	14	24	0.634(16)	-	-	-	0.63(8)
SU(2)	2.0	-0.92	12	24	0.665(9)	-	-	-	0.66(3)
SU(2)	2.0	-0.9	12	24	0.770(16)	-	-	-	0.79(8)
SU(2)	2.0	-0.88	10	20	0.842(5)	0.855(14)	0.855(14)	-	-
Sp(4)	7.2	-0.799	32	40	-	0.37(2)	0.37(2)	-	0.57(6)
Sp(4)	7.2	-0.794	28	36	0.397(16)	0.368(12)	0.368(12)	-	0.47(7)
Sp(4)	7.2	-0.79	24	36	0.387(13)	-	-	-	0.36(6)
Sp(4)	7.2	-0.78	24	36	0.418(7)	0.43(2)	0.45(2)	-	0.43(5)
Sp(4)	7.2	-0.77	24	36	0.456(8)	0.450(6)	0.450(6)	0.459(7)	-
Sp(4)	7.2	-0.76	16	36	-	0.511(13)	0.512(13)	-	0.59(3)
Sp(4)	6.9	-0.924	24	32	-	-	-	-	0.60(8)
Sp(4)	6.9	-0.92	24	32	-	0.51(4)	0.52(4)	0.486(16)	0.40(6)
Sp(4)	6.9	-0.92	16	32	0.49(3)	0.46(2)	0.46(2)	0.50(2)	0.45(13)
Sp(4)	6.9	-0.91	16	32	0.560(14)	0.59(4)	0.59(4)	0.560(13)	0.59(4)
Sp(4)	6.9	-0.91	14	24	0.541(9)	0.58(3)	0.58(3)	-	-
Sp(4)	6.9	-0.9	16	32	0.611(9)	-	-	-	0.63(3)
Sp(4)	6.9	-0.9	14	24	0.619(16)	0.614(12)	0.615(12)	0.620(9)	0.63(3)
Sp(4)	6.9	-0.9	12	24	0.610(6)	0.620(15)	0.620(15)	0.612(5)	-
Sp(4)	6.9	-0.89	14	24	0.69(2)	0.680(16)	0.681(16)	0.69(2)	0.72(4)
Sp(4)	6.9	-0.89	12	24	0.661(9)	0.660(5)	0.660(5)	0.660(10)	-
Sp(4)	6.9	-0.87	12	24	0.782(13)	0.80(4)	0.80(4)	-	0.80(2)
Sp(4)	6.9	-0.87	10	20	0.764(9)	0.763(6)	0.763(6)	-	-

Table 9: Determination of the masses of the pseudoscalar singlets using different techniques for removing the constant term in the correlator. The method used in the main part of this work is compared to: i) Direct calculation and subtraction of $\langle 0|O_{\eta'}|0\rangle$ ii) Ignoring the constant and restricting the fit to early time-slices iii) Performing a three-parameter fit of the decaying exponential plus a term modelling the constant. iv) Removing the constant using a numerical derivative but without any modelling of the connected part.

	β	m_0	L	T	m_σ	$m_\sigma^{(i)}$	$m_\sigma^{(\mathrm{ii})}$	$m_\sigma^{(\mathrm{iii})}$
SU(2)	2.0	-0.947	20	32	0.53(4)	0.53(3)	0.58(5)	0.54(4)
SU(2)	2.0	-0.94	14	24	-	0.64(5)	0.61(4)	0.64(5)
SU(2)	2.0	-0.935	16	32	-	0.47(10)	0.55(8)	0.47(10)
SU(2)	2.0	-0.93	14	24	-	-	0.62(9)	-
SU(2)	2.0	-0.925	14	24	-	-	-	-
SU(2)	2.0	-0.92	12	24	-	0.71(7)	0.75(13)	0.72(7)
SU(2)	2.0	-0.9	12	24	-	-	-	-
SU(2)	2.0	-0.88	10	20	-	-	-	-
Sp(4)	7.2	-0.799	32	40	0.36(5)	0.35(8)	0.41(4)	0.38(8)
Sp(4)	7.2	-0.794	28	36	-	0.55(8)	-	0.55(8)
Sp(4)	7.2	-0.79	24	36	0.56(6)	0.56(6)	0.48(7)	0.65(12)
Sp(4)	7.2	-0.78	24	36	-	-	0.55(6)	-
Sp(4)	7.2	-0.77	24	36	-	-	-	-
Sp(4)	7.2	-0.76	16	36	0.64(12)	0.64(7)	-	-
Sp(4)	6.9	-0.924	24	32	0.46(3)	0.46(3)	0.45(3)	0.48(7)
Sp(4)	6.9	-0.92	24	32	0.42(2)	0.43(3)	0.45(3)	-
Sp(4)	6.9	-0.92	16	32	0.45(6)	0.40(8)	0.42(7)	0.37(11)
Sp(4)	6.9	-0.91	16	32	-	-	-	0.71(8)
Sp(4)	6.9	-0.91	14	24	0.41(3)	0.41(3)	-	-
Sp(4)	6.9	-0.9	16	32	-	-	-	-
Sp(4)	6.9	-0.9	14	24	0.57(4)	0.56(4)	0.48(5)	0.51(10)
Sp(4)	6.9	-0.9	12	24	0.55(2)	0.56(4)	-	0.57(3)
Sp(4)	6.9	-0.89	14	24	0.57(9)	0.56(9)	0.61(9)	0.59(9)
Sp(4)	6.9	-0.89	12	24	0.62(7)	-	0.64(4)	-
Sp(4)	6.9	-0.87	12	24	0.80(15)	0.76(11)	-	0.72(7)
Sp(4)	6.9	-0.87	10	20	-	0.70(6)	-	-

Table 10: Results on the masses of the scalar singlet σ using the standard approach of a numerical derivative as well as (i) a direct calculation of the vacuum term $\langle 0|O_\sigma|0\rangle$ and (ii) a numerical derivative without an explicit subtraction of excited states in the connected piece.

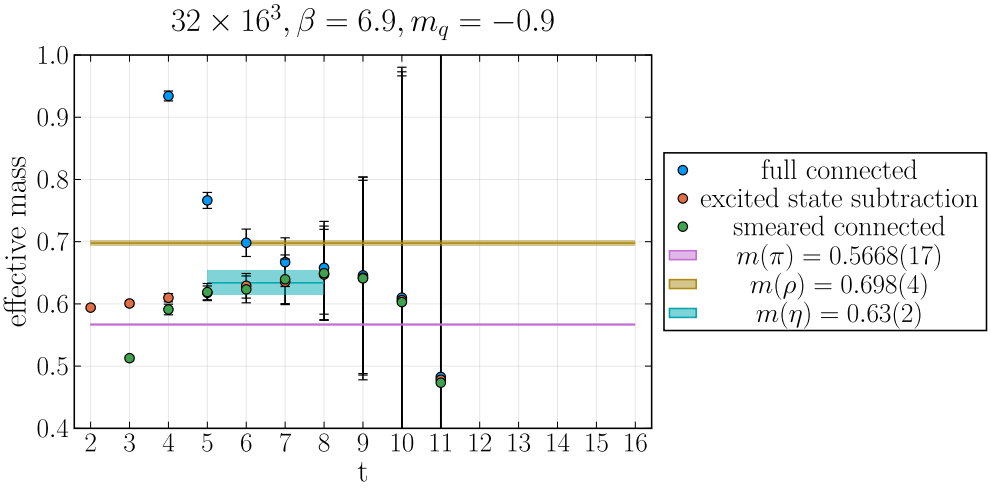

Figure 19: Comparison of excited state subtraction by modelling the connected part of the correlator as a single exponential term to smeared operators on a preliminary set of configurations for a single ensemble. Both methods of removing excited state contaminations agree remarkably well.

correlator was defined as

$$C^{\text{smeared}}_{\text{conn.}}(t) \equiv \frac{C_{N,0}(t)^2}{C_{N,N}(t)}\,, \tag{224}$$

by squaring the connected correlator with N steps of source smearing and no sink smearing and divide that by the connected correlator with an equal amount of smearing steps at both the source and the sink. This correlator has the same large-t behaviour and the same normalization as a non-smeared one. This allows a construction of the full correlator of the singlet meson. In Fig. 19 the full singlet correlator obtained from Eq. (224) was compared to using Wuppertal smearing with $N = 60$ smearing steps, to the correlator obtained using the single-exponential modelling and subtraction of the connected piece. The subtracted correlator and the smeared correlator agree remarkably well in the interesting, plateau region.

3.5 Dark Matter self-scattering: $\pi\pi$ scattering lengths

In Sec. 1.1.3 it was pointed out that self-interacting Dark Matter can address several small-scale structure problems, provided that the self-interaction strength of the 2DM $\to$ 2DM process is sufficiently strong while avoiding experimental constraints. A direct lattice determination can provide insight into the viability of the DM model. Furthermore, a lattice calculation allows a direct test of the chiral effective theory. General expressions for meson-meson scattering have been derived for every breaking pattern considered in 1.2.8. For the scattering length a_0^I chiral perturbation theory predicts for $N_f \geq 2$ mass-degenerate fermions [182]

$$m_\pi a_0^{I=0} = -\frac{m_\pi^2}{f_\pi^2}\left(\frac{4N_f-1}{32} - \frac{1}{32N_f}\right), \tag{225}$$

$$m_\pi a_0^{I=1} = -\frac{m_\pi^2}{f_\pi^2}\left(\frac{N_f-1}{48}\right), \tag{226}$$

$$m_\pi a_0^{I=2} = -\frac{m_\pi^2}{32f_\pi^2}. \tag{227}$$

As noted in Sec 2.5.2, the scattering processes at maximal isospin $I = 2$ are likely less noisy than the channels corresponding to isospin $I = 0, 1$. Furthermore, the isospin 2 channel does not contain any contributions from meson resonances since the associated representation is 14-dimensional and no meson state transforming under this representation exists. This is in contrast to the 10-dimensional representation of isospin $I = 1$ scattering where the vector mesons will contribute, and the singlet channel $I = 0$ scattering where the extremely noisy scalar singlet needs to be taken into account.

Thus, the scattering lengths at isospin 2 are a good starting point for investigations into PNGB scattering. The scattering length can be understood as the first order expansion in the scattering phase shift $\delta(k)$ in the momentum k. This has been recently applied to PNGB DM models with $I = 0$ self-scattering enhancement through the dark σ meson. The numerical determination of the scattering length can be seen in this context as a step towards the determination of the full phase shift via Lüscher's formalism [120, 122].

Numerically, the scattering lengths in SU(2) gauge theory with $N_f = 2$ have first been explored in [106]. As a proof of principle, the isospin 2 scattering length is studied on the ensemble with the highest available statistics given by the bare gauge coupling $\beta = 6.9$ and a degenerate, bare fermion mass $m_0 = -0.9$ on a 24×12^3 lattice. The energy shift $\delta E_{\pi\pi}$ is

extracted from the ratio of correlators [106]

$$R(t) = \frac{C_{\pi\pi}(t) - C_{\pi\pi}(t+1)}{C_\pi^2(t) - C_\pi^2(t+1)}. \tag{228}$$

At first, one would expect that it is sufficient to only consider the ratio of the single pion correlator C_π and the two-pion correlator $C_{\pi\pi}$ as

$$R(t) = \frac{C_{\pi\pi}(t)}{C_\pi^2(t)}, \tag{229}$$

since the correlator $C_{\pi\pi}$ gives the energy of two-interacting pions and C_π^2 gives the energy of two non-interaction dark pions. The ratio $R(t)$ at large times t should then be proportional to the mass difference that enters the determination of the scattering length in Eq. (134). However, as in the case of the singlets, an additional constant contribution to the two-pion correlator appears [172]. Similarly, as in Sec. 3.4 this can be removed by a numerical derivative. The choice in (228) ensures that both single-pion and two-pion correlator have the same symmetry with respect to the lattice mid-point $T/2$ and at large times t the ratio behaves as

$$R(t \to \infty) = A\left[\cosh\left(\delta E_{\pi\pi}(t - T/2)\right) + \sinh\left(\delta E_{\pi\pi}(t - T/2)\right) \coth\left(m_\pi(t - T/2)\right)\right]. \tag{230}$$

From this the energy difference $\delta E_{\pi\pi}$ can be extracted using (134) with coefficients $c_1 = -2.837$ and $c_2 = 6.375$ [121]. As a proof of principle, the scattering length is calculated for the ensemble with the highest available statistics. This corresponds to the 24×12^3 lattice with an inverse coupling of $\beta = 6.9$ and a bare, degenerate fermion mass of $m_0 = -0.90$ [3, 183]. A value of

$$\delta E_{\pi\pi} = -0.010(4), \tag{231}$$

has been obtained on this single ensemble [6]. This corresponds to a scattering length of

$$a_0^{I=2} = -0.6(3). \tag{232}$$

This is substantially lower than the prediction from chiral perturbation theory which suggests a value of $a_0^{\chi PT} = -1.6(3)$. Using $\sigma = \pi a_0^2$ the result is compared with experimental constraints on $\sigma/m_\pi^{phys.}$. The physical lattice spacing a was not yet fixed. From the experimental

[6] Note the different sign compared to the value reported in [3]

constraints $\sigma/m_\pi^{phys.} < 0.19\ \mathrm{cm}^2 g^{-1}$ [15] and $\sigma/m_\pi^{phys.} < 0.13\ \mathrm{cm}^2 g^{-1}$ [14] a lower limit for the physical dark pion mass of $m_\pi > 80$MeV is obtained. This is consistent with the constraints of the Dark Matter relic density [25] and thus provides a hint that the ensemble corresponds to a phenomenologically interesting points in parameter space. It is important to note, that this is only a rough lower bound. The mismatch between the direct calculation and chiral perturbation theory could be caused by the large fermion masses or by unaccounted for systematic effects. A larger value of the scattering length will increase the lower bound on the PNGB mass in physical units. This is particularly relevant, since the isospin $I = 0$ might have a larger magnitude of the scattering length as predicted by chiral perturbation theory (225).

Eventually, a full scattering analysis is needed. This result has been obtained only on a fixed volume for one lattice spacing and one (degenerate) fermion mass. More investigations on finer lattices with different physical volumes are needed. It was pointed out in Ref. [106] that finite volume effects are expected to be large in this system. The current constraints [14, 15] are so strong that the core-vs-cusp problem might not be resolved by a velocity-independent cross-section but that rather an explicit velocity dependence $\sigma(v)$ is needed. This further motivates going beyond a study of the scattering length to fully velocity-dependent $\pi\pi$ scattering.

Chapter 4

Summary and Conclusion

In this thesis the low-lying spectrum of Sp(4) gauge theory with two fundamental fermions has been calculated from first principles on the lattice. This is motivated by the models of SIMP Dark Matter [25–27] for which this theory is the simplest realization, with Sp(4) being the smallest non-SU(N) gauge group that can provide exactly five PNGBs which are needed for the $3 \to 2$ semi-annihilation process. The lattice results are crucial input parameters for the low-energy effective description of this theory as reviewed in Sec. 1.3.

For non-degenerate fermions the symmetry of the multiplets under the remaining $\mathrm{SU}(2)_u \times \mathrm{SU}(2)_d$ have been derived in Sec. 3.1. The PNGB five-plet π decomposes into a degenerate four-plet and a singlet for non-degenerate fermions. This has profound implications for this theory as a DM model as the singlet PNGB will no longer be protected from decay into the SM by flavour symmetry. Thus, a different mechanism needs to ensure that the singlet PNGB is sufficiently long-lived for setting the correct DM relic density via the $3 \to 2$ process in the SIMP model. This is not the case if mass-differences between PNGBs is induced by radiative corrections, where the five-plet can be split into a doublet and triplet as was shown in [2]. The ten-plet of vector mesons splits into a degenerate flavoured four-plet and an unflavoured six-plet – more specifically two triplets under the individual $\mathrm{SU}(2)_{u/d}$ symmetries. This multiplet also includes the state that would source the vector singlet ω in two-flavour QCD. Thus, no singlet vector meson appears as long as the theory is studied in isolation. This is different from QCD and two-flavour theories with complex fermion representations in general.

Numerically, the case for non-degenerate fermions was studied for moderately heavy fermions due to the increased computational cost compared to the degenerate case. It was found that the flavour-diagonal, singlet PNGB π^0 is the lightest state of the theory. Similarly, as in QCD, the flavoured PNGB states are heavier. The same pattern has been observed for the vector meson masses as well as both vector and pseudoscalar decay constants. No

sizeable finite volume effects were found for the meson masses and decay constants. The finite size effects of meson mass ratios were within statistical uncertainties. For the decay constant the finite size effects were of the order of 10% for the PNGBs and around 20% for the vector mesons. As caveat, it needs to be mentioned that the decay constants were renormalized using one-loop lattice perturbation theory and no non-perturbative approach was used. The lightest fermions used in this investigation correspond to a ratio of $m_\pi/m_\rho \approx 0.7$ in the degenerate limit. In [91] it was found that at this point the PNGB squared depends linearly on the fermion mass as predicted by LO chiral perturbation theory. The masses considered in this thesis are almost always heavier, and the EFT at leading order is not expected to hold. However, a consistency check of the construction for non-degenerate fermions was performed in Sec. 3.3.4 where it was found that the non-degenerate EFT breaks down at roughly a fermion mass ratio of 2. This does *not* guarantee that the EFT provides a correct description. Given the relatively heavy fermions is even unlikely to be applicable in this case. This consistency check shows that the construction can be adequate for small mass splitting. Still, a more thorough investigation at lighter fermion masses would be extremely illuminating. It would also be advantageous to test the EFT with quantities that do not need renormalization. A prime candidate for this would be PNGB scattering.

In Sec. 3.4 the singlet spectrum of two-flavour Sp(4) gauge theory was studied. This was the first determination of any singlet meson in any Sp($N_c \geq 4$). For the first time the mass hierarchy between the pseudoscalar singlet η' associated with the axial anomaly and the PNGBs was established in any symplectic gauge theory. For fermion masses corresponding to $m_\pi/m_\rho > 0.7$ it was found to be lighter than the vector mesons and relatively close to the other PNGBs for Sp(4). In SU(2) gauge theory the same pattern was observed for $m_\pi/m_\rho > 0.75$. For the lightest masses, the masses of the η' and the vector mesons are comparable within the relatively large uncertainties of the pseudoscalar singlets. The overall behaviour at intermediate to heavy fermion masses was found to be in agreement with the literature on two-flavour QCD. This suggests that this is a generic pattern of two-flavour theories. The agreement between SU(2), SU(3) and Sp(4) indicates that the behaviour of the η' meson differs significantly from the behaviour at small fermion masses where the mass difference between the PNGBs π and the η' is suppressed by $1/N_c$. It will be interesting to see if the expected scaling N_f persists in further dedicated lattice investigations. The singlet spectrum was also studied for non-degenerate fermions. For the relatively heavy fermion masses the connected-only approximation of the π^0 was found to be justified over the entire range of mass splittings studied. At some point this behaviour is expected to change when approaching the chiral limit but no signs of it have been observed for fermions as light as $m_\pi/m_\rho \approx 0.8$. For the scalar singlet signs of sizeable finite spacing effects have been observed

in Sp(4). On a coarse lattice the scalar singlet σ was often comparable or even lighter than the PNGBs, whereas on a finer lattice their masses were comparable to those of the vector mesons. It is unclear if the scalar singlet masses will be even heavier on finer lattices or if it remains a light meson that is kinematically protected from strong decays.

Further studies are needed to resolve its properties better. Given the challenging nature of the scalar singlet a multitude of improvements might be required. The standard Wilson action could be replaced by its $\mathcal{O}(a)$ improved version. Alternatively, a chiral fermion action which automatically includes $\mathcal{O}(a)$ improvement could be used. This would also pave the way for further studies closer to the chiral limit. The analysis could be improved by switching to a full variational analysis or to investigate the use of Bayesian approaches to correlator fitting.

Finally, an exploratory analysis of PNGB scattering has been performed in Sec. 3.5. It was found that the regime of moderately heavy fermions might be compatible with experimental constraints. However, a rather large number of caveats appear. First, this is based on only a single ensemble at a fixed volume and on a fixed lattice spacing. The contribution of discretization artefacts is completely unclear. Secondly, only the isospin channel $I = 2$ has been studied for purely technical convenience. For a correct comparison with experimental constraints the scattering information of all channels is needed. Given the predictions of chiral perturbation theory, the different channels *cannot* be assumed to be similar. Lastly, the scattering length only provide scattering information at vanishing velocity while a velocity dependent scattering cross-section might be preferred by astrophysics and a full determination of the scattering phase shift will be needed. Thus, this investigation can only be seen as a technical proof of principle towards a description of $\pi\pi \to \pi\pi$ and $\pi\pi\pi \to \pi\pi$ scattering on the lattice.

In summary, the low-lying spectrum of hadrons in two-flavour Sp(4) gauge theory was calculated for moderately heavy fermions. The determination of the mesonic masses and their decay constants provide crucial lattice input for further phenomenological investigations. The results highlight potentially important differences from SM QCD. A comparatively light pseudoscalar singlet was observed and in the case of non-degenerate fermions a change in mass hierarchy as a function of the fermion masses was observed. This all points towards the necessity to include non-PNGB states in phenomenological models. The results are a stepping stone towards more elaborate simulations of Sp($2N$) gauge theory on a finite lattice including meson spectroscopy at lighter fermion masses and the scattering of mesons. In light of all this, symplectic gauge groups with fermions remain a valid and interesting model of composite Dark Matter.

Appendix A

Definitions

A.1 Gamma and Pauli matrices

The Dirac γ matrices in Euclidean metric are defined through their anti-commutation relations

$$\{\gamma_\mu, \gamma_\nu\} = 2\delta_{\mu\nu}, \qquad \mu, \nu = 0, 1, 2, 3. \tag{233}$$

Additionally, the fifth gamma matrix is introduced as

$$\gamma_5 = \gamma_1\gamma_2\gamma_3\gamma_0. \tag{234}$$

It anti-commutes with all other γ_μ and similarly squares to $\mathbb{1}$. Using the Minkowski metric they obey $\left\{\gamma_\mu^M, \gamma_\nu^M\right\} = 2\eta_{\mu\nu}$, with $\eta_{\mu\nu} = \mathrm{diag}(1, -1, -1, -1)$. They are connected to Euclidean ones by $\gamma_i^M = i\gamma_i$ for the spatial gamma matrices with $i = 1, 2, 3$ while $\gamma_0 = \gamma_0^M$ holds for the temporal γ matrix. A particularly useful representation for the purposes of this thesis is the chiral representation, in which γ_5 is block-diagonal.

$$\gamma_1 = \begin{pmatrix} 0 & 0 & 0 & -i \\ 0 & 0 & -i & 0 \\ 0 & i & 0 & 0 \\ i & 0 & 0 & 0 \end{pmatrix} \quad \gamma_2 = \begin{pmatrix} 0 & 0 & 0 & -1 \\ 0 & 0 & 1 & 0 \\ 0 & 1 & 0 & 0 \\ -1 & 0 & 0 & 0 \end{pmatrix} \quad \gamma_3 = \begin{pmatrix} 0 & 0 & -i & 0 \\ 0 & 0 & 0 & i \\ i & 0 & 0 & 0 \\ 0 & -i & 0 & 0 \end{pmatrix}$$
$$\gamma_0 = \begin{pmatrix} 0 & 0 & 1 & 0 \\ 0 & 0 & 0 & 1 \\ 1 & 0 & 0 & 0 \\ 0 & 1 & 0 & 0 \end{pmatrix} \quad \gamma_5 = \begin{pmatrix} 1 & 0 & 0 & 0 \\ 0 & 1 & 0 & 0 \\ 0 & 0 & -1 & 0 \\ 0 & 0 & 0 & -1 \end{pmatrix}. \tag{235}$$

In this form they can be recast as block-diagonal matrices in terms of the Pauli matrices σ_i with $i = 1, 2, 3$ which are the generators of SU(2) satisfying $[\sigma_i, \sigma_j] = 2\epsilon_{ijk}\sigma_k$, where ϵ_{ijk} is the Levi-Civita symbol, and the Einstein summation convention is implied. Explicitly, they are given by

$$\sigma_1 = \begin{pmatrix} 0 & 1 \\ 1 & 0 \end{pmatrix} \quad \sigma_2 = \begin{pmatrix} 0 & -i \\ i & 0 \end{pmatrix} \quad \sigma_3 = \begin{pmatrix} 1 & 0 \\ 0 & -1 \end{pmatrix}. \tag{236}$$

The γ matrices in the chiral representation (235) can then be written as

$$\gamma_i = \begin{pmatrix} 0 & -i\sigma_i \\ i\sigma_i & 0 \end{pmatrix} \quad \gamma_0 = \begin{pmatrix} 0 & \mathbb{1}_{2\times 2} \\ \mathbb{1}_{2\times 2} & 0 \end{pmatrix} \quad \gamma_5 = \begin{pmatrix} \mathbb{1}_{2\times 2} & 0 \\ 0 & -\mathbb{1}_{2\times 2} \end{pmatrix}. \tag{237}$$

The charge conjugation operator C in general is defined as

$$C = \gamma_\mu C^{-1} = -\gamma_\mu^T, \tag{238}$$

and in the chiral representation it is explicitly given as

$$C = i\gamma_2\gamma_0. \tag{239}$$

A.2 Defining properties of $\mathrm{Sp}(2N)$

The fundamental representation of any $\mathrm{Sp}(2N)$ group is pseudo-real. The representation is isomorphic to its complex conjugate representation. This can be seen from the defining

property of the Sp($2N$) group: it is the subgroup of SU($2N$) that leaves

$$E = \begin{pmatrix} 0 & \mathbb{1}_N \\ -\mathbb{1}_N & 0 \end{pmatrix} \tag{240}$$

invariant. It consists of all SU($2N$) transformations that fulfil $U^* = EUE^\dagger$. Here the notation E for the invariant tensor in the context of $2p(2N)$ flavour symmetry is used. In the context of colour groups the invariant tensor is as S to make the context unambiguous. The following relations hold:

$$E^\dagger = E^{-1} = E^T = -E, \quad E^2 = -\mathbb{1}_{2N}. \tag{241}$$

On the level of the generators T^a using $U = \exp(i\alpha^a T^a)$ this is equivalent to

$$T^{a*} = -ET^aE^\dagger, \tag{242}$$

which fulfils the pseudo-reality condition (27).

A.3 SU(4) and Sp(4) generators

The generators with normalization $\mathrm{Tr}\{T^a T^b\} = \frac{1}{2}\delta^{ab}$ are given by [184]

$$
\begin{aligned}
T^1 &= \tfrac{1}{\sqrt{8}}\begin{pmatrix} 0 & 1 & 0 & 0 \\ 1 & 0 & 0 & 0 \\ 0 & 0 & 0 & 1 \\ 0 & 0 & 1 & 0 \end{pmatrix} \qquad
T^2 = \tfrac{1}{\sqrt{8}}\begin{pmatrix} 0 & -i & 0 & 0 \\ i & 0 & 0 & 0 \\ 0 & 0 & 0 & i \\ 0 & 0 & -i & 0 \end{pmatrix} \qquad
T^3 = \tfrac{1}{\sqrt{8}}\begin{pmatrix} 1 & 0 & 0 & 0 \\ 0 & -1 & 0 & 0 \\ 0 & 0 & 1 & 0 \\ 0 & 0 & 0 & -1 \end{pmatrix} \\
T^4 &= \tfrac{1}{\sqrt{8}}\begin{pmatrix} 0 & 0 & 0 & -i \\ 0 & 0 & i & 0 \\ 0 & -i & 0 & 0 \\ i & 0 & 0 & 0 \end{pmatrix} \qquad
T^5 = \tfrac{1}{\sqrt{8}}\begin{pmatrix} 0 & 0 & 0 & 1 \\ 0 & 0 & -1 & 0 \\ 0 & -1 & 0 & 0 \\ 1 & 0 & 0 & 0 \end{pmatrix} \qquad
T^6 = \tfrac{1}{\sqrt{8}}\begin{pmatrix} 0 & 0 & -i & 0 \\ 0 & 0 & 0 & -i \\ i & 0 & 0 & 0 \\ 0 & i & 0 & 0 \end{pmatrix} \\
T^7 &= \tfrac{1}{\sqrt{8}}\begin{pmatrix} 0 & 0 & 0 & -i \\ 0 & 0 & -i & 0 \\ 0 & i & 0 & 0 \\ i & 0 & 0 & 0 \end{pmatrix} \qquad
T^8 = \tfrac{1}{\sqrt{8}}\begin{pmatrix} 0 & -i & 0 & 0 \\ i & 0 & 0 & 0 \\ 0 & 0 & 0 & -i \\ 0 & 0 & i & 0 \end{pmatrix} \qquad
T^9 = \tfrac{1}{\sqrt{8}}\begin{pmatrix} 0 & 0 & -i & 0 \\ 0 & 0 & 0 & i \\ i & 0 & 0 & 0 \\ 0 & -i & 0 & 0 \end{pmatrix} \\
T^{10} &= \tfrac{1}{2}\begin{pmatrix} 0 & 0 & 1 & 0 \\ 0 & 0 & 0 & 0 \\ 1 & 0 & 0 & 0 \\ 0 & 0 & 0 & 0 \end{pmatrix} \qquad
T^{11} = \tfrac{1}{\sqrt{8}}\begin{pmatrix} 0 & 0 & 0 & 1 \\ 0 & 0 & 1 & 0 \\ 0 & 1 & 0 & 0 \\ 1 & 0 & 0 & 0 \end{pmatrix} \qquad
T^{12} = \tfrac{1}{2}\begin{pmatrix} 0 & 0 & 0 & 0 \\ 0 & 0 & 0 & 1 \\ 0 & 0 & 0 & 0 \\ 0 & 1 & 0 & 0 \end{pmatrix} \\
T^{13} &= \tfrac{1}{2\sqrt{2}}\begin{pmatrix} 0 & 1 & 0 & 0 \\ 1 & 0 & 0 & 0 \\ 0 & 0 & 0 & -1 \\ 0 & 0 & -1 & 0 \end{pmatrix} \qquad
T^{14} = \tfrac{1}{\sqrt{8}}\begin{pmatrix} 1 & 0 & 0 & 0 \\ 0 & -1 & 0 & 0 \\ 0 & 0 & -1 & 0 \\ 0 & 0 & 0 & 1 \end{pmatrix} \qquad
T^{15} = \tfrac{1}{\sqrt{8}}\begin{pmatrix} 1 & 0 & 0 & 0 \\ 0 & 1 & 0 & 0 \\ 0 & 0 & -1 & 0 \\ 0 & 0 & 0 & -1 \end{pmatrix}.
\end{aligned}
\tag{243}
$$

The totally antisymmetric structure constants $f^{a,b,c}$ of the $SU(4)$ group are defined as

$$
\left[T^a, T^b\right] = i f^{abc} T^c \tag{244}
$$

and all non-zero structure constants are given by

$$
f^{1,2,14} = f^{2,3,13} = f^{2,4,6} = f^{3,5,7} = -f^{1,3,8} = -f^{1,5,9} = -f^{3,4,11} = -f^{4,5,15} = \frac{1}{\sqrt{2}} \tag{245}
$$

$$
f^{1,4,10} = f^{2,5,10} = f^{2,5,12} = -f^{1,4,12} = \frac{1}{2}. \tag{246}
$$

The group $SU(4)$ has 15 generators and the subgroup Sp(4) has 10 generators. From (242) follows the relation

$$FT^a + (T^a)^T F = 0 \quad \text{for } a = 6, \ldots, 15 \tag{247}$$

for the generators of the Sp(4) subgroup while the other 5 generators satisfy

$$FT^a - (T^a)^T F = 0 \quad \text{for } a = 1, \ldots, 5. \tag{248}$$

Occasionally it is convenient to use another basis of the generators than the one in (243). A different basis of SU(4) and Sp(4) algebras is obtained by exchanging the second row with the third row and the second column with the third column. In this form, all generators are either block-diagonal or anti-block-diagonal where the different blocks are either the identity matrix $\mathbb{1}$ or one of the Pauli matrices σ_i,

$$\begin{aligned}
\tilde{T}^1 &= \frac{1}{2\sqrt{2}} \begin{pmatrix} 0 & \mathbb{1}_2 \\ \mathbb{1}_2 & 0 \end{pmatrix} & \tilde{T}^2 &= \frac{1}{2\sqrt{2}} \begin{pmatrix} 0 & -i\sigma_3 \\ i\sigma_3 & 0 \end{pmatrix} & \tilde{T}^3 &= \frac{1}{2\sqrt{2}} \begin{pmatrix} \mathbb{1}_2 & 0 \\ 0 & -\mathbb{1}_2 \end{pmatrix} \\
\tilde{T}^4 &= \frac{1}{2\sqrt{2}} \begin{pmatrix} 0 & -i\sigma_1 \\ i\sigma_1 & 0 \end{pmatrix} & \tilde{T}^5 &= \frac{1}{2\sqrt{2}} \begin{pmatrix} 0 & i\sigma_2 \\ -i\sigma_2 & 0 \end{pmatrix} & \tilde{T}^6 &= \frac{1}{2\sqrt{2}} \begin{pmatrix} \sigma_2 & 0 \\ 0 & \sigma_2 \end{pmatrix} \\
\tilde{T}^7 &= \frac{1}{2\sqrt{2}} \begin{pmatrix} 0 & \sigma_2 \\ \sigma_2 & 0 \end{pmatrix} & \tilde{T}^8 &= \frac{1}{2\sqrt{2}} \begin{pmatrix} 0 & -i\mathbb{1}_2 \\ i\mathbb{1}_2 & 0 \end{pmatrix} & \tilde{T}^9 &= \frac{1}{2\sqrt{2}} \begin{pmatrix} \sigma_2 & 0 \\ 0 & -\sigma_2 \end{pmatrix} \\
\tilde{T}^{10} &= \frac{1}{2} \begin{pmatrix} \sigma_1 & 0 \\ 0 & 0 \end{pmatrix} & \tilde{T}^{11} &= \frac{1}{2\sqrt{2}} \begin{pmatrix} 0 & \sigma_1 \\ \sigma_1 & 0 \end{pmatrix} & \tilde{T}^{12} &= \frac{1}{2} \begin{pmatrix} 0 & 0 \\ 0 & \sigma_1 \end{pmatrix} \\
\tilde{T}^{13} &= \frac{1}{2\sqrt{2}} \begin{pmatrix} 0 & \sigma_3 \\ \sigma_3 & 0 \end{pmatrix} & \tilde{T}^{14} &= \frac{1}{2\sqrt{2}} \begin{pmatrix} \sigma_3 & 0 \\ 0 & -\sigma_3 \end{pmatrix} & \tilde{T}^{15} &= \frac{1}{2\sqrt{2}} \begin{pmatrix} \sigma_3 & 0 \\ 0 & \sigma_3 \end{pmatrix}.
\end{aligned} \tag{249}$$

Then, the symplectic matrix F is written as

$$\tilde{F} = \begin{pmatrix} i\sigma_2 & 0 \\ 0 & i\sigma_2 \end{pmatrix}. \tag{250}$$

In this basis, all $\mathrm{SU}(2)_u \times \mathrm{SU}(2)_d$ generators and thus transformations are fully block-diagonal:

$$\begin{aligned}
\tilde{T}^1_u = \tilde{T}^{10} = \frac{1}{2}\begin{pmatrix}\sigma_1 & 0\\ 0 & 0\end{pmatrix}, \tilde{T}^2_u = \frac{(\tilde{T}^6 + \tilde{T}^9)}{\sqrt{2}} = \frac{1}{2}\begin{pmatrix}\sigma_2 & 0\\ 0 & 0\end{pmatrix}, \tilde{T}^3_u = \frac{(\tilde{T}^{14} + \tilde{T}^{15})}{\sqrt{2}} = \frac{1}{2}\begin{pmatrix}\sigma_3 & 0\\ 0 & 0\end{pmatrix},\\
\tilde{T}^1_d = \tilde{T}^{12} = \frac{1}{2}\begin{pmatrix}0 & 0\\ 0 & \sigma_1\end{pmatrix}, \tilde{T}^2_d = \frac{(\tilde{T}^6 - \tilde{T}^9)}{\sqrt{2}} = \frac{1}{2}\begin{pmatrix}0 & 0\\ 0 & \sigma_2\end{pmatrix}, \tilde{T}^3_d = \frac{(\tilde{T}^{15} - \tilde{T}^{14})}{\sqrt{2}} = \frac{1}{2}\begin{pmatrix}0 & 0\\ 0 & \sigma_3\end{pmatrix}.
\end{aligned} \tag{251}$$

Another useful basis can be obtained by considering the matrix of the Goldstone bosons in (48) as well as the matrices of the spin-1 states in (62). Requiring that all off-diagonal elements contain only one field defines a new basis as

$$\begin{aligned}
&T^A = \frac{1}{\sqrt{2}}\left(T^1 - iT^2\right) && T^B = \frac{1}{\sqrt{2}}\left(T^1 + iT^2\right) && T^C = T^3\\
&T^D = \frac{1}{\sqrt{2}}\left(T^5 - iT^4\right) && T^E = \frac{1}{\sqrt{2}}\left(T^5 + iT^4\right) && T^F = T^{10} - \frac{i}{\sqrt{2}}\left(T^6 + T^9\right)\\
&T^G = \frac{1}{\sqrt{2}}\left(T^{11} - iT^7\right) && T^H = \frac{1}{\sqrt{2}}\left(T^{13} - iT^8\right) && T^I = T^{12} - \frac{i}{\sqrt{2}}\left(T^6 - T^9\right)\\
&T^J = -T^{10} - \frac{i}{\sqrt{2}}\left(T^6 + T^9\right) && T^K = \frac{-1}{\sqrt{2}}\left(T^{11} + iT^7\right) && T^L = -T^{12} - \frac{i}{\sqrt{2}}\left(T^6 - T^9\right)\\
&T^M = \frac{1}{\sqrt{2}}\left(T^{13} + iT^8\right) && T^N = T^{14} && T^O = T^{15}.
\end{aligned} \tag{252}$$

Appendix B

States and Sp(4) multiplets

The meson spin-0 and spin-1 fermion bilinears have already been constructed in [29]. They have the same structure as those appearing in a $N_f = 1$ theory [137]. For completeness table 11 gives the operators that source the $J^D = 0^-, 1^+$ and 1^- multiplets of Sp(4), i.e. the pseudoscalars, axial-vectors and vectors constructed from the generators in the basis of (243) and (252), respectively. The other spin-0 and spin-1 states are the scalar 5-plet as well as the scalar flavour singlet which differ from the flavour structure of the pseudoscalars only by the extra γ_5 in the bilinears.

	$-\Psi^T SCT^n E\Psi + \bar{\Psi} E T^n SC\bar{\Psi}^T$		$-\Psi^T SCT^N E\Psi + \bar{\Psi} E T^N SC\bar{\Psi}^T$	J^P	J^D
π_1	$\frac{1}{\sqrt{2}}\left(\bar{u}\gamma_5 d + \bar{d}\gamma_5 u\right)$	π^A	$\bar{u}\gamma_5 d$	0^-	0^-
π_2	$\frac{i}{\sqrt{2}}\left(\bar{d}\gamma_5 u - \bar{u}\gamma_5 d\right)$	π^B	$\bar{d}\gamma_5 u$	0^-	0^-
π_3	$\frac{1}{\sqrt{2}}\left(\bar{u}\gamma_5 u - \bar{d}\gamma_5 d\right)$	π^C	$\frac{1}{\sqrt{2}}\left(\bar{u}\gamma_5 u - \bar{d}\gamma_5 d\right)$	0^-	0^-
π_4	$\frac{i}{\sqrt{2}}\left(\bar{d}\gamma_5 SC\bar{u}^T - d^T SC\gamma_5 u\right)$	π^D	$\bar{d}\gamma_5 SC\bar{u}^T$	0^+	0^-
π_5	$\frac{1}{\sqrt{2}}\left(\bar{d}\gamma_5 SC\bar{u}^T + d^T SC\gamma_5 u\right)$	π^E	$d^T SC\gamma_5 u$	0^+	0^-

	$-\Psi^T SCT^0 E\Psi + \bar{\Psi} E T^0 SC\bar{\Psi}^T$		$-\Psi^T SCT^0 E\Psi + \bar{\Psi} E T^0 SC\bar{\Psi}^T$	J^P	J^D
η'	$\frac{1}{\sqrt{2}}\left(\bar{u}\gamma_5 u + \bar{d}\gamma_5 d\right)$	η'	$\frac{1}{\sqrt{2}}\left(\bar{u}\gamma_5 u + \bar{d}\gamma_5 d\right)$	0^-	0^-

	$2\bar{\Psi} T^n \gamma_\mu \Psi$		$2\bar{\Psi} T^N \gamma_\mu \Psi$	J^P	J^D
ρ_1	$\frac{1}{\sqrt{2}}\left(\bar{u}\gamma_\mu\gamma_5 d + \bar{d}\gamma_\mu\gamma_5 u\right)$	a^A	$\bar{d}\gamma_\mu\gamma_5 u$	1^+	1^+
ρ_2	$\frac{i}{\sqrt{2}}\left(\bar{d}\gamma_\mu\gamma_5 u - \bar{u}\gamma_\mu\gamma_5 d\right)$	a^B	$\bar{u}\gamma_\mu\gamma_5 d$	1^+	1^+
ρ_3	$\frac{1}{\sqrt{2}}\left(\bar{u}\gamma_\mu\gamma_5 u - \bar{d}\gamma_\mu\gamma_5 d\right)$	a^C	$\frac{1}{\sqrt{2}}\left(\bar{u}\gamma_\mu\gamma_5 u - \bar{d}\gamma_\mu\gamma_5 d\right)$	1^+	1^+
ρ_4	$\frac{i}{\sqrt{2}}\left(\bar{d}SC\gamma_\mu\gamma_5\bar{u}^T - d^T SC\gamma_\mu\gamma_5 u\right)$	a^D	$d^T SC\gamma_\mu\gamma_5 u$	1^-	1^+
ρ_5	$\frac{1}{\sqrt{2}}\left(\bar{d}SC\gamma_\mu\gamma_5\bar{u}^T + d^T SC\gamma_\mu\gamma_5 u\right)$	a^E	$\bar{d}\gamma_\mu\gamma_5 SC\bar{u}^T$	1^-	1^+

	$2\bar{\Psi} T^n \gamma_\mu \Psi$		$2\bar{\Psi} T^N \gamma_\mu \Psi$	J^P	J^D
ρ_6	$\frac{i}{\sqrt{2}}\big(\bar{u}\gamma_\mu SCP_L\bar{u}^T + u^T SC\gamma_\mu P_L u$ $+\bar{d}\gamma_\mu SCP_L\bar{d}^T + d^T SC\gamma_\mu P_L d\big)$	ρ^F	$u^T SC\gamma_\mu P_L u$	1^+	1^-
ρ_7	$\frac{i}{\sqrt{2}}\left(\bar{u}\gamma_\mu SC\bar{d}^T + u^T SC\gamma_\mu d\right)$	ρ^G	$u^T SC\gamma_\mu d$	1^+	1^-
ρ_8	$\frac{i}{\sqrt{2}}\left(-\bar{u}\gamma_\mu d + \bar{d}\gamma_\mu u\right)$	ρ^H	$\bar{d}\gamma_\mu u$	1^-	1^-
ρ_9	$\frac{i}{\sqrt{2}}\big(\bar{u}\gamma_\mu SCP_L\bar{u}^T + u^T SC\gamma_\mu P_L u$ $-\bar{d}\gamma_\mu SCP_L\bar{d}^T - d^T SC\gamma_\mu P_L d\big)$	ρ^I	$d^T SC\gamma_\mu P_L d$	1^+	1^-
ρ_{10}	$u^T SC\gamma_\mu P_L u - \bar{u}\gamma_\mu SCP_L\bar{u}^T$	ρ^J	$\bar{u}\gamma_\mu SCP_L\bar{u}^T$	1^+	1^-
ρ_{11}	$\frac{1}{\sqrt{2}}\left(-\bar{u}\gamma_\mu SC\bar{d}^T + u^T SC\gamma_\mu d\right)$	ρ^K	$\bar{u}\gamma_\mu SC\bar{d}^T$	1^+	1^-
ρ_{12}	$d^T SC\gamma_\mu P_L d - \bar{d}\gamma_\mu SCP_L\bar{d}^T$	ρ^L	$\bar{d}\gamma_\mu SCP_L\bar{d}^T$	1^+	1^-
ρ_{13}	$\frac{1}{\sqrt{2}}\left(\bar{u}\gamma_\mu d + \bar{d}\gamma_\mu u\right)$	ρ^M	$\bar{u}\gamma_\mu d$	1^-	1^-
ρ_{14}	$\frac{1}{\sqrt{2}}\left(\bar{u}\gamma_\mu u - \bar{d}\gamma_\mu d\right)$	ρ^N	$\frac{1}{\sqrt{2}}\left(\bar{u}\gamma_\mu u - \bar{d}\gamma_\mu d\right)$	1^-	1^-
ρ_{15}	$\frac{1}{\sqrt{2}}\left(\bar{u}\gamma_\mu u + \bar{d}\gamma_\mu d\right)$	ρ^O	$\frac{1}{\sqrt{2}}\left(\bar{u}\gamma_\mu u + \bar{d}\gamma_\mu d\right)$	1^-	1^-

Table 11: Fermion bilinears of the $J^D = 0^-, 1^\pm$ meson multiplets constructed from the generators in the basis of (243) (left) and (252) (right) respectively. In addition, the J^P quantum numbers are shown.

Appendix C

Tabulated results and additional plots

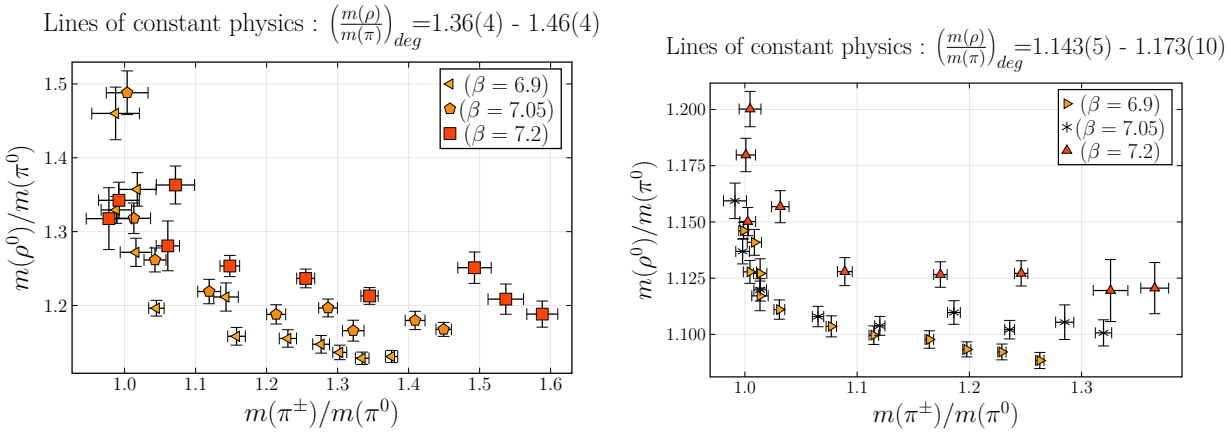

Figure 20: Ratio of the flavour-neutral vector and pseudoscalar mesons against the pseudoscalar mesons' mass ratio for the ensembles not depicted in Sec. 3.3.3.

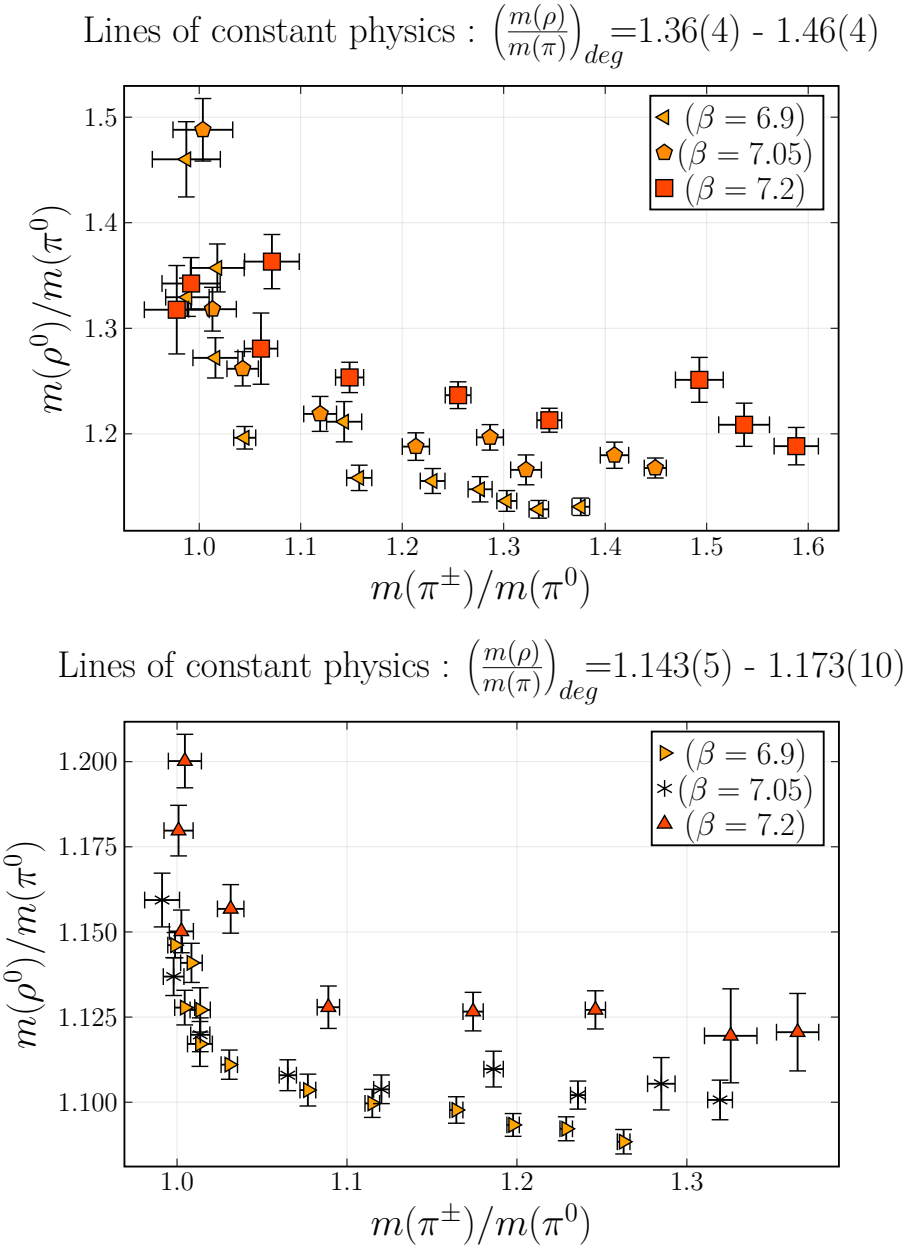

Figure 21: Ratio of the flavour-neutral vector and pseudoscalar mesons against the pseudoscalar mesons' mass ratio for the ensembles not depicted in Sec. 3.3.3.

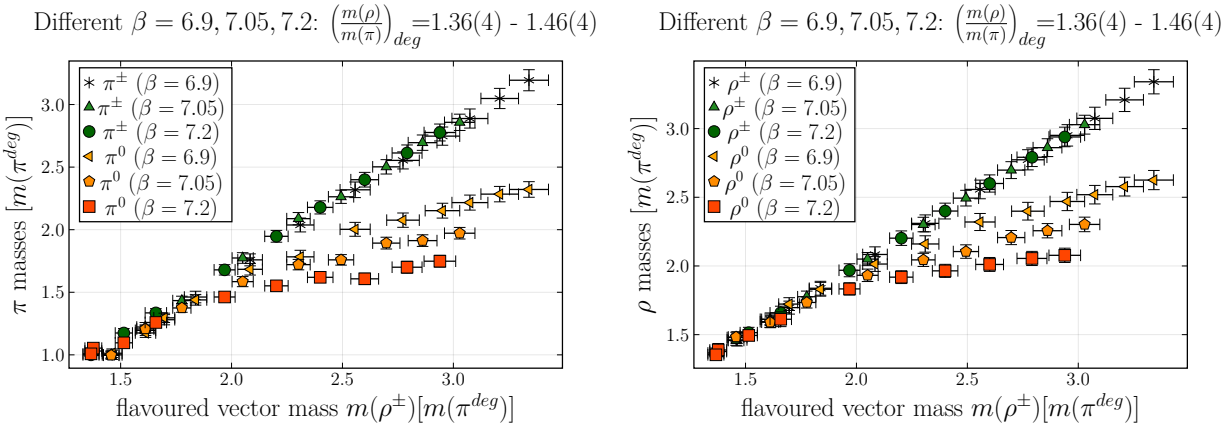

Figure 22: Masses of the pseudo-Goldstones (left) and vector mesons (right) for different values of the inverse coupling β in units of the pseudo-Goldstone mass degeneracy for the set of ensembles with comparatively heavy fermions .

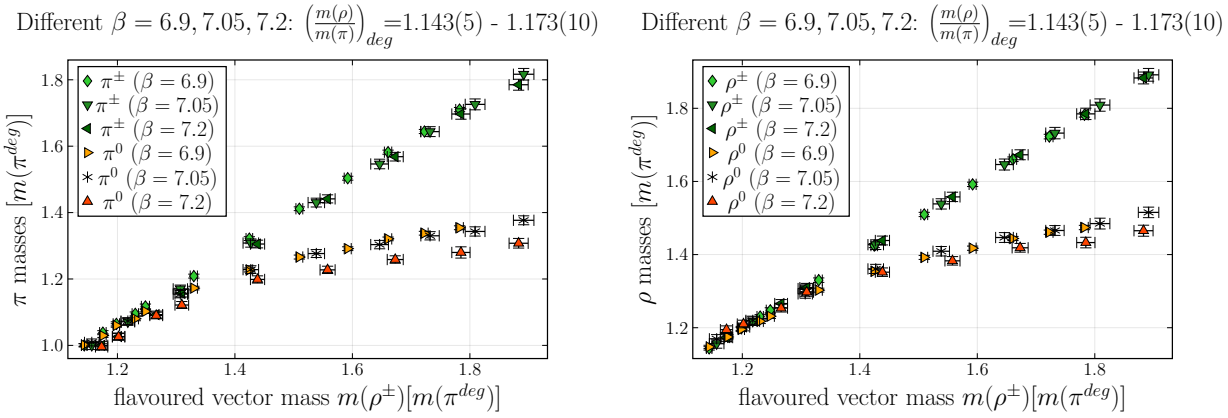

Figure 23: Masses of the pseudo-Goldstones (left) and vector mesons (right) for different values of the inverse coupling β in units of the pseudo-Goldstone mass degeneracy for the set of ensembles with comparatively heavy fermions .

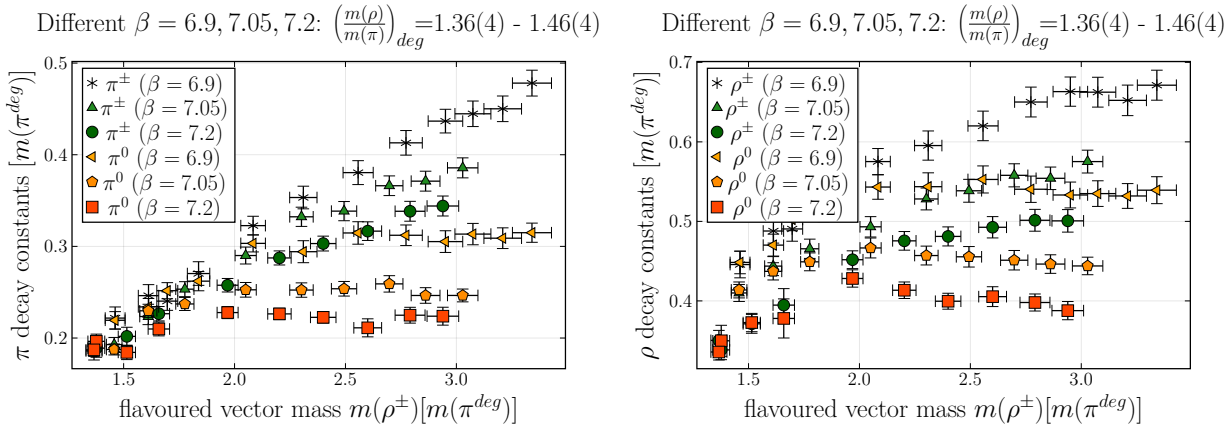

Figure 24: Decay constants of the pseudo-Goldstones and vector mesons for different values of the inverse coupling β in units of the pseudo-Goldstone mass degeneracy for the set of ensembles with comparatively light fermions.

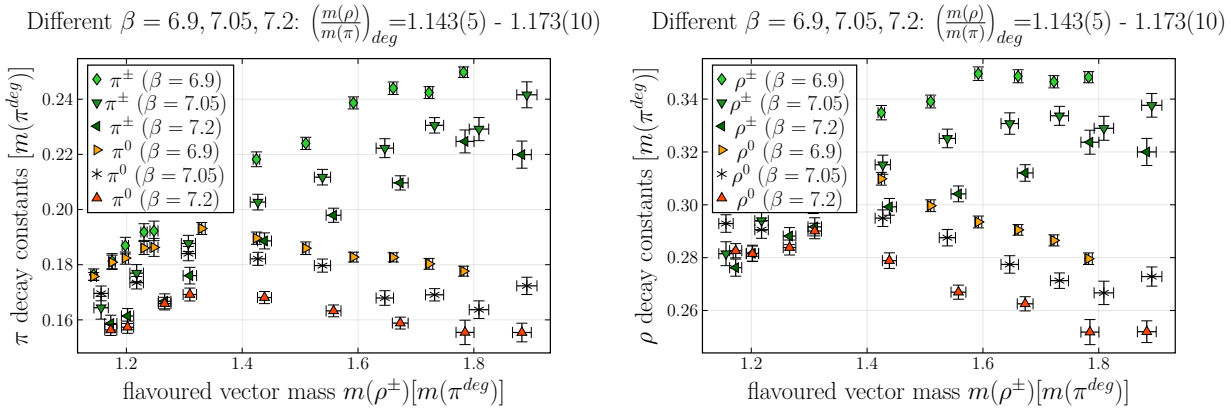

Figure 25: Decay constants of the pseudo-Goldstones and vector mesons for different values of the inverse coupling β in units of the pseudo-Goldstone mass degeneracy for the set of ensembles with comparatively light fermions.

β	T	L	am_u^0	am_d^0	$\langle P \rangle$	$am(\pi^A)$	$am(\pi^C)$	$af(\pi^A)$	$af(\pi^C)$	$am(\rho^M)$	$am(\rho^N)$	$af(\rho^M)$	$af(\rho^N)$	$a\bar{m}_{\mathrm{PCAC}}$
6.9	24	12	-0.9	-0.5	0.5333(2)	1.228(3)	0.930(3)	0.179(2)	0.129(2)	1.284(2)	1.028(3)	0.254(2)	0.208(2)	0.372(7)
6.9	24	12	-0.9	-0.55	0.5345(2)	1.181(2)	0.912(3)	0.177(2)	0.124(2)	1.239(2)	1.018(3)	0.253(2)	0.206(2)	0.340(6)
6.9	24	12	-0.9	-0.6	0.53655(8)	1.122(1)	0.891(2)	0.173(1)	0.1229(9)	1.185(1)	0.996(2)	0.252(1)	0.205(1)	0.306(3)
6.9	24	12	-0.9	-0.65	0.5386(1)	1.056(3)	0.868(3)	0.162(2)	0.122(2)	1.132(3)	0.980(3)	0.249(2)	0.210(2)	0.270(6)
6.9	24	14	-0.9	-0.7	0.54098(8)	0.993(2)	0.849(2)	0.160(1)	0.126(1)	1.070(1)	0.959(2)	0.247(1)	0.213(1)	0.236(3)
6.9	24	14	-0.9	-0.75	0.54393(8)	0.920(2)	0.820(2)	0.155(1)	0.128(1)	1.005(2)	0.929(2)	0.245(1)	0.218(1)	0.200(3)
6.9	24	14	-0.9	-0.8	0.54736(8)	0.826(2)	0.769(2)	0.142(1)	0.126(1)	0.921(2)	0.882(2)	0.233(1)	0.218(1)	0.163(3)
6.9	24	14	-0.9	-0.85	0.55163(7)	0.713(2)	0.695(2)	0.128(1)	0.123(1)	0.823(2)	0.812(2)	0.219(1)	0.217(1)	0.122(3)
6.9	24	14	-0.9	-0.86	0.5523(1)	0.694(3)	0.682(3)	0.124(2)	0.122(1)	0.805(2)	0.801(2)	0.216(2)	0.217(1)	0.110(3)
6.9	24	14	-0.9	-0.87	0.5538(1)	0.660(4)	0.653(3)	0.119(2)	0.119(2)	0.783(3)	0.771(3)	0.216(2)	0.209(2)	0.103(3)
6.9	24	14	-0.9	-0.88	0.5547(1)	0.636(4)	0.626(3)	0.120(2)	0.114(2)	0.756(3)	0.746(3)	0.212(2)	0.204(2)	0.096(3)
6.9	24	14	-0.9	-0.89	0.55582(9)	0.603(4)	0.596(3)	0.113(2)	0.111(1)	0.730(2)	0.725(2)	0.206(2)	0.201(1)	0.086(3)
6.9	24	14	-0.9	-0.9	0.5569(2)	0.560(4)	0.569(3)	0.104(2)	0.109(1)	0.699(3)	0.697(2)	0.199(2)	0.198(1)	0.077(3)
7.05	24	12	-0.835	-0.5	0.5603(1)	1.025(3)	0.738(5)	0.139(2)	0.093(2)	1.081(3)	0.847(3)	0.202(2)	0.160(2)	0.274(7)
7.05	24	12	-0.835	-0.55	0.5618(2)	0.965(4)	0.730(5)	0.136(2)	0.096(2)	1.026(3)	0.829(4)	0.202(2)	0.162(2)	0.248(6)
7.05	24	12	-0.835	-0.6	0.5636(1)	0.903(3)	0.702(5)	0.131(2)	0.094(2)	0.967(3)	0.807(3)	0.197(2)	0.160(2)	0.216(6)
7.05	24	12	-0.835	-0.65	0.5654(1)	0.828(4)	0.669(5)	0.123(2)	0.092(2)	0.901(4)	0.775(4)	0.192(2)	0.161(2)	0.182(6)
7.05	24	14	-0.835	-0.7	0.5678(1)	0.750(3)	0.642(5)	0.117(2)	0.094(2)	0.828(3)	0.751(4)	0.186(2)	0.165(2)	0.149(4)
7.05	24	14	-0.835	-0.75	0.5700(1)	0.659(4)	0.612(5)	0.110(2)	0.100(2)	0.746(4)	0.711(4)	0.178(2)	0.170(2)	0.118(4)
7.05	24	14	-0.835	-0.8	0.5731(1)	0.542(7)	0.532(4)	0.092(3)	0.091(2)	0.650(4)	0.644(4)	0.166(2)	0.164(2)	0.079(4)
7.05	24	14	-0.835	-0.82	0.5742(1)	0.496(7)	0.485(4)	0.086(3)	0.085(2)	0.615(4)	0.610(4)	0.161(2)	0.161(2)	0.064(4)
7.05	24	14	-0.835	-0.83	0.5749(1)	0.472(6)	0.469(5)	0.085(3)	0.085(2)	0.590(4)	0.593(4)	0.158(2)	0.160(2)	0.061(4)
7.05	24	14	-0.835	-0.835	0.5755(2)	0.445(6)	0.447(5)	0.077(2)	0.081(2)	0.575(4)	0.578(3)	0.153(2)	0.155(2)	0.051(3)
7.2	24	14	-0.78	-0.5	0.58108(7)	0.842(2)	0.582(4)	0.108(1)	0.074(1)	0.897(2)	0.685(2)	0.159(1)	0.128(1)	0.211(4)
7.2	24	14	-0.78	-0.55	0.58222(7)	0.778(2)	0.566(4)	0.103(1)	0.074(1)	0.838(2)	0.668(2)	0.157(1)	0.129(1)	0.181(4)
7.2	24	14	-0.78	-0.6	0.58342(7)	0.718(3)	0.560(4)	0.102(1)	0.077(1)	0.782(2)	0.659(3)	0.158(1)	0.133(1)	0.153(4)
7.2	24	14	-0.78	-0.65	0.58484(6)	0.638(3)	0.542(4)	0.093(1)	0.079(1)	0.716(2)	0.639(3)	0.153(1)	0.137(1)	0.127(3)
7.2	24	14	-0.78	-0.7	0.58634(6)	0.558(3)	0.513(4)	0.086(2)	0.080(1)	0.644(2)	0.612(3)	0.147(1)	0.140(1)	0.097(3)
7.2	32	16	-0.78	-0.73	0.58743(6)	0.484(5)	0.446(5)	0.078(3)	0.069(2)	0.573(5)	0.551(4)	0.131(3)	0.125(2)	0.078(4)
7.2	32	16	-0.78	-0.75	0.58818(6)	0.438(5)	0.433(6)	0.069(3)	0.072(3)	0.536(4)	0.524(7)	0.125(3)	0.122(4)	0.064(4)
7.2	32	16	-0.78	-0.77	0.58892(6)	0.396(8)	0.387(6)	0.069(4)	0.065(2)	0.493(5)	0.492(4)	0.120(3)	0.116(2)	0.054(4)
7.2	32	16	-0.78	-0.78	0.58923(4)	0.382(6)	0.389(5)	0.067(2)	0.068(2)	0.482(4)	0.484(3)	0.117(2)	0.116(2)	0.049(3)

Table 12: Tabulated results for the ensembles with $m_\rho/m_\pi \approx 1.25$ including the bare inverse gauge coupling β, the bare fermion masses am_u^0 and am_u^0 — where a is the lattice spacing — as well as the lattice dimensions $T \times L^3$. The reported decay constants have been renormalized. In addition, the average plaquette $\langle P \rangle$ that is used in the renormalization is reported. The last column contains the average PCAC-mass.

β	T	L	am_u^0	am_d^0	$\langle P \rangle$	$am(\pi^A)$	$am(\pi^C)$	$af(\pi^A)$	$af(\pi^C)$	$am(\rho^M)$	$am(\rho^N)$	$af(\rho^M)$	$af(\rho^N)$	$a\bar{m}_{\mathrm{PCAC}}$
6.9	24	12	-0.92	-0.5	0.5349(2)	1.198(3)	0.871(5)	0.179(2)	0.118(2)	1.253(3)	0.985(4)	0.252(2)	0.202(4)	0.358(9)
6.9	24	12	-0.92	-0.55	0.5364(2)	1.144(4)	0.857(5)	0.169(3)	0.116(3)	1.204(4)	0.967(4)	0.245(3)	0.200(3)	0.314(7)
6.9	24	12	-0.92	-0.6	0.5385(2)	1.084(4)	0.832(6)	0.167(3)	0.118(3)	1.154(3)	0.945(5)	0.249(3)	0.201(3)	0.28(1)
6.9	24	12	-0.92	-0.65	0.5399(2)	1.031(4)	0.807(7)	0.164(2)	0.115(3)	1.107(3)	0.927(6)	0.249(2)	0.200(3)	0.257(8)
6.9	24	12	-0.92	-0.7	0.5427(2)	0.958(5)	0.779(7)	0.155(3)	0.117(3)	1.040(4)	0.900(5)	0.244(3)	0.203(3)	0.217(9)
6.9	24	12	-0.92	-0.75	0.5459(2)	0.870(5)	0.752(7)	0.143(3)	0.118(3)	0.959(4)	0.870(5)	0.233(3)	0.207(3)	0.180(8)
6.9	24	12	-0.92	-0.8	0.5498(2)	0.765(6)	0.669(9)	0.133(3)	0.110(3)	0.867(4)	0.810(7)	0.223(4)	0.204(4)	0.143(8)
6.9	24	14	-0.92	-0.85	0.5538(1)	0.660(5)	0.632(5)	0.121(2)	0.114(2)	0.782(4)	0.756(4)	0.216(2)	0.204(2)	0.106(4)
6.9	24	14	-0.92	-0.88	0.5572(3)	0.55(1)	0.540(7)	0.101(4)	0.098(3)	0.690(6)	0.687(6)	0.195(3)	0.194(3)	0.073(5)
6.9	24	14	-0.92	-0.9	0.5594(1)	0.480(9)	0.486(6)	0.090(3)	0.094(2)	0.637(6)	0.646(4)	0.184(3)	0.189(2)	0.057(3)
6.9	24	14	-0.92	-0.91	0.5607(1)	0.45(1)	0.441(6)	0.092(4)	0.088(3)	0.605(7)	0.598(5)	0.183(3)	0.176(2)	0.048(4)
6.9	24	14	-0.92	-0.92	0.5621(2)	0.38(1)	0.380(8)	0.083(4)	0.082(3)	0.548(9)	0.555(6)	0.167(4)	0.168(3)	0.038(4)
7.05	24	14	-0.85	-0.5	0.5614(1)	0.999(4)	0.690(4)	0.135(2)	0.086(2)	1.059(3)	0.805(4)	0.201(2)	0.155(2)	0.261(8)
7.05	24	14	-0.85	-0.55	0.5628(1)	0.943(3)	0.669(6)	0.130(2)	0.086(2)	1.001(3)	0.789(4)	0.194(2)	0.156(2)	0.233(7)
7.05	24	14	-0.85	-0.6	0.5648(1)	0.875(4)	0.662(7)	0.128(2)	0.091(2)	0.943(3)	0.772(5)	0.195(3)	0.158(2)	0.204(7)
7.05	24	14	-0.85	-0.65	0.5666(1)	0.791(5)	0.615(5)	0.118(2)	0.089(2)	0.872(4)	0.736(4)	0.188(3)	0.159(3)	0.173(6)
7.05	24	14	-0.85	-0.7	0.5685(1)	0.730(5)	0.602(5)	0.116(3)	0.088(2)	0.805(4)	0.715(4)	0.185(2)	0.160(2)	0.138(6)
7.05	24	14	-0.85	-0.75	0.5712(2)	0.620(5)	0.554(7)	0.101(2)	0.088(2)	0.717(4)	0.676(4)	0.172(2)	0.163(2)	0.106(5)
7.05	24	14	-0.85	-0.8	0.5739(1)	0.501(5)	0.481(5)	0.089(2)	0.083(2)	0.621(3)	0.606(4)	0.163(2)	0.157(2)	0.072(3)
7.05	24	14	-0.85	-0.83	0.57590(8)	0.427(8)	0.422(6)	0.078(2)	0.080(2)	0.563(5)	0.556(4)	0.155(2)	0.153(2)	0.047(3)
7.05	24	14	-0.85	-0.85	0.57736(7)	0.350(8)	0.348(6)	0.067(2)	0.066(2)	0.510(4)	0.518(3)	0.143(2)	0.145(1)	0.035(2)
7.2	24	14	-0.794	-0.45	0.5808(1)	0.874(4)	0.550(7)	0.108(2)	0.070(3)	0.925(4)	0.654(5)	0.158(2)	0.122(2)	0.227(7)
7.2	24	14	-0.794	-0.5	0.5816(1)	0.823(5)	0.535(8)	0.107(2)	0.071(2)	0.879(4)	0.647(5)	0.158(2)	0.125(2)	0.201(7)
7.2	24	14	-0.794	-0.55	0.5829(1)	0.755(4)	0.506(8)	0.100(2)	0.066(3)	0.819(3)	0.633(5)	0.155(2)	0.128(2)	0.172(7)
7.2	24	14	-0.794	-0.6	0.58408(5)	0.686(2)	0.510(4)	0.095(1)	0.070(1)	0.755(2)	0.618(3)	0.151(1)	0.126(1)	0.144(3)
7.2	24	14	-0.794	-0.65	0.58543(6)	0.613(3)	0.488(4)	0.090(1)	0.071(1)	0.693(2)	0.604(3)	0.150(1)	0.130(1)	0.117(3)
7.2	24	14	-0.794	-0.7	0.58696(6)	0.529(3)	0.460(5)	0.081(1)	0.072(1)	0.620(2)	0.577(3)	0.142(1)	0.135(1)	0.086(3)
7.2	32	16	-0.794	-0.75	0.58878(5)	0.420(4)	0.396(5)	0.071(2)	0.066(2)	0.522(9)	0.51(1)	0.124(6)	0.119(7)	0.059(2)
7.2	32	16	-0.794	-0.77	0.5895(1)	0.370(7)	0.345(6)	0.064(3)	0.058(2)	0.477(4)	0.470(4)	0.117(2)	0.117(2)	0.043(3)
7.2	32	16	-0.794	-0.78	0.58988(6)	0.324(8)	0.332(7)	0.059(3)	0.062(2)	0.433(6)	0.44(1)	0.107(3)	0.110(6)	0.039(3)
7.2	32	16	-0.794	-0.794	0.59032(6)	0.315(8)	0.317(5)	0.059(3)	0.059(2)	0.430(5)	0.426(4)	0.110(3)	0.106(2)	0.032(2)

Table 13: Tabulated results for the ensembles with $m_\rho/m_\pi \approx 1.4$ including the bare inverse gauge coupling β, the bare fermion masses am_u^0 and am_u^0 — where a is the lattice spacing — as well as the lattice dimensions $T \times L^3$. The reported decay constants have been renormalized. In addition, the average plaquette $\langle P \rangle$ that is used in the renormalization is reported. The last column contains the average PCAC-mass.

β	T	L	am_u^0	am_d^0	$\langle P \rangle$	$am(\pi^A)$	$am(\pi^C)$	$af(\pi^A)$	$af(\pi^C)$	$am(\rho^M)$	$am(\rho^N)$	$af(\rho^M)$	$af(\rho^N)$	$a\bar{m}_{\mathrm{PCAC}}$
6.9	24	12	-0.87	-0.5	0.5309(1)	1.268(2)	1.004(3)	0.185(1)	0.132(1)	1.322(2)	1.093(2)	0.258(1)	0.207(2)	0.400(5)
6.9	24	12	-0.87	-0.55	0.5326(1)	1.219(2)	0.992(2)	0.180(2)	0.134(1)	1.278(2)	1.084(2)	0.257(2)	0.213(1)	0.361(6)
6.9	24	12	-0.87	-0.6	0.5341(1)	1.173(2)	0.980(2)	0.181(2)	0.135(1)	1.232(2)	1.071(2)	0.259(2)	0.215(1)	0.334(5)
6.9	24	12	-0.87	-0.65	0.5361(1)	1.115(2)	0.958(3)	0.177(2)	0.136(1)	1.181(2)	1.051(2)	0.259(2)	0.218(2)	0.300(5)
6.9	24	12	-0.87	-0.7	0.5384(1)	1.047(2)	0.939(3)	0.166(2)	0.138(2)	1.120(2)	1.033(2)	0.251(2)	0.222(2)	0.260(5)
6.9	24	12	-0.87	-0.75	0.5411(1)	0.980(3)	0.910(3)	0.162(2)	0.141(2)	1.057(2)	1.004(2)	0.248(2)	0.230(2)	0.226(5)
6.9	24	12	-0.87	-0.8	0.5444(1)	0.896(3)	0.870(3)	0.152(2)	0.143(2)	0.986(3)	0.966(2)	0.244(2)	0.235(1)	0.187(5)
6.9	24	12	-0.87	-0.83	0.5470(2)	0.829(5)	0.818(4)	0.143(3)	0.138(2)	0.925(4)	0.913(3)	0.234(3)	0.228(3)	0.164(7)
6.9	24	12	-0.87	-0.84	0.5478(2)	0.812(3)	0.801(4)	0.142(2)	0.138(2)	0.913(2)	0.903(3)	0.237(2)	0.231(2)	0.156(5)
6.9	24	12	-0.87	-0.85	0.5485(1)	0.790(4)	0.786(3)	0.139(2)	0.135(2)	0.889(3)	0.887(2)	0.230(2)	0.226(2)	0.150(4)
6.9	24	12	-0.87	-0.86	0.5497(1)	0.770(4)	0.764(3)	0.134(2)	0.134(2)	0.872(3)	0.871(2)	0.227(2)	0.229(2)	0.137(5)
6.9	24	12	-0.87	-0.87	0.5504(2)	0.742(2)	0.743(2)	0.131(2)	0.1303(9)	0.848(2)	0.851(2)	0.224(2)	0.224(1)	0.129(3)
7.05	24	12	-0.8	-0.45	0.5566(1)	1.137(4)	0.862(4)	0.151(3)	0.108(2)	1.184(3)	0.949(3)	0.211(2)	0.171(2)	0.340(9)
7.05	24	12	-0.8	-0.5	0.5581(2)	1.080(4)	0.841(4)	0.143(2)	0.102(2)	1.132(3)	0.930(4)	0.206(2)	0.167(2)	0.304(9)
7.05	24	12	-0.8	-0.55	0.55938(9)	1.029(2)	0.833(2)	0.144(1)	0.106(1)	1.084(2)	0.918(2)	0.209(1)	0.170(1)	0.277(4)
7.05	24	12	-0.8	-0.6	0.5611(1)	0.968(3)	0.816(3)	0.139(2)	0.105(1)	1.031(2)	0.906(2)	0.207(2)	0.174(1)	0.244(5)
7.05	24	12	-0.8	-0.65	0.56321(9)	0.895(2)	0.799(2)	0.133(1)	0.112(1)	0.963(2)	0.882(2)	0.204(1)	0.180(1)	0.213(4)
7.05	24	12	-0.8	-0.7	0.56537(9)	0.819(3)	0.769(3)	0.127(1)	0.114(1)	0.893(2)	0.852(2)	0.197(1)	0.185(1)	0.178(4)
7.05	24	12	-0.8	-0.75	0.56774(9)	0.733(3)	0.723(3)	0.117(2)	0.115(1)	0.818(2)	0.809(2)	0.190(2)	0.188(1)	0.146(4)
7.05	24	12	-0.8	-0.78	0.5695(1)	0.670(3)	0.672(2)	0.111(2)	0.109(1)	0.762(3)	0.764(2)	0.184(2)	0.182(1)	0.123(4)
7.05	24	12	-0.8	-0.8	0.5708(1)	0.626(6)	0.632(3)	0.103(2)	0.106(1)	0.724(4)	0.732(3)	0.176(2)	0.183(1)	0.105(4)
7.2	24	12	-0.75	-0.45	0.5787(1)	0.950(4)	0.696(5)	0.117(2)	0.083(2)	1.002(3)	0.780(5)	0.170(2)	0.134(2)	0.262(8)
7.2	24	12	-0.75	-0.5	0.5797(2)	0.903(4)	0.681(7)	0.120(2)	0.083(2)	0.950(3)	0.763(5)	0.172(2)	0.134(2)	0.236(7)
7.2	24	12	-0.75	-0.55	0.58086(7)	0.835(2)	0.670(3)	0.112(1)	0.0846(9)	0.891(2)	0.755(2)	0.166(1)	0.1398(9)	0.203(4)
7.2	24	12	-0.75	-0.6	0.58208(6)	0.767(2)	0.653(3)	0.105(1)	0.0869(9)	0.829(2)	0.736(2)	0.1619(9)	0.1421(9)	0.174(3)
7.2	24	12	-0.75	-0.65	0.58353(6)	0.695(3)	0.638(3)	0.100(1)	0.0895(9)	0.766(2)	0.720(2)	0.159(1)	0.148(1)	0.145(3)
7.2	24	12	-0.75	-0.7	0.58512(7)	0.616(4)	0.597(3)	0.094(1)	0.090(1)	0.697(3)	0.691(2)	0.155(1)	0.154(1)	0.117(3)
7.2	24	12	-0.75	-0.72	0.58586(7)	0.582(3)	0.580(3)	0.089(1)	0.088(1)	0.674(2)	0.667(2)	0.153(1)	0.1511(9)	0.103(3)
7.2	24	12	-0.75	-0.74	0.58661(7)	0.547(4)	0.546(3)	0.086(1)	0.084(1)	0.640(2)	0.644(2)	0.150(1)	0.150(1)	0.092(3)
7.2	24	12	-0.75	-0.75	0.58690(6)	0.532(4)	0.530(3)	0.084(2)	0.0832(8)	0.624(2)	0.636(2)	0.147(1)	0.1505(8)	0.086(3)

Table 14: Tabulated results for the ensembles with $m_\rho/m_\pi \approx 1.15$ including the bare inverse gauge coupling β, the bare fermion masses am_u^0 and am_u^0 — where a is the lattice spacing — as well as the lattice dimensions $T \times L^3$. The reported decay constants have been renormalized. In addition, the average plaquette $\langle P \rangle$ that is used in the renormalization is reported. The last column contains the average PCAC-mass.

Appendix D

Isospin breaking as a perturbation

D.1 Expansion of the path integral

If the isospin breaking due to non-degenerate fermion masses is small. The breaking effects can be including perturbatively using measurements on purely iso-symmetric configurations. This is achieved by splitting the fermionic part of the action into an iso-symmetric part and a perturbation proportional to $m_u - m_d$ [185]:

$$\begin{aligned}\mathcal{L} &= (m_u + m_d)(\bar{u}u + \bar{d}d)/2 + (m_u - m_d)(\bar{u}u - \bar{d}d)/2 \\ &= m(\bar{u}u + \bar{d}d) + \Delta m(\bar{u}u - \bar{d}d) = \mathcal{L}_{0,1} + \Delta m \mathcal{L}_{IB,1}\end{aligned} \tag{253}$$

This splitting has been used for QCD at first and second order in [145, 185] to induce strong isospin breaking from a $N_f = 2 + 1$ to a $N_f = 1 + 1 + 1$ theory. In this case the breaking term is itself symmetric and both fermion masses are perturbed, i.e. $m_u = m - \Delta m$ and $m_d = m \pm \Delta m$. However, a different splitting can be chosen by setting

$$\mathcal{L} = m(\bar{u}u + \bar{d}d) + \Delta m(\bar{d}d) = \mathcal{L}_{0,2} + \Delta m \mathcal{L}_{IB,2}, \tag{254}$$

such that only one fermion mass is perturbed $m_d = m_u + \Delta m = m + \Delta m$. In this case the perturbation is itself no longer symmetric. For now, a generic breaking term is considered. Denoting $S_{IB} = \sum_x \mathcal{L}_{IB}$ a generic expectation value of an observable $\mathcal{O}$ is

$$\langle \mathcal{O} \rangle = \frac{1}{Z} \int D\phi \; \mathcal{O} e^{-S} = \frac{\int D\phi \; \mathcal{O} e^{-(S_0 + \Delta m S_{IB})}}{\int D\phi \; e^{-(S_0 + \Delta m S_{IB})}} \tag{255}$$

At first order the expansion of (255) gives

$$\begin{aligned}\langle\mathcal{O}\rangle &\approx \frac{\langle\mathcal{O}\rangle_0 - \Delta m\langle\mathcal{O}S_{IB}\rangle_0}{1-\Delta m\langle S_{IB}\rangle_0}\\ &= \langle\mathcal{O}\rangle_0 + \Delta m\left[\langle S_{IB}\rangle_0\langle\mathcal{O}\rangle_0 - \langle\mathcal{O}S_{IB}\rangle_0\right] + \mathcal{O}(\Delta m^2).\end{aligned} \tag{256}$$

Note, that for the specific form the first order correction to the partition function Z is proportional to S_{IB} evaluated on a symmetric theory denoted by $\langle S_{IB}\rangle_0$ which vanishes for $S_{IB,1}$ due to the anti-symmetry w.r.t u and d. For some observables the first order corrections vanish and the terms proportional to Δm^2 are the leading order iso-spin breaking effects [145]. At second order the expansion is given by

$$\begin{aligned}\langle\mathcal{O}\rangle &\approx \frac{\langle\mathcal{O}\rangle_0 - \Delta m\langle\mathcal{O}S_{IB}\rangle_0 + \frac{1}{2}\Delta m^2\langle\mathcal{O}S_{IB}^2\rangle_0}{1-\Delta m\langle S_{IB}\rangle_0 + \frac{1}{2}\Delta m^2\langle S_{IB}^2\rangle_0}\\ &= \langle\mathcal{O}\rangle_0 + \Delta m\left[\langle\mathcal{O}\rangle_0\langle S_{IB}\rangle_0 - \langle\mathcal{O}S_{IB}\rangle_0\right]\\ &\quad + \frac{1}{2}\Delta m^2\left[\langle\mathcal{O}S_{IB}^2\rangle_0 - 2\langle S_{IB}^2\rangle_0\langle\mathcal{O}\rangle_0 - \langle S_{IB}\rangle_0\langle\mathcal{O}S_{IB}\rangle_0\right] + \mathcal{O}(\Delta m^3)\end{aligned} \tag{257}$$

where it was *not* used that $\langle\mathcal{S}_{\mathcal{IB}}\rangle_0$ vanishes and even more extra terms arise in comparison with [145, 185]. For the case of the difference between two observables that are degenerate in the iso-symmetric limit the expression simplifies even further. Denoting the operators as $\mathcal{O}_A$ and $\mathcal{O}_B$ with $\langle\mathcal{O}_A\rangle_0 = \langle\mathcal{O}_B\rangle_0$ it follows that

$$\langle\mathcal{O}_A\rangle - \langle\mathcal{O}_B\rangle \approx -\Delta m\left[\langle\mathcal{O}_A S_{IB}\rangle - \langle\mathcal{O}_B S_{IB}\rangle\right] + \frac{\Delta m^2}{2}\left[\langle\mathcal{O}_A S_{IB}^2\rangle - \langle\mathcal{O}_B S_{IB}^2\rangle\right], \tag{258}$$

and all additional terms cancel. Only $\langle\mathcal{O}S_{IB}^n\rangle$ needs to be in order to obtain the difference between two otherwise degenerate observables for a generic isospin breaking term S_{IB}. Let us first consider $\langle\mathcal{O}S_{IB,2}\rangle$ for meson mass differences where $\mathcal{O}$ is a single meson correlator such as $O_{\pi^\pm}$ and O_{π^0}. The following fermion contractions need to be performed

$$\begin{aligned}\langle\bar{u}(x)\Gamma d(x)\bar{d}(y)\Gamma u(y)\mathcal{L}_{IB,2}\rangle_F &= \langle\bar{u}(x)\Gamma d(x)\bar{d}(y)\Gamma u(y)\bar{d}(z)d(z)\rangle_F\\ \langle\bar{u}(x)\Gamma u(x)\bar{u}(y)\Gamma u(y)\mathcal{L}_{IB,2}\rangle_F &= \langle\bar{u}(x)\Gamma u(x)\bar{u}(y)\Gamma u(y)\bar{d}(z)d(z)\rangle_F\\ \langle\bar{u}(x)\Gamma u(x)\bar{d}(y)\Gamma d(y)\mathcal{L}_{IB,2}\rangle_F &= \langle\bar{u}(x)\Gamma u(x)\bar{d}(y)\Gamma d(y)\bar{d}(z)d(z)\rangle_F\\ \langle\bar{d}(x)\Gamma d(x)\bar{d}(y)\Gamma d(y)\mathcal{L}_{IB,2}\rangle_F &= \langle\bar{d}(x)\Gamma d(x)\bar{d}(y)\Gamma d(y)\bar{d}(z)d(z)\rangle_F\end{aligned} \tag{259}$$

where the first contraction is needed for non-singlet mesons and the other three are needed for singlet mesons after symmetry breaking such as the η meson or the π^0. Instead of calculating all these contractions directly it is useful to observe a few patterns. The general form of these contractions are

$$\sum_z \langle \mathcal{O}\mathcal{L}_{IB,2}(z)\rangle_F = \sum_z \langle \mathcal{O}\bar{d}(z)d(z)\rangle_F. \tag{260}$$

If the two quark fields of $L_{IB,2}$ are contracted an extra factor of $\sum_z \mathrm{tr}[G(z|z)] = \mathrm{tr}[\mathcal{S}_{IB}]$ appears - where $G(x|y)$ is the quark propagator from x to y - times all the usual fermion contractions. Diagrammatically, this means the every fermion contraction is multiplied by this factor and yields

$$\langle \text{usual fermion contraction of } \mathcal{O}\rangle_F \times \sum_z \text{(z)} \Delta m. \tag{261}$$

In the case of the symmetric breaking term there is such a diagram both for the u and the d quark with opposing sign and these diagrams cancel. This can also be understood as a consequence of the tracelessnes of $\mathcal{L}_{IB,1}$ in flavour space [185]. For the case of the non-symmetric breaking operator this is not the case. However, since these expressions are evaluated on symmetric gauge configurations these contributions cancel in expressions like (258).

If the additional quark fields are contracted with a quark field of the operator $\mathcal{O}$ of the same flavour (in this case d) one propagator of a quark from some point on the lattice x to the inserted point z and due to the second adjoint quark field a corresponding propagator to another point y (which can coincide with x) results in the contraction. Diagrammatically this corresponds to an insertion of an additional quark propagator into an existing d-quark propagator [185] while keeping the u-quark propagators unchanged

$$\text{x} \longrightarrow \text{y} \quad \rightarrow \quad \sum_z \quad \text{x} \longrightarrow \text{(z)} \longrightarrow \text{y}. \tag{262}$$

In case of the symmetric isospin breaking operator these insertions are also present for the u-quark propagators. Note, that in the first order expansion only one insertion per product of diagrams is allowed since every insertion comes with a factor of Δm.

The situation is similar at second order for the operators $\langle \mathcal{O}_B S_{IB}(x) S_{IB}(y)\rangle$. If the fermion operators of are contracted with themselves the usual contracted diagrams times a all

possible contractions in $S_{IB}(x)S_{IB}(y)$ are obtained. Even in the case of a symmetric breaking term this does not vanish. However, when considering the difference of two observables that are degenerate in the isosymmetric limit these contributions cancel for every breaking operator.

The contractions of $S_{IB}(x)S_{IB}(y)$ with other quark fields in $\mathcal{O}$ lead either to a double insertion of an extra d-quark propagator into one quark line or two separate insertions in one product of diagram, i.e. replacements of the form

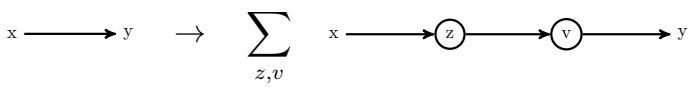

(263)

and

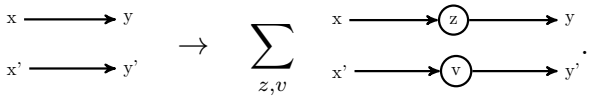

(264)

With these diagrammatic replacement rules the relevant diagrams for measuring isospin breaking effects can be constructed. Only need the usual diagrams after fermion contraction and the ones after applying the insertion rules derived above need to be considered. In the case of the iso-symmetric breaking operator this is sufficient to calculate **all** isospin breaking corrections to all operators at first order in Δm. For non-symmetric breaking operators and higher orders with the symmetric operator this is only sufficient for obtaining the difference between observables that are degenerate in the isosymmetric limit like $m_{\pi^\pm} - m_{\pi^0}$. For other observables (like meson properties of a bound state like $m_{\pi^\pm}$ or m_η) $\langle \mathcal{L}_{IB} \rangle_0$ needs to be measured for the first order expansion and $\langle \mathcal{L}_{IB}^2 \rangle_0$ for the second order expansion.

The relevant diagrams depend on the specific meson and theory at hand as well as on the desired breaking pattern. The isospin breaking effects of $N_f = 2 \to 1 + 1$ as well as $N_f = 3 \to 1 + 1 + 1$ and $N_f = 3 \to 2 + 1$ for mesonic operators will be discussed here. For concreteness, the pseudoscalar mesons will be discussed. The other J^P mesons can be obtained by exactly the same procedure. [1]

The relevant diagrams after fermion contraction for the pions are given in (137) and (138). For the kaons of the three-flavour theories the diagrams are the same as for the $\pi^\pm$ above after suitable replacements of u and d by s.

[1] In some cases like the vector mesons of Sp(4) gauge theory the disconnected contributions of the diagrams are vanishing even in the non-isosymmetric case and thus this method might become even easier.

D.2 Two flavour theories: $N_f = 2 \to 1 + 1$

Only have bound states of u and d quarks appear. For the isosymmetric breaking operator the contributions to the pions cancel at first order in Δm since both the u and the d quark propagator receive the same correction with opposing sign. The breaking effects at second order are [185]

$$\mathcal{L}_{IB,1}: \qquad C_{\pi^0\pi^0} - C_{\pi^\pm\pi^\pm} = -2 \left[\right. \quad - \quad \left. \right] \tag{265}$$

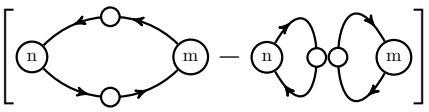

where the blank, white circles denote the insertions and summation over all lattice points of insertions is implied and the quark propagators are the isosymmetric ones. Even for the non-symmetric isospin breaking operator the pion mass difference has no leading order contribution

$$\mathcal{L}_{IB,2}: \qquad C_{\pi^0\pi^0} - C_{\pi^\pm\pi^\pm} = -\frac{1}{2} \left[\right. \quad - \quad + 4 \quad \left. \right] \tag{266}$$

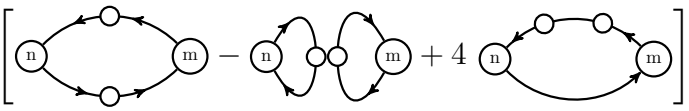

In both cases an $N_f = 1{+}1$ theory is obtained. Note that in both cases disconnected diagrams appear. They arise because isospin breaking turns the neutral pion into a singlet. If the global symmetry preserves a multiplet structure of these mesons then also the contributions vanish as is the case for the ρ mesons in Sp(4) gauge theory.

The key difference between the two different methods of parameterizing the isospin breaking that in the first case both u and d type quarks get corrections whereas in the second case only the u type quark changes:

$$\mathcal{L}_{IB,1}: \quad \begin{array}{l} m_d \\ m_u, m_d \\ m_u \end{array} \quad 2\Delta m \qquad\qquad \mathcal{L}_{IB,2}: \quad \begin{array}{l} m_d \\ m_u, m_d \\ m_u \end{array} \quad \Delta m \tag{267}$$

D.3 Three flavour theories: $N_f = 3$

The choice of breaking operator matters in $N_f = 3$ theories where they lead two different breaking patterns. The usual term $L_{IB,1}$ shifts the masses of both the u and d quark but keeps the third mass m_S unchanged. This leads to the same diagrams as above but the

overall theory breaks down to $N_f = 1 + 1 + 1$.

$$\mathcal{L}_{IB,1}: \quad \begin{array}{lll} & m_d & \\ m_d,m_u,m_s & m_s & 2\,\Delta m \\ & m_u & \end{array} \tag{268}$$

The other operator only shifts the mass of the d upwards. In this case a $N_f = 2 + 1$ theory results.

$$\mathcal{L}_{IB,2}: \quad \begin{array}{ll} m_d & \\ & \Delta m \\ m_d,m_u,m_s & m_u,m_s \end{array} \tag{269}$$

There are of course other additional particles present in these theories (the K, the η mesons, ...) which also receive isospin breaking correction. The corresponding diagrams can be derived as outlined above.

D.4 Relevance of the disconnected diagrams

The disconnected diagrams need to be evaluated to compute the corrections of strong isospin breaking to the pion masses. Since these are not identical to usual ones but come with extra insertions of quark propagators it is a priori not known if they suffer as badly from statistical noise as the other disconnected terms.

In [145] these terms have been evaluated for QCD using the *rotated twisted mass* (RTM) scheme for an ensemble with a degenerate pion mass of ≈ 260MeV. It was found that the connected and disconnected contributions are roughly of the same size and that the signal-to-noise ratio is significantly worse for the disconnected diagrams. When choosing the breaking operator $\mathcal{L}_{IB,2}$, a third connected diagram appears. This third diagram has not yet been computed in the literature but it could lead to a situation where the connected diagrams dominate.

Bibliography

[1] Bennett, H. Hsiao, J.-W. Lee, B. Lucini, A. Maas, M. Piai et al., *Singlets in gauge theories with fundamental matter*, 2304.07191.

[2] S. Kulkarni, A. Maas, S. Mee, M. Nikolic, J. Pradler and F. Zierler, *Low-energy effective description of dark $Sp(4)$ theories*, *SciPost Phys.* **14** (2023) 044 [2202.05191].

[3] F. Zierler, J.-W. Lee, A. Maas and F. Pressler, *Singlet Mesons in Dark $Sp(4)$ Theories*, *PoS* **LATTICE2022** (2023) 225 [2210.11187].

[4] F. Zierler, S. Kulkarni, A. Maas, S. Mee, M. Nikolic and J. Pradler, *Strongly Interacting Dark Matter from Sp(4) Gauge Theory*, *EPJ Web Conf.* **274** (2022) 08014 [2211.11272].

[5] A. Maas and F. Zierler, *Strong isospin breaking in $\boldsymbol{Sp}(4)$ gauge theory*, *PoS* **LATTICE2021** (2022) 130 [2109.14377].

[6] F. Zierler and A. Maas, *$Sp(4)$ SIMP Dark Matter on the Lattice*, *PoS* **LHCP2021** (2021) 162.

[7] G. Bertone, D. Hooper and J. Silk, *Particle dark matter: Evidence, candidates and constraints*, *Phys. Rept.* **405** (2005) 279 [hep-ph/0404175].

[8] S. Profumo, *An Introduction to Particle Dark Matter*, World Scientific (2017), 10.1142/q0001.

[9] A.M. Green, *Dark matter in astrophysics/cosmology*, *SciPost Phys. Lect. Notes* **37** (2022) 1 [2109.05854].

[10] K.C. Freeman, *On the disks of spiral and SO Galaxies*, *Astrophys. J.* **160** (1970) 811.

[11] V.C. Rubin and W.K. Ford, Jr., *Rotation of the Andromeda Nebula from a Spectroscopic Survey of Emission Regions*, *Astrophys. J.* **159** (1970) 379.

[12] J.A. Tyson, G.P. Kochanski and I.P. Dell'Antonio, *Detailed mass map of CL0024+1654 from strong lensing*, *Astrophys. J. Lett.* **498** (1998) L107 [astro-ph/9801193].

[13] D. Clowe, M. Bradac, A.H. Gonzalez, M. Markevitch, S.W. Randall, C. Jones et al., *A direct empirical proof of the existence of dark matter*, *Astrophys. J. Lett.* **648** (2006) L109 [astro-ph/0608407].

[14] K.E. Andrade, J. Fuson, S. Gad-Nasr, D. Kong, Q. Minor, M.G. Roberts et al., *A stringent upper limit on dark matter self-interaction cross-section from cluster strong lensing*, *Mon. Not. Roy. Astron. Soc.* **510** (2021) 54 [2012.06611].

[15] D. Eckert, S. Ettori, A. Robertson, R. Massey, E. Pointecouteau, D. Harvey et al., *Constraints on dark matter self-interaction from the internal density profiles of X-COP galaxy clusters*, *Astron. Astrophys.* **666** (2022) A41 [2205.01123].

[16] B. Famaey and S. McGaugh, *Modified Newtonian Dynamics (MOND): Observational Phenomenology and Relativistic Extensions*, *Living Rev. Rel.* **15** (2012) 10 [1112.3960].

[17] Particle Data Group collaboration, *Review of Particle Physics*, *PTEP* **2022** (2022) 083C01.

[18] J.S. Bullock and M. Boylan-Kolchin, *Small-Scale Challenges to the ΛCDM Paradigm*, *Ann. Rev. Astron. Astrophys.* **55** (2017) 343 [1707.04256].

[19] S. Tulin and H.-B. Yu, *Dark Matter Self-interactions and Small Scale Structure*, *Phys. Rept.* **730** (2018) 1 [1705.02358].

[20] S.Y. Kim, A.H.G. Peter and J.R. Hargis, *Missing Satellites Problem: Completeness Corrections to the Number of Satellite Galaxies in the Milky Way are Consistent with Cold Dark Matter Predictions*, *Phys. Rev. Lett.* **121** (2018) 211302 [1711.06267].

[21] S. Adhikari et al., *Astrophysical Tests of Dark Matter Self-Interactions*, 2207.10638.

[22] D.N. Spergel and P.J. Steinhardt, *Observational evidence for selfinteracting cold dark matter*, *Phys. Rev. Lett.* **84** (2000) 3760 [astro-ph/9909386].

[23] L. Sagunski, S. Gad-Nasr, B. Colquhoun, A. Robertson and S. Tulin, *Velocity-dependent Self-interacting Dark Matter from Groups and Clusters of Galaxies*, *JCAP* **01** (2021) 024 [2006.12515].

[24] V.H. Robles, T. Kelley, J.S. Bullock and M. Kaplinghat, *The Milky Way's halo and subhaloes in self-interacting dark matter*, *Mon. Not. Roy. Astron. Soc.* **490** (2019) 2117 [1903.01469].

[25] Y. Hochberg, E. Kuflik, T. Volansky and J.G. Wacker, *Mechanism for Thermal Relic Dark Matter of Strongly Interacting Massive Particles*, *Phys. Rev. Lett.* **113** (2014) 171301 [1402.5143].

[26] Y. Hochberg, E. Kuflik, H. Murayama, T. Volansky and J.G. Wacker, *Model for Thermal Relic Dark Matter of Strongly Interacting Massive Particles*, *Phys. Rev. Lett.* **115** (2015) 021301 [1411.3727].

[27] Y. Hochberg, E. Kuflik and H. Murayama, *SIMP Spectroscopy*, *JHEP* **05** (2016) 090 [1512.07917].

[28] C. Gattringer and C.B. Lang, *Quantum chromodynamics on the lattice*, vol. 788, Springer, Berlin (2010), 10.1007/978-3-642-01850-3.

[29] E. Bennett, D.K. Hong, J.-W. Lee, C.-J.D. Lin, B. Lucini, M. Mesiti et al., *$Sp(4)$ gauge theories on the lattice: quenched fundamental and antisymmetric fermions*, *Phys. Rev. D* **101** (2020) 074516 [1912.06505].

[30] H.D. Politzer, *Reliable Perturbative Results for Strong Interactions?*, *Phys. Rev. Lett.* **30** (1973) 1346.

[31] D.J. Gross and F. Wilczek, *Ultraviolet Behavior of Nonabelian Gauge Theories*, *Phys. Rev. Lett.* **30** (1973) 1343.

[32] J. Greensite, *The Confinement problem in lattice gauge theory*, *Prog. Part. Nucl. Phys.* **51** (2003) 1 [hep-lat/0301023].

[33] R. Alkofer and J. Greensite, *Quark Confinement: The Hard Problem of Hadron Physics*, *J. Phys. G* **34** (2007) S3 [hep-ph/0610365].

[34] S.L. Adler, *Axial vector vertex in spinor electrodynamics*, *Phys. Rev.* **177** (1969) 2426.

[35] E. Witten, *Current Algebra Theorems for the U(1) Goldstone Boson*, *Nucl. Phys. B* **156** (1979) 269.

[36] G. Veneziano, *U(1) Without Instantons*, *Nucl. Phys. B* **159** (1979) 213.

[37] Y. Aoki, Z. Fodor, S.D. Katz and K.K. Szabo, *The QCD transition temperature: Results with physical masses in the continuum limit*, *Phys. Lett. B* **643** (2006) 46 [hep-lat/0609068].

[38] M. Cheng et al., *The Transition temperature in QCD*, *Phys. Rev. D* **74** (2006) 054507 [hep-lat/0608013].

[39] Y. Aoki, S. Borsanyi, S. Durr, Z. Fodor, S.D. Katz, S. Krieg et al., *The QCD transition temperature: results with physical masses in the continuum limit II.*, *JHEP* **06** (2009) 088 [0903.4155].

[40] B.G.-g. Chen, D. Derbes, D. Griffiths, B. Hill, R. Sohn and Y.-S. Ting, eds., *Lectures of Sidney Coleman on Quantum Field Theory*, WSP, Hackensack (12, 2018), 10.1142/9371.

[41] J. Goldstone, A. Salam and S. Weinberg, *Broken Symmetries*, *Phys. Rev.* **127** (1962) 965.

[42] RM123 collaboration, *Leading isospin breaking effects on the lattice*, *Phys. Rev. D* **87** (2013) 114505 [1303.4896].

[43] W.E. Caswell, *Asymptotic Behavior of Nonabelian Gauge Theories to Two Loop Order*, *Phys. Rev. Lett.* **33** (1974) 244.

[44] T. Banks and A. Zaks, *On the Phase Structure of Vector-Like Gauge Theories with Massless Fermions*, *Nucl. Phys. B* **196** (1982) 189.

[45] G. Cacciapaglia, C. Pica and F. Sannino, *Fundamental Composite Dynamics: A Review*, *Phys. Rept.* **877** (2020) 1 [2002.04914].

[46] V. Drach, *Composite electroweak sectors on the lattice*, *PoS* **LATTICE2019** (2020) 242 [2005.01002].

[47] T. DeGrand, *Lattice tests of beyond Standard Model dynamics*, *Rev. Mod. Phys.* **88** (2016) 015001 [1510.05018].

[48] O. Witzel, *Review on Composite Higgs Models*, *PoS* **LATTICE2018** (2019) 006 [1901.08216].

[49] L. von Smekal, *Universal Aspects of QCD-like Theories*, *Nucl. Phys. B Proc. Suppl.* **228** (2012) 179 [1205.4205].

[50] J.B. Kogut, M.A. Stephanov, D. Toublan, J.J.M. Verbaarschot and A. Zhitnitsky, *QCD - like theories at finite baryon density*, *Nucl. Phys. B* **582** (2000) 477 [hep-ph/0001171].

[51] F. Gürsey, *Relation of charge independence and baryon conservation to Pauli's transformation*, *Nuovo Cim.* **7** (1958) 411.

[52] W. Pauli, *On the conservation of the Lepton charge*, *Nuovo Cim.* **6** (1957) 204.

[53] D.A. Kosower, *SYMMETRY BREAKING PATTERNS IN PSEUDOREAL AND REAL GAUGE THEORIES*, *Phys. Lett. B* **144** (1984) 215.

[54] R. Lewis, C. Pica and F. Sannino, *Light Asymmetric Dark Matter on the Lattice: SU(2) Technicolor with Two Fundamental Flavors*, *Phys. Rev. D* **85** (2012) 014504 [1109.3513].

[55] J. Preskill, *Subgroup Alignment in Hypercolor Theories*, *Nucl. Phys. B* **177** (1981) 21.

[56] M.E. Peskin, *The Alignment of the Vacuum in Theories of Technicolor*, *Nucl. Phys. B* **175** (1980) 197.

[57] U.-G. Meißner and A. Rusetsky, *Effective Field Theories*, Cambridge University Press (8, 2022), 10.1017/9781108689038.

[58] S. Scherer, *Introduction to chiral perturbation theory*, *Adv. Nucl. Phys.* **27** (2003) 277 [hep-ph/0210398].

[59] R. Penco, *An Introduction to Effective Field Theories*, 2006.16285.

[60] E. Witten, *Global Aspects of Current Algebra*, *Nucl. Phys. B* **223** (1983) 422.

[61] J. Wess and B. Zumino, *Consequences of anomalous Ward identities*, *Phys. Lett. B* **37** (1971) 95.

[62] E. Witten, *Current Algebra, Baryons, and Quark Confinement*, *Nucl. Phys. B* **223** (1983) 433.

[63] E. Bennett, D.K. Hong, J.-W. Lee, C.J.D. Lin, B. Lucini, M. Piai et al., *Sp(4) gauge theory on the lattice: towards SU(4)/Sp(4) composite Higgs (and beyond)*, *JHEP* **03** (2018) 185 [1712.04220].

[64] V. Drach, T. Janowski, C. Pica and S. Prelovsek, *Scattering of Goldstone Bosons and resonance production in a Composite Higgs model on the lattice*, *JHEP* **04** (2021) 117 [2012.09761].

[65] F. Erben, J.R. Green, D. Mohler and H. Wittig, *Rho resonance, timelike pion form factor, and implications for lattice studies of the hadronic vacuum polarization*, *Phys. Rev. D* **101** (2020) 054504 [1910.01083].

[66] C. Alexandrou, L. Leskovec, S. Meinel, J. Negele, S. Paul, M. Petschlies et al., *P-wave $\pi\pi$ scattering and the ρ resonance from lattice QCD*, *Phys. Rev. D* **96** (2017) 034525 [1704.05439].

[67] K. Kawarabayashi and M. Suzuki, *Partially conserved axial vector current and the decays of vector mesons*, *Phys. Rev. Lett.* **16** (1966) 255.

[68] Riazuddin and Fayyazuddin, *Algebra of current components and decay widths of rho and K* mesons*, *Phys. Rev.* **147** (1966) 1071.

[69] R.C. Johnson, *Simple derivation of the ksrf relation*, *Nucl. Phys. B* **23** (1970) 247.

[70] T. Brauner and H. Kolešová, *Gauged Wess-Zumino terms for a general coset space*, *Nucl. Phys. B* **945** (2019) 114676 [1809.05310].

[71] Extended Twisted Mass, ETM collaboration, *The ρ-resonance from $N_f = 2$ lattice QCD including the physical pion mass*, *Phys. Lett. B* **819** (2021) 136449 [2006.13805].

[72] A. Rodas, J.J. Dudek and R.G. Edwards, *Constraining the quark mass dependence of the lightest resonance in QCD*, 2304.03762.

[73] A. Rodas, J.J. Dudek and R.G. Edwards, *The quark mass dependence of $\pi\pi$ scattering in isospin 0, 1 and 2 from lattice QCD*, 2303.10701.

[74] Lattice Strong Dynamics (LSD) collaboration, *Goldstone boson scattering with a light composite scalar*, *Phys. Rev. D* **105** (2022) 034505 [2106.13534].

[75] LatKMI collaboration, *Light composite scalar in twelve-flavor QCD on the lattice*, *Phys. Rev. Lett.* **111** (2013) 162001 [1305.6006].

[76] LatKMI collaboration, *Light composite scalar in eight-flavor QCD on the lattice*, *Phys. Rev. D* **89** (2014) 111502 [1403.5000].

[77] LatKMI collaboration, *Light flavor-singlet scalars and walking signals in $N_f = 8$ QCD on the lattice*, *Phys. Rev. D* **96** (2017) 014508 [1610.07011].

[78] A. Athenodorou, Bennett, G. Bergner and B. Lucini, *Investigating the conformal behavior of SU(2) with one adjoint Dirac flavor*, *Phys. Rev. D* **104** (2021) 074519 [2103.10485].

[79] Lattice Strong Dynamics collaboration, *Nonperturbative investigations of SU(3) gauge theory with eight dynamical flavors*, *Phys. Rev. D* **99** (2019) 014509 [1807.08411].

[80] T. Appelquist et al., *Strongly interacting dynamics and the search for new physics at the LHC*, *Phys. Rev. D* **93** (2016) 114514 [1601.04027].

[81] R.C. Brower, A. Hasenfratz, C. Rebbi, E. Weinberg and O. Witzel, *Composite Higgs model at a conformal fixed point*, *Phys. Rev. D* **93** (2016) 075028 [1512.02576].

[82] W.A. Bardeen, C.N. Leung and S.T. Love, *The Dilaton and Chiral Symmetry Breaking*, *Phys. Rev. Lett.* **56** (1986) 1230.

[83] T. Appelquist, J. Ingoldby and M. Piai, *Dilaton Effective Field Theory*, *Universe* **9** (2023) 10 [2209.14867].

[84] F. Sannino, *Conformal Windows of SP(2N) and SO(N) Gauge Theories*, *Phys. Rev. D* **79** (2009) 096007 [0902.3494].

[85] J.-W. Lee, *Conformal window from conformal expansion*, *Phys. Rev. D* **103** (2021) 076006 [2008.12223].

[86] M. Hansen, K. Langæble and F. Sannino, *SIMP model at NNLO in chiral perturbation theory*, *Phys. Rev. D* **92** (2015) 075036 [1507.01590].

[87] ALPHA collaboration, *Critical slowing down and error analysis in lattice QCD simulations*, *Nucl. Phys. B* **845** (2011) 93 [1009.5228].

[88] N. Bernal, X. Chu and J. Pradler, *Simply split strongly interacting massive particles*, *Phys. Rev. D* **95** (2017) 115023 [1702.04906].

[89] J. Barnard, T. Gherghetta and T.S. Ray, *UV descriptions of composite Higgs models without elementary scalars*, *JHEP* **02** (2014) 002 [1311.6562].

[90] G. Cacciapaglia and F. Sannino, *Fundamental Composite (Goldstone) Higgs Dynamics*, *JHEP* **04** (2014) 111 [1402.0233].

[91] E. Bennett, D.K. Hong, J.-W. Lee, C.J.D. Lin, B. Lucini, M. Piai et al., *Sp(4) gauge theories on the lattice: $N_f = 2$ dynamical fundamental fermions*, *JHEP* **12** (2019) 053 [1909.12662].

[92] E. Bennett, J. Holligan, D.K. Hong, H. Hsiao, J.-W. Lee, C.J.D. Lin et al., *$Sp(2N)$ Lattice Gauge Theories and Extensions of the Standard Model of Particle Physics*, 2304.01070.

[93] Bennett, D.K. Hong, H. Hsiao, J.-W. Lee, C.J.D. Lin, B. Lucini et al., *Lattice studies of the Sp(4) gauge theory with two fundamental and three antisymmetric Dirac fermions*, *Phys. Rev. D* **106** (2022) 014501 [2202.05516].

[94] T.A. Ryttov and F. Sannino, *Ultra Minimal Technicolor and its Dark Matter TIMP*, *Phys. Rev. D* **78** (2008) 115010 [0809.0713].

[95] J.M. Cline, Z. Liu, G.D. Moore and W. Xue, *Composite strongly interacting dark matter*, *Phys. Rev. D* **90** (2014) 015023 [1312.3325].

[96] S. Bhattacharya, B. Melić and J. Wudka, *Pionic Dark Matter*, *JHEP* **02** (2014) 115 [1307.2647].

[97] W. Detmold, M. McCullough and A. Pochinsky, *Dark nuclei. II. Nuclear spectroscopy in two-color QCD*, *Phys. Rev. D* **90** (2014) 114506 [1406.4116].

[98] N. Yamanaka, S. Fujibayashi, S. Gongyo and H. Iida, *Dark matter in the hidden gauge theory*, 1411.2172.

[99] V. Drach, A. Hietanen, C. Pica, J. Rantaharju and F. Sannino, *Template Composite Dark Matter: $SU(2)$ gauge theory with 2 fundamental flavours*, *PoS* **LATTICE2015** (2016) 234 [1511.04370].

[100] V. Beylin, M. Khlopov, V. Kuksa and N. Volchanskiy, *New physics of strong interaction and Dark Universe*, *Universe* **6** (2020) 196 [2010.13678].

[101] Y.-D. Tsai, R. McGehee and H. Murayama, *Resonant Self-Interacting Dark Matter from Dark QCD*, *Phys. Rev. Lett.* **128** (2022) 172001 [2008.08608].

[102] D. Kondo, R. McGehee, T. Melia and H. Murayama, *Linear sigma dark matter*, *JHEP* **09** (2022) 041 [2205.08088].

[103] A. Hietanen, R. Lewis, C. Pica and F. Sannino, *Fundamental Composite Higgs Dynamics on the Lattice: SU(2) with Two Flavors*, *JHEP* **07** (2014) 116 [1404.2794].

[104] R. Arthur, V. Drach, M. Hansen, A. Hietanen, C. Pica and F. Sannino, *SU(2) gauge theory with two fundamental flavors: A minimal template for model building*, *Phys. Rev. D* **94** (2016) 094507 [1602.06559].

[105] V. Drach, T. Janowski and C. Pica, *Update on SU(2) gauge theory with NF = 2 fundamental flavours*, *EPJ Web Conf.* **175** (2018) 08020 [1710.07218].

[106] R. Arthur, V. Drach, M. Hansen, A. Hietanen, C. Pica and F. Sannino, *Scattering lengths in SU(2) gauge theory with two fundamental fermions*, *PoS* **LATTICE2014** (2014) 271 [1412.4771].

[107] V. Drach, P. Fritzsch, A. Rago and F. Romero-López, *Singlet channel scattering in a composite Higgs model on the lattice*, *Eur. Phys. J. C* **82** (2022) 47 [2107.09974].

[108] V. Drach, T. Janowski, C. Pica, J. Rantaharju and F. Sannino, *The scalar sector of $SU(2)$ gauge theory with $N_F = 2$ fundamental flavours*, *PoS* **LATTICE2016** (2017) 229.

[109] R. Arthur, V. Drach, A. Hietanen, C. Pica and F. Sannino, *$SU(2)$ Gauge Theory with Two Fundamental Flavours: Scalar and Pseudoscalar Spectrum*, 1607.06654.

[110] M. Creutz, *Quarks, Gluons and Lattices*, Oxford University Press (1983), 10.1017/9781009290395.

[111] H.J. Rothe, *Lattice Gauge Theories : An Introduction (Fourth Edition)*, vol. 43, World Scientific Publishing Company (2012), 10.1142/8229.

[112] I. Montvay and G. Munster, *Quantum fields on a lattice*, Cambridge Monographs on Mathematical Physics, Cambridge University Press (3, 1997), 10.1017/CBO9780511470783.

[113] T. DeGrand and C.E. Detar, *Lattice methods for quantum chromodynamics*, World Scientific (2006).

[114] M. Golterman, *Applications of chiral perturbation theory to lattice QCD*, in *Les Houches Summer School: Session 93: Modern perspectives in lattice QCD: Quantum field theory and high performance computing*, pp. 423–515, 12, 2009 [0912.4042].

[115] J. Gasser and H. Leutwyler, *Light Quarks at Low Temperatures*, *Phys. Lett. B* **184** (1987) 83.

[116] K.G. Wilson, *Confinement of Quarks*, *Phys. Rev. D* **10** (1974) 2445.

[117] N. Metropolis, A.W. Rosenbluth, M.N. Rosenbluth, A.H. Teller and E. Teller, *Equation of state calculations by fast computing machines*, *J. Chem. Phys.* **21** (1953) 1087.

[118] L. Del Debbio, A. Patella and C. Pica, *Higher representations on the lattice: Numerical simulations. SU(2) with adjoint fermions*, *Phys. Rev. D* **81** (2010) 094503 [0805.2058].

[119] B. Efron, *The Jackknife, the Bootstrap and Other Resampling Plans*, Society for Industrial and Applied Mathematics (1982), 10.1137/1.9781611970319, [https://epubs.siam.org/doi/pdf/10.1137/1.9781611970319].

[120] M. Luscher, *Volume Dependence of the Energy Spectrum in Massive Quantum Field Theories. 1. Stable Particle States*, *Commun. Math. Phys.* **104** (1986) 177.

[121] M. Luscher, *Volume Dependence of the Energy Spectrum in Massive Quantum Field Theories. 2. Scattering States*, *Commun. Math. Phys.* **105** (1986) 153.

[122] M. Luscher, *Two particle states on a torus and their relation to the scattering matrix*, *Nucl. Phys. B* **354** (1991) 531.

[123] M. Fukugita, Y. Kuramashi, M. Okawa, H. Mino and A. Ukawa, *Hadron scattering lengths in lattice QCD*, *Phys. Rev. D* **52** (1995) 3003 [hep-lat/9501024].

[124] X. Feng, K. Jansen and D.B. Renner, *The pi+ pi+ scattering length from maximally twisted mass lattice QCD*, *Phys. Lett. B* **684** (2010) 268 [0909.3255].

[125] S.-J. Dong and K.-F. Liu, *Stochastic estimation with Z(2) noise*, *Phys. Lett. B* **328** (1994) 130 [hep-lat/9308015].

[126] P.A. Boyle, A. Juttner, C. Kelly and R.D. Kenway, *Use of stochastic sources for the lattice determination of light quark physics*, *JHEP* **08** (2008) 086 [0804.1501].

[127] W. Wilcox, *Noise methods for flavor singlet quantities*, in *Interdisciplinary Workshop on Numerical Challenges in Lattice QCD*, pp. 127–141, 8, 1999 [hep-lat/9911013].

[128] J. Foley, K. Jimmy Juge, A. O'Cais, M. Peardon, S.M. Ryan and J.-I. Skullerud, *Practical all-to-all propagators for lattice QCD*, *Comput. Phys. Commun.* **172** (2005) 145 [hep-lat/0505023].

[129] E. Endress, C. Pena and K. Sivalingam, *Variance reduction with practical all-to-all lattice propagators*, *Comput. Phys. Commun.* **195** (2015) 35 [1402.0831].

[130] W.H. Press, S.A. Teukolsky, W.T. Vetterling and B.P. Flannery, *Numerical Recipes in FORTRAN: The Art of Scientific Computing*, .

[131] S. Capitani, *Lattice perturbation theory*, *Phys. Rept.* **382** (2003) 113 [hep-lat/0211036].

[132] G. Martinelli and Y.-C. Zhang, *The Connection Between Local Operators on the Lattice and in the Continuum and Its Relation to Meson Decay Constants*, *Phys. Lett. B* **123** (1983) 433.

[133] M. Constantinou, M. Hadjiantonis, H. Panagopoulos and G. Spanoudes, *Singlet versus nonsinglet perturbative renormalization of fermion bilinears*, *Phys. Rev. D* **94** (2016) 114513 [1610.06744].

[134] Particle Data Group collaboration, *Review of Particle Physics*, *PTEP* **2020** (2020) 083C01.

[135] Bern-Graz-Regensburg (BGR) collaboration, *Lattice calculation of low energy constants with Ginsparg-Wilson type fermions*, *Phys. Rev. D* **72** (2005) 094510 [hep-lat/0509003].

[136] Flavour Lattice Averaging Group (FLAG) collaboration, *FLAG Review 2021*, *Eur. Phys. J. C* **82** (2022) 869 [2111.09849].

[137] A. Francis, R.J. Hudspith, R. Lewis and S. Tulin, *Dark Matter from Strong Dynamics: The Minimal Theory of Dark Baryons*, *JHEP* **12** (2018) 118 [1809.09117].

[138] M.E. Peskin and D.V. Schroeder, *An Introduction to quantum field theory*, Addison-Wesley, Reading, USA (1995).

[139] "GitHub - claudiopica/HiRep: HiRep repository — github.com." https://github.com/claudiopica/HiRep.

[140] "GitHub - sa2c/HiRep: HiRep repository — github.com." https://github.com/sa2c/HiRep.

[141] J. Bezanson, A. Edelman, S. Karpinski and V.B. Shah, *Julia: A fresh approach to numerical computing*, *SIAM Review* **59** (2017) 65.

[142] "GitHub - julianlsolvers/lsqfit.jl — github.com." https://github.com/JuliaNLSolvers/LsqFit.jl.

[143] S. Christ, D. Schwabeneder, C. Rackauckas, M.K. Borregaard and T. Breloff, *Plots.jl – a user extendable plotting api for the julia programming language*, .

[144] A. Berlin, N. Blinov, S. Gori, P. Schuster and N. Toro, *Cosmology and Accelerator Tests of Strongly Interacting Dark Matter*, *Phys. Rev. D* **97** (2018) 055033 [1801.05805].

[145] R. Frezzotti, G. Gagliardi, V. Lubicz, G. Martinelli, F. Sanfilippo and S. Simula, *First direct lattice calculation of the chiral perturbation theory low-energy constant $\ell 7$*, *Phys. Rev. D* **104** (2021) 074513 [2107.11895].

[146] UKQCD collaboration, *Light hadron spectroscopy with O(a) improved dynamical fermions*, *Phys. Rev. D* **60** (1999) 034507 [hep-lat/9808016].

[147] UKQCD collaboration, *The η and η' mesons in QCD*, *Phys. Lett. B* **491** (2000) 123 [hep-lat/0006020].

[148] TXL, T(X)L collaboration, *Flavor singlet pseudoscalar masses in N(f) = 2 QCD*, *Phys. Rev. D* **63** (2001) 074503 [hep-lat/0010005].

[149] TXL, T(X)L collaboration, *Static potentials and glueball masses from QCD simulations with Wilson sea quarks*, *Phys. Rev. D* **62** (2000) 054503 [hep-lat/0003012].

[150] CP-PACS collaboration, *Flavor singlet meson mass in the continuum limit in two flavor lattice QCD*, *Phys. Rev. D* **67** (2003) 074503 [hep-lat/0211040].

[151] UKQCD collaboration, *Improved Wilson QCD simulations with light quark masses*, *Phys. Rev. D* **70** (2004) 014501 [hep-lat/0403007].

[152] European Twisted Mass collaboration, *Lattice QCD with two light Wilson quarks and maximally twisted mass*, *PoS* **LATTICE2007** (2007) 022 [0710.1517].

[153] ETM collaboration, *The eta-prime meson from lattice QCD*, *Eur. Phys. J. C* **58** (2008) 261 [0804.3871].

[154] K. Hashimoto and T. Izubuchi, *eta-prime meson from two flavor dynamical domain wall fermions*, *Prog. Theor. Phys.* **119** (2008) 599 [0803.0186].

[155] W. Sun, L.-C. Gui, Y. Chen, M. Gong, C. Liu, Y.-B. Liu et al., *Glueball spectrum from $N_f = 2$ lattice QCD study on anisotropic lattices*, *Chin. Phys. C* **42** (2018) 093103 [1702.08174].

[156] P. Dimopoulos et al., *Topological susceptibility and η' meson mass from $N_f = 2$ lattice QCD at the physical point*, *Phys. Rev. D* **99** (2019) 034511 [1812.08787].

[157] X. Jiang, W. Sun, F. Chen, Y. Chen, M. Gong, Z. Liu et al., *η-glueball mixing from $N_f = 2$ lattice QCD*, 2205.12541.

[158] SCALAR collaboration, *Scalar mesons in lattice QCD*, *Phys. Rev. D* **70** (2004) 034504 [hep-ph/0310312].

[159] UKQCD collaboration, *A Lattice study of the masses of singlet 0++ mesons*, *Phys. Rev. D* **74** (2006) 114504 [hep-lat/0608026].

[160] S. Prelovsek, T. Draper, C.B. Lang, M. Limmer, K.-F. Liu, N. Mathur et al., *Lattice study of light scalar tetraquarks with I=0,2,1/2,3/2: Are \sigma and \kappa tetraquarks?*, *Phys. Rev. D* **82** (2010) 094507 [1005.0948].

[161] Z. Fu, *Preliminary lattice study of σ meson decay width*, *JHEP* **07** (2012) 142 [1202.5834].

[162] Hadron Spectrum collaboration, *Resonances in coupled $\pi K - \eta K$ scattering from quantum chromodynamics*, *Phys. Rev. Lett.* **113** (2014) 182001 [1406.4158].

[163] M. Wakayama, T. Kunihiro, S. Muroya, A. Nakamura, C. Nonaka, M. Sekiguchi et al., *Lattice QCD study of four-quark components of the isosinglet scalar mesons: Significance of disconnected diagrams*, *Phys. Rev. D* **91** (2015) 094508 [1412.3909].

[164] R.A. Briceno, J.J. Dudek, R.G. Edwards and D.J. Wilson, *Isoscalar $\pi\pi$ scattering and the σ meson resonance from QCD*, *Phys. Rev. Lett.* **118** (2017) 022002 [1607.05900].

[165] R.A. Briceno, J.J. Dudek, R.G. Edwards and D.J. Wilson, *Isoscalar $\pi\pi, K\overline{K}, \eta\eta$ scattering and the σ, f_0, f_2 mesons from QCD*, *Phys. Rev. D* **97** (2018) 054513 [1708.06667].

[166] D. Guo, A. Alexandru, R. Molina, M. Mai and M. Döring, *Extraction of isoscalar $\pi\pi$ phase-shifts from lattice QCD*, *Phys. Rev. D* **98** (2018) 014507 [1803.02897].

[167] Y. Aoki et al., *Flavor-singlet spectrum in multi-flavor QCD*, *EPJ Web Conf.* **175** (2018) 08023 [1710.06549].

[168] LatKMI collaboration, *SU(3) gauge theory with four degenerate fundamental fermions on the lattice*, *PoS* **LATTICE2015** (2016) 215 [1512.00957].

[169] Z. Fodor, K. Holland, J. Kuti, S. Mondal, D. Nogradi and C.H. Wong, *Status of a minimal composite Higgs theory*, *Int. J. Mod. Phys. A* **32** (2017) 1747001.

[170] S. Aoki, H. Fukaya, S. Hashimoto and T. Onogi, *Finite volume QCD at fixed topological charge*, *Phys. Rev. D* **76** (2007) 054508 [0707.0396].

[171] G.S. Bali, S. Collins, S. Dürr and I. Kanamori, *$D_s \to \eta, \eta'$ semileptonic decay form factors with disconnected quark loop contributions*, *Phys. Rev. D* **91** (2015) 014503 [1406.5449].

[172] T. Umeda, *A Constant contribution in meson correlators at finite temperature*, *Phys. Rev. D* **75** (2007) 094502 [hep-lat/0701005].

[173] Lattice Strong Dynamics (LSD) collaboration, G. Fleming, "Update on light composite scalar in eight-flavor su(3) gauge theory."

[174] H. Neff, N. Eicker, T. Lippert, J.W. Negele and K. Schilling, *On the low fermionic eigenmode dominance in QCD on the lattice*, *Phys. Rev. D* **64** (2001) 114509 [hep-lat/0106016].

[175] RQCD collaboration, *Masses and decay constants of the η and η' mesons from lattice QCD*, *JHEP* **08** (2021) 137 [2106.05398].

[176] T. Feldmann, P. Kroll and B. Stech, *Mixing and decay constants of pseudoscalar mesons: The Sequel*, *Phys. Lett. B* **449** (1999) 339 [hep-ph/9812269].

[177] T. Feldmann, P. Kroll and B. Stech, *Mixing and decay constants of pseudoscalar mesons*, *Phys. Rev. D* **58** (1998) 114006 [hep-ph/9802409].

[178] T. Feldmann, *Quark structure of pseudoscalar mesons*, *Int. J. Mod. Phys. A* **15** (2000) 159 [hep-ph/9907491].

[179] H. Hsiao, Bennett, D.K. Hong, J.-W. Lee, C.J.D. Lin, B. Lucini et al., *Spectroscopy of chimera baryons in a $Sp(4)$ lattice gauge theory*, 2211.03955.

[180] H. Hsiao, E. Bennett, D.K. Hong, J.-W. Lee, C.J.D. Lin, B. Lucini et al., *Spectroscopy of chimera baryons in a Sp(4) lattice gauge theory*, *PoS* **LATTICE2022** (2023) 211 [2210.08154].

[181] S. Gusken, U. Low, K.H. Mutter, R. Sommer, A. Patel and K. Schilling, *Nonsinglet Axial Vector Couplings of the Baryon Octet in Lattice QCD*, *Phys. Lett. B* **227** (1989) 266.

[182] J. Bijnens and J. Lu, *Meson-meson Scattering in QCD-like Theories*, *JHEP* **03** (2011) 028 [1102.0172].

[183] F. Pressler, *Lattice spectroscopy of strongly interacting dark matter candidates*, bachelor's thesis, University of Graz, 2019.

[184] J.-W. Lee, B. Lucini and M. Piai, *Symmetry restoration at high-temperature in two-color and two-flavor lattice gauge theories*, *JHEP* **04** (2017) 036 [1701.03228].

[185] G.M. de Divitiis et al., *Isospin breaking effects due to the up-down mass difference in Lattice QCD*, *JHEP* **04** (2012) 124 [1110.6294].